Republic of Iraq

Ministry of Higher Education & Scientific Research

University of Kerbala

College of Engineering

Department of Mechanical Engineering

Vibration Control of a Half-Car Model Using a Smart Damper

A Thesis Submitted to the Council of the College of Engineering, University of Kerbala in Partial Fulfillment of the Requirements for the Degree of Master of Science in Mechanical Engineering

(Applied Mechanics)

Prepared by

Ahmed Mohammed Ali Hassan Al-Khafaji

Supervised by

Prof. Dr. Ahmed Abdullah Hassan Al-Rajihy

May 2025 Dhu al-Qi’da 1446

Republic of Iraq

Ministry of Higher Education & Scientific Research

University of Kerbala

College of Engineering

Mechanical Engineering Department

Vibration Control of a Half-Car Model Using a Smart Damper

A Thesis Submitted to the Council of the Faculty of the College of Engineering/University Of Kerbala in Partial Fulfillment of the Requirements for the Master's Degree in /Applied Mechanical Engineering

Prepared by

Ahmed Mohammed Ali Hassan Al-Khafaji

Supervised by

Prof. Dr. Ahmed Abdullah Hassan Al-Rajihy

May 2025 Dhu al-Qi’da 1446

بِسْمِ اللَّهِ الرَّحْمَنِ الرَّحِيمِ

يَرْفَعِ اللَّهُ الَّذِينَ آمَنُوا مِنكُمْ وَالَّذِينَ أُوتُوا الْعِلْمَ دَرَجَاتٍ

صدق الله العلي العظيم

(المجادلة: من الآية 11)

Examination committee certification

We certify that we have read the thesis entitled "**Vibration Control of a Half-Car Model Using a Smart Damper** " and as an examining committee, we examined the student " **Ahmed Mohammed Ali Hassan Al-Khafaji**" in its content and in what is connected with it and that in our opinion it is adequate as a thesis for the degree of Master of Science in Mechanic Engineering.

Signature:
Name:. Prof. Dr. Ahmed A. Al-Rajihy
Date: 25 / 9 / 2025
Superviser

Signature:
Name :. Prof. Dr. Amjad Al-Hamood
Date: 25 / 9 / 2025
Member

Signature:
Name :. Assoc. Prof. Dr. Fawaz F. Al-Bakri
Date 25 / 9 / 2025
Member

Signature:
Name :. Prof. Dr. Emad Qasem Hussein
Date: 25 / 9 / 2025
Chairman

Approval of Head of Mechanic Engineering Department

Signature:
Name : Pro. Dr. Salah N. Alnomani
Date: 28 / 9 / 2025

Approval of Deanery of the College of Engineering

Signature:
Name : Pro. Dr. Haider Nadhom Azizz
Date: 28 / 9 / 2025

Supervisor certificate

I certify that the thesis entitled **"Vibration Control of a Half-Car Model Using a Smart Damper "** was prepared by **Ahmed Mohammed Ali Hassan Al-Khafaji** under our supervision at the Department of Mechanic Engineering, Faculty of Engineering, University of Kerbala as a partial of fulfilment of the requirements for the Degree of Master of Science in Mechanic Engineering.

Signature:

Prof. Dr. Ahmed Abdullah Hassan Al-Rajihy

Date: 24/ 9/ 2025

Linguistic certificate

I certify that the thesis entitled " **Vibration Control of a Half-Car Model Using a Smart Damper** " which has been submitted by **Ahmed Mohammed Ali Hassan Al-Khafaji,** has been proofread and its language has been amended to meet the English style.

Signature:

Dr. Hasan Qahtan Hussain

Date: 23/ 9/ 2025

Undertaking

I certify that research work titled " **Vibration Control of a Half-Car Model Using a Smart Damper** " is my own work. The work has not been presented elsewhere for assessment. Where material has been used from other sources, it has been properly acknowledged/referred.

Signature:

Ahmed Mohammed Ali Hassan Al-Khafaji

Date: 23/ 9/ 2025

Dedication

To my parents' spirit, who provided me with all the required support, to my wife, who urged me to stay on course, and to my entire family.

Ahmed. M. Ali

Acknowledgments

To everyone who helped me finish this thesis, I would like to sincerely thank you for your contributions.

First and foremost, I want to express my gratitude to Prof. Dr. Ahmed Abdullah Hassan Al-Rajihy, my supervisor, for his invaluable advice and unwavering support. His counsel has been invaluable in helping me develop my thoughts, and I am very grateful for it.

Additionally, I would like to express my gratitude to Dr. Muslim Mohsen Al-Shraefi, all doctors of Kerbala University, Mr. Ali Taban, Mr. Waleed Khalid Ali with his work stuff, Mr. Haider Al-Dulaimi, Mr. Salim Mousaibawy, Mr. Mahmood Hatem Gamah with his work stuff, Mr. Aqeel Al-kenani, Mr. Khalil Abd Ali and Mr.Talib Fadil Abbas for their help and support in times of need. I've found inspiration in our conversations and thought exchanges.

Lastly, I want to express my gratitude to my family for their unwavering encouragement and support during my academic career. Without them, I could not have finished this work.

Many thanks to all of you!

Abstract

Automobiles vibrate due to different road irregularities, which affects safety and ride comfort. To reduce these effects, Half-car model with four degrees of freedom is adopted, considering vertical motions of the front and rear wheels and rotational motion about the vehicle's center. The model is tested with and without modifications to the damping system. The damping system is altered by applying two external hydraulic control valves and two check valves fitted to the front and rear dampers. This model's response is investigated theoretically under step road input and practically under impulse close to sine road input. The parameters: mass, damping factor, and spring stiffness are adjusted to achieve improved performance. The objective of the optimization is to minimize (settling time, peak overshoot percentage, and steady-state error). Matlab-Simulink program is used for simulation, combined with an optimization technique called the" line search method". The optimal front control valve parameter values are found to be: mass of 2 grams, damping factor of 7 N.s/m and spring stiffness of 9000 N/m, while for the rear one, the mass is 2 grams, damping factor is 8 N.s/m and spring stiffness is 13000 N/m. Results show that this approach enhances the overall dynamic response compared with the approach of a passive damper system; the center sprung mass settling time for the smart damper case was reduced by 65 % and the peak overshoot by 55% as contrasted with the passive damper, providing more ride comfort and vehicle stability.

Table of Contents

List of Tables

List of Figures

List of Symbols

Symbol	Description	Unit
A_{DP}	Damper piston area	m^2
A_{DR}	Damper piston rod area	m^2
A_{net}	Damper piston net area	m^2
A_v	Control valve flow area	m^2
A_{vp}	Control valve projected area	m^2
b_1	Half-automobile model rear damper damping constant	N.s/m
b_2	Half-automobile model front damper damping constant	$\mathrm{N.s/m}$
b_3	Rear tire damping constant for the half-automobile model	N.s/m
b_4	Front tire damping constant for the half-automobile model	N.s/m
b_v	Control valve damping constant	$\mathrm{N.s/m}$
C	A damper damping constant.	N.s/m
c_{cr}	Critical damping.	N.s/m
c_f	Coefficient of discharge	--------
D_v	Control valve conical mass diameter	m
F	The force that results from the main spring's expansion during the rebound stroke due to the damper's hydraulic fluid pressure	N
f_f	Front side control valve force	N

Symbol	Description	Unit
f_r	Rear side control valve force	N
F_{vf}	Control valve momentum force due to the hydraulic liquid flow	N
F_{vP}	Control valve pressure force	N
H	Road excitation delay time between the half-automobile model front and rear tires	s
J_c	Sprung mass, mass moment of inertia, rotating about a horizontal axis passing through its center of gravity	$\mathrm{Kg.m^2}$
k_1	Rear spring stiffness of a half-automobile model	$\mathrm{N/m}$
k_2	Front spring stiffness of a half-automobile model	$\mathrm{N/m}$
k_3	Rear tire stiffness for the half-automobile model	$\mathrm{N/m}$
k_4	Front tire stiffness for the half-automobile model	$\mathrm{N/m}$
k_v	Control valve spring stiffness	$\mathrm{N/m}$
k	Spring stiffness. For the control valve	$\mathrm{N/m}$
L_1	Distance between the half-automobile model sprung mass center and the top of the rear damper	m
L_2	Distance between the sprung mass center and the top of the front damper	m
m_s	Sprung mas for the half automobile model	Kg
m	Sprung mass effect on the front half-automobile side	Kg
m_{u1}	Half-automobile model rear unsprung mass	Kg
m_{u2}	Half-automobile model front unsprung mass	Kg
m_v	Control valve conical mass	Kg
P	Hydraulic pressure due to the main spring force	$\mathrm{N/m^2}$

Symbol	Description	Unit
P_1	Pressure below the damper piston.	$\mathrm{N/m^2}$
P_2	Pressure above the damper piston.	$\mathrm{N/m^2}$
Q_p	The hydraulic liquid flow rate that leaves the damper during the rebound stroke	$\mathrm{m^3/s}$
Q_v	The hydraulic liquid flow rate that enters the control valve during the rebound stroke	$\mathrm{m^3/s}$
U	Hydraulic flow velocity	$\mathrm{m/s}$
$U_{1\ or\ 2}$	Hydraulic liquid velocity above or below the damper piston sides, respectively.	$\mathrm{m/s}$
V	Half-automobile test rig conveying belt velocity	$\mathrm{m/s}$
x_1	The amplitude of the first peak of the response	m
x_2	The amplitude of the second peak of the response	m
y_2	Half-automobile center sprung mass displacement	m
$\dot{y}_2$	Half-automobile model center sprung mass velocity	$\mathrm{m/s}$
$\ddot{y}_2$	Half-automobile model, center-sprung mass acceleration	$\mathrm{m/s^2}$
y_{1f}	The half-automobile model front unsprung mass displacement	m
$\dot{y}_{1f}$	The half-automobile model front unsprung mass velocity	$\mathrm{m/s}$
$\ddot{y}_{1f}$	The half-automobile model front unsprung mass acceleration	$\mathrm{m/s^2}$
y_{2f}	The half-automobile model's front side sprung mass displacement	m
$\dot{y}_{2f}$	Half-automobile model's front side sprung mass velocity	$\mathrm{m/s}$

Symbol	Description	Unit
y_{1r}	The half-automobile model rear unsprung mass displacement	m
$\dot{y}_{1r}$	The half-automobile model rear unsprung mass velocity	m/s
$\ddot{y}_{1r}$	The half-automobile model rear unsprung mass acceleration	m/s^2
y_{2r}	The half-automobile model's rear side sprung mass displacement	m
$\dot{y}_{2r}$	The half-automobile model's rear side sprung mass velocity	m/s
y_{rf}	Half-automobile model front road excitation displacement	m
$\dot{y}_{rf}$	Half-automobile model front road excitation velocity	m/s
y_{rr}	Half-automobile model rear road excitation displacement	m
$\dot{y}_{rr}$	Half-automobile model rear road excitation velocity	m/s
y_v	Control valve conical mass displacement	m
$\dot{y}_v$	Control valve conical mass velocity	m/s
$\ddot{y}_v$	Control valve conical mass acceleration	m/s^2
θ	Half automobile model sprung mass angle of rotation	rad
$\dot{\theta}$	Half automobile model's sprung mass angle of rotation first derivative	rad/s
$\ddot{\theta}$	Half automobile model sprung mass angle of rotation second derivative	rad/s^2

Symbol	Description	Unit
Δ	Logarithmic decrement	-------
$\mathcal{f}$	Hydraulic fluid density	Kg/m^3
Z	Damping ratio	-------
$\propto$	Control valve mass angle	Degree

List of Abbreviations

RMS	Root mean square
EMD	Electromagnetic damper
MFAFLC	Model-free adaptive fuzzy logic controller
ANN	Artificial neural network
FLC	Fuzzy logic controller
LQR	Linear quadratic regulator
MPC-LQR	Model predictive control-linear quadratic regulator
S-SAS	Semi-active stability augmentation system
FS-SAS	Fuzzy semi-active stability augmentation system
PID	Proportional integral-derivative
SMC	Sliding mode control
CCU	Closed-loop Current Control Unit
PEMSS	Passive electromagnetic suspension system
CDC	Continuous damping control
PSO	Particle swarm optimization

Chapter One

Introduction

Chapter One: Introduction

1.1 Overall View

During the motion of an automobile, it is exposed to vibrations due to external disturbances as a result of road profiles, causing riding discomfort. Vibration takes the form of pitching, rolling, and yawing. A variety of early treatments for this undesirable phenomenon, included adding springs and hydraulic dampers. It is known that these first treated means were based on constant stiffness and damping factors, which partially meet the demands of ride comfort, road handling, and stability. Therefore, more studies were conducted, which led to the invention of semi-active and active dampers that help to provide more vehicle stability and road handling, as well as ride comfort. The pitching and rolling motions of the vehicle can contribute significant energy to the overall excitation of the vehicle and payload[1] Controlling automobile vibration mechanically and /or electrically has a significant role in automobile road handling and passenger comfort. This is achieved by attaching a stepper motor for each shock absorber, which helps in adjusting the bleed orifice to a certain position that alternates the hydraulic oil flow in the shock absorber between the piston's chamber during the process of compression and rebound[2], [3]. "The results show that the smart damper attenuates the vibrations of the sprung mass in a short period compared with other types of dampers,"[4].

1.2 Types of Suspension Systems

The suspension systems can be categorized as follows:

I. Independent Suspension: Independent suspension is usually used in vehicles that allow each wheel to move vertically independently of the others and afford better handling, comfort,

and traction by separating each wheel's movement. This type can be divided as below:

1. MacPherson Strut suspension: It consists of a damper and a coil spring into a single unit to minimize the required space and is easy to maintain. This design is low in cost for a wide range of vehicles. This suspension type can be shown in Figure (1-1):

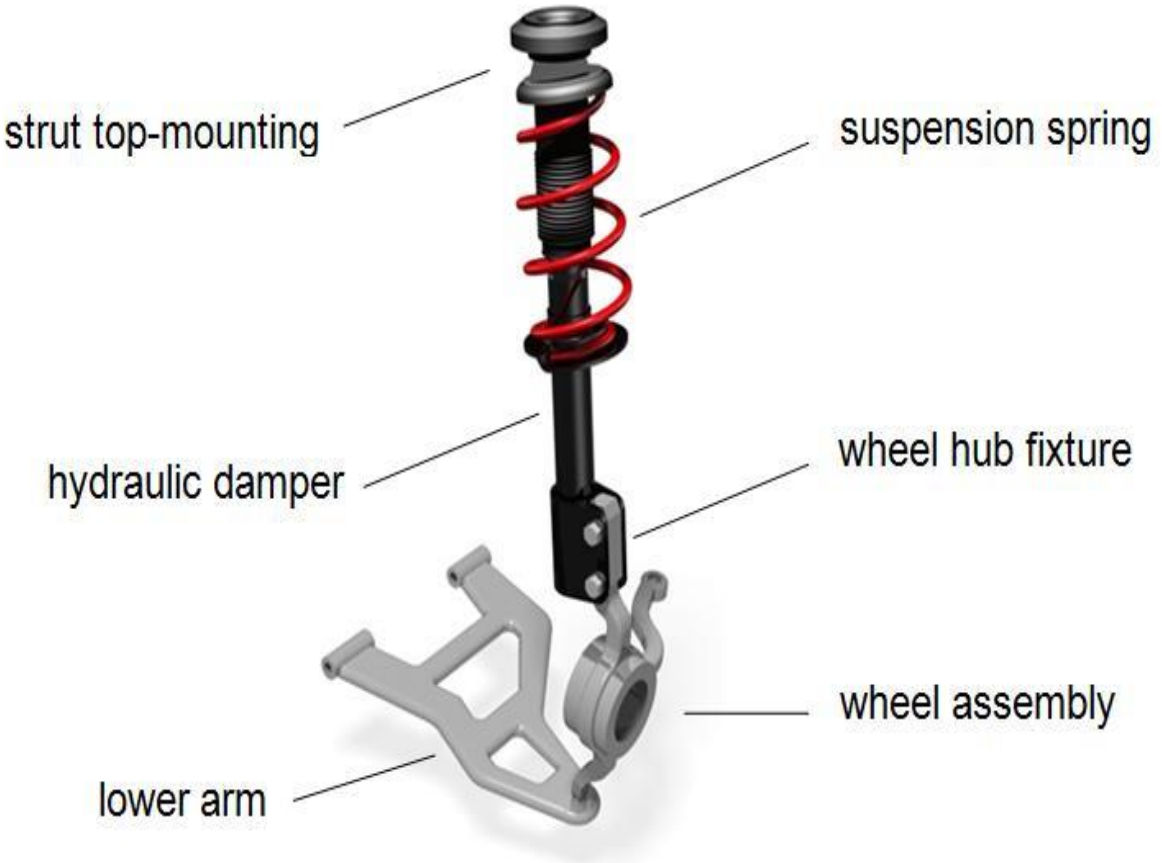

Figure (1-1): MacPherson Strut suspension.

2. Double Wishbone suspension: Double Wishbone suspension is an advanced independent suspension system. Two control arms formed as wishbones to connect the wheel hub to the chassis. This design provides better car steering, good road handling

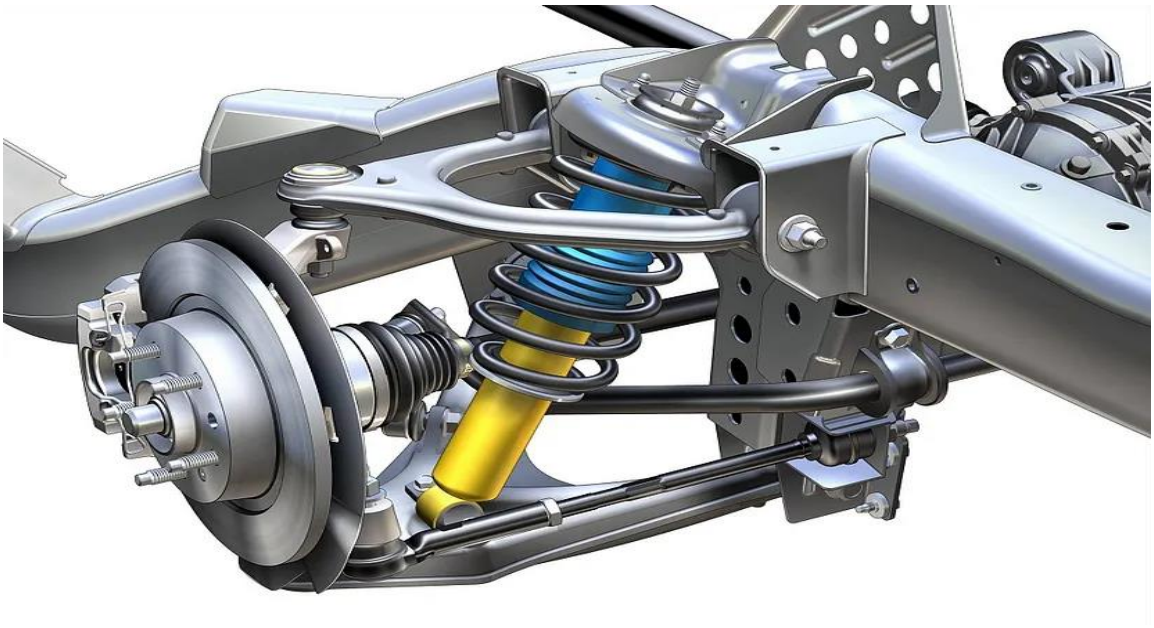

Figure (1-2): Double Wishbone suspension system.

during cornering, and eliminates tire wear. It can be illustrated in Figure (1-2).

3. Multi-link suspension: This suspension type uses multiple control arms to connect the wheel hub to the chassis, providing precise control over wheel movement. This advantage gives cars equipped with this type of suspension, especially sports cars, comfortable steering control during traction and cornering. Figure (1- 3) illustrates this system.

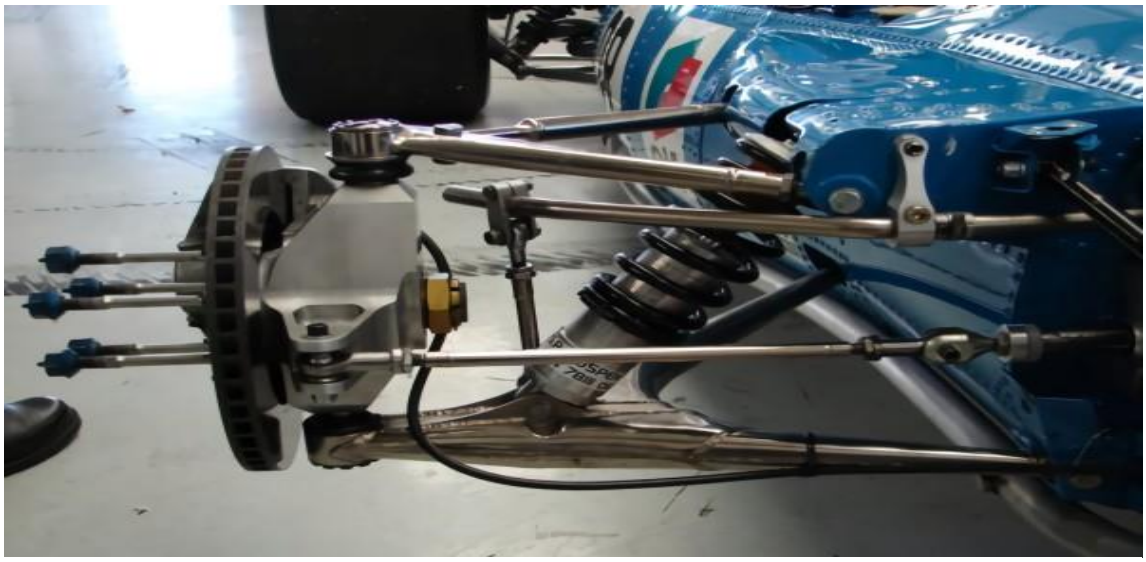

Figure (1-3): Multi-link suspension system.

II. Dependent Suspension: This suspension system is rougher in ride quality than an independent suspension system because each wheel's displacement partially affects the other displacement lying on the same axle. This design causes less stability and road handling, particularly on uneven road profiles. This design is simple to manufacture and costs little to hand. It can be found in the vehicle's rear axle in two forms as follows:

1. Solid Axle: In this type, two or more wheels that lie on the same axle are linked to a single rigid beam or axle housing. This design minimizes control links and reduces road handling, especially on uneven roads. The design of a solid axle has the advantage of durability and the capability to carry high loads; therefore, it is used in heavy-duty trucks. Figure (1-4) shows this type.

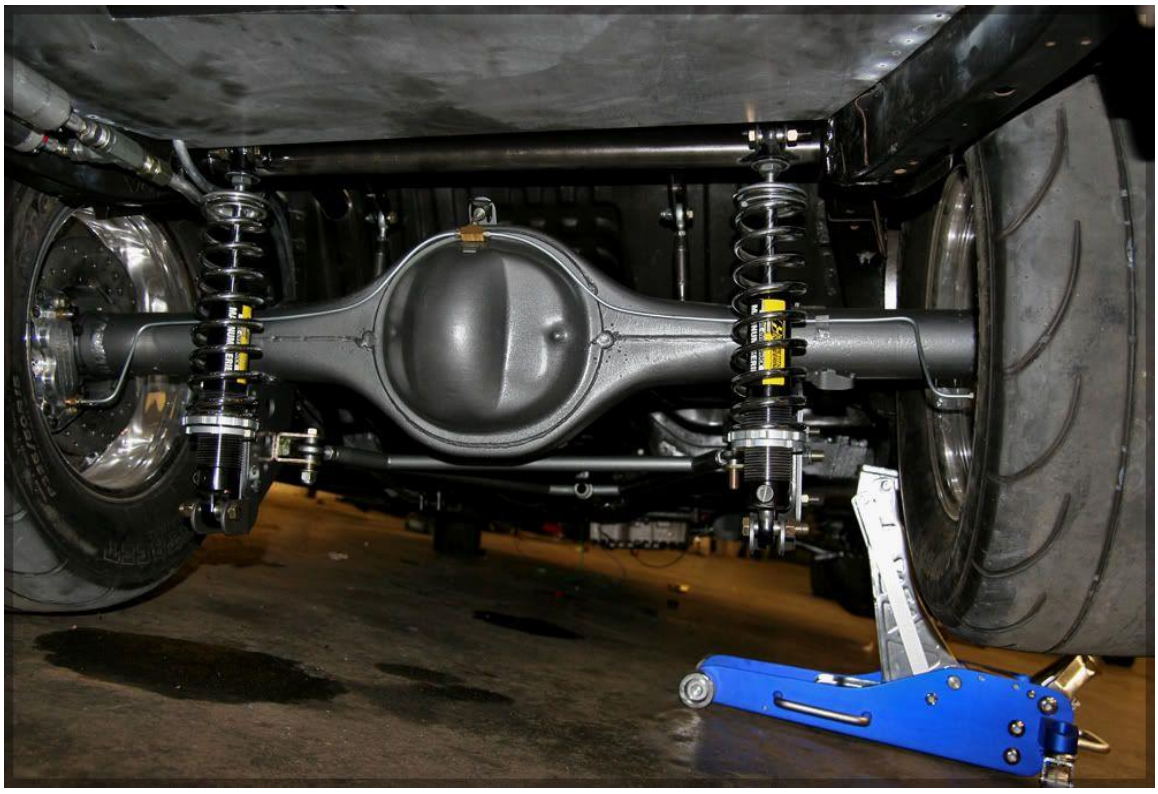

Figure (1-4): Solid axle suspension system.

2. Torsion Beam: This type involves a solid beam that joins the wheels on the same axle, permitting partial independent displacement. It is simple in design, has low-cost maintenance, and requires little space. For that reason, it is used for a variety of car models, providing a good balance between vehicle stability and ride comfort. Figure (1-5) illustrates the suspension type.

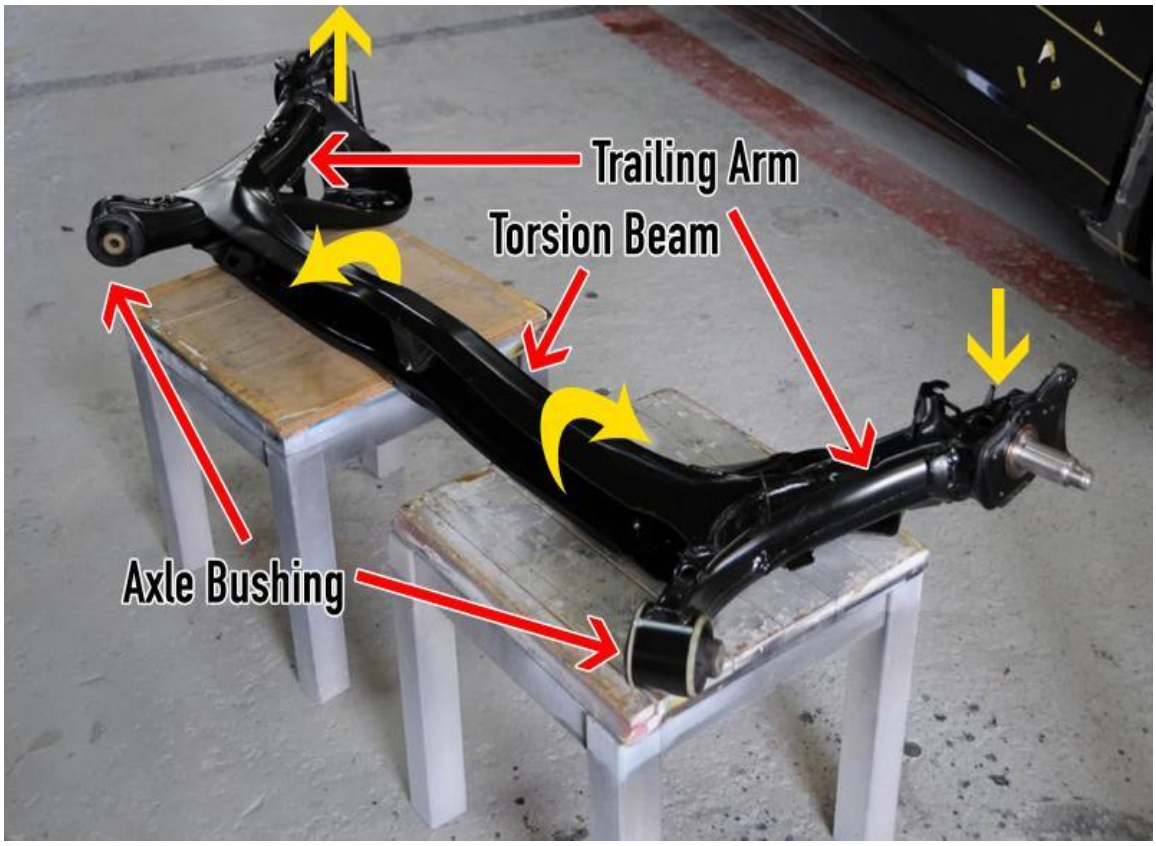

Figure (1-5): Torsion beam suspension system.

3. Semi-Active and Active Suspension: Semi-active suspension systems vary the damping rates according to the road profiles and driving dynamics, providing a balance between passenger comfort and road handling without the difficulty of active systems. Figure (1-6) shows a semi-active damper with electric coils. When energized, the Magnetorheological fluid changes its characteristics, resulting in adjusted damper stiffness

accordingly. Active suspension systems use sensors and actuators to control damping rates continuously, enhancing comfort and vehicle stability noticeably. Figures (1-7) and (1-8) illustrate an active suspension system.

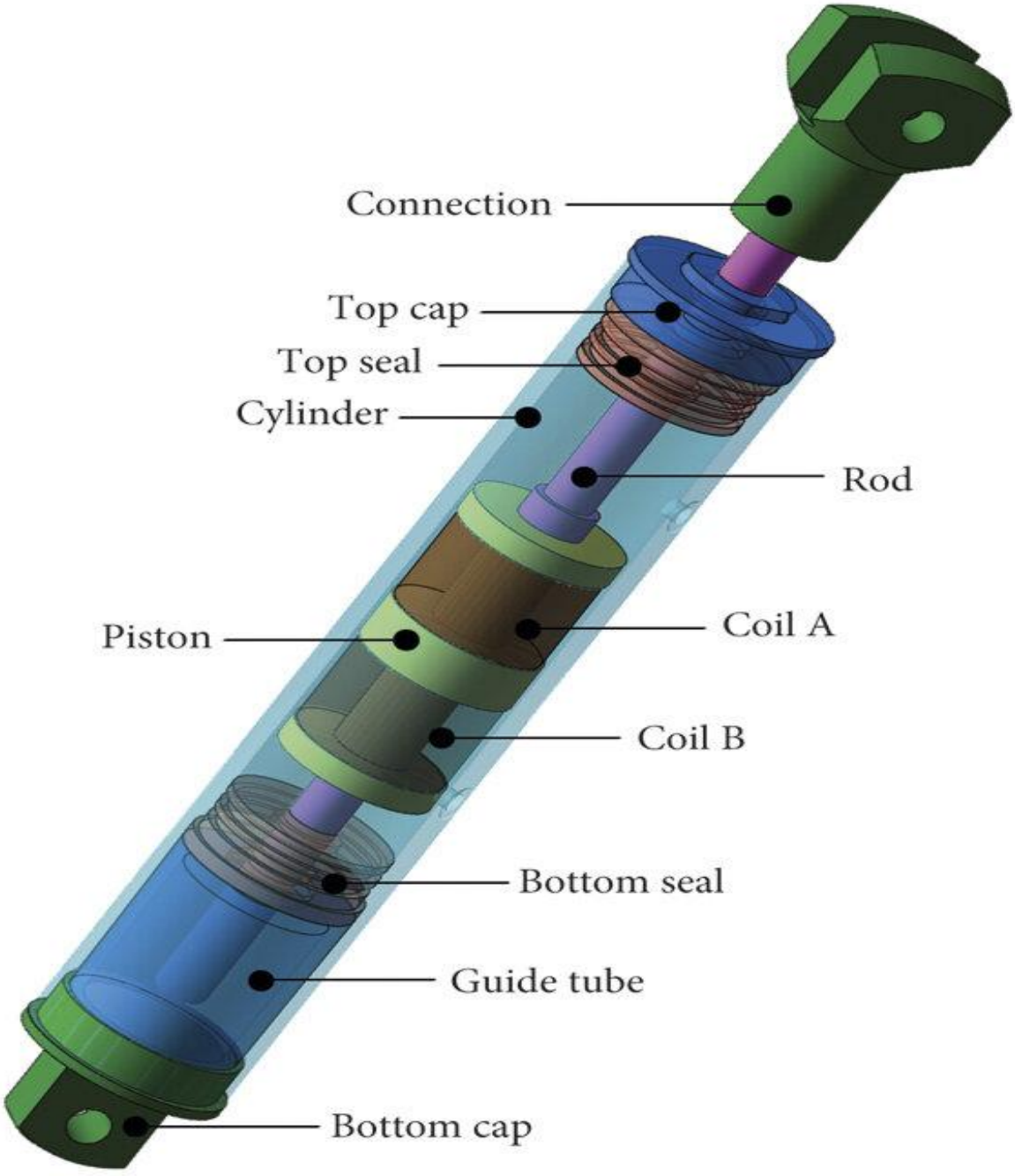

Figure (1-6): semi-active damper with electric coils.

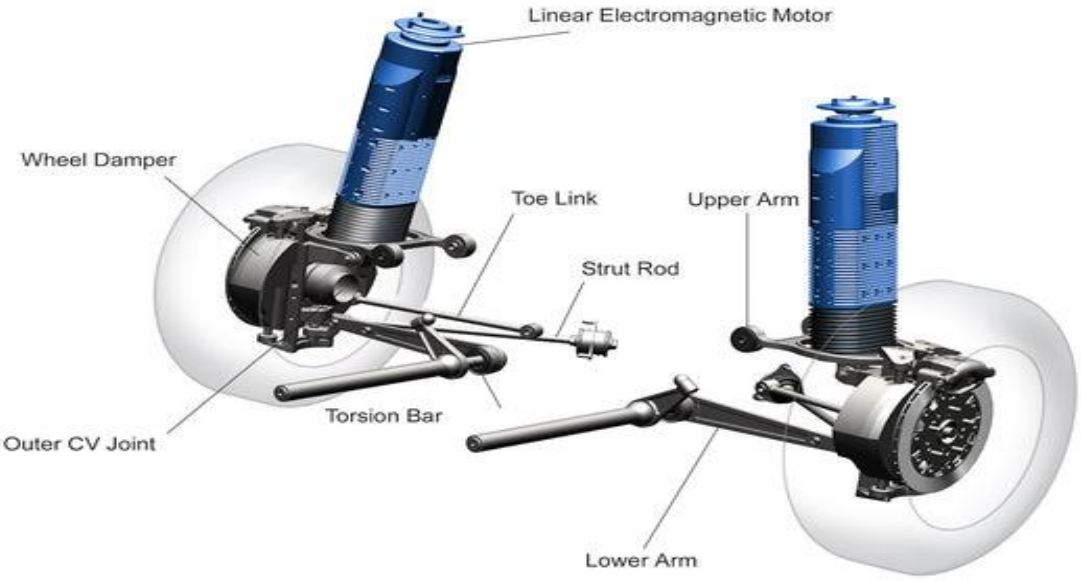

Figure (1-7): Bose electromagnetic car (active) suspension.

Figure (1-8): A car with Bose Active Suspension floats along the road and through corners.

1.3 Viscous Damper Composition

Viscous dampers are hydraulic devices that restrict the fluid stream to control motion and dampen vibrations. In cars, they are simple in design, thus they can be produced in mass production to meet market demands and requirements, and can be trusted for safety because they can work at different temperature ranges. "Dampers are largely responsible for determining a car's driving character, so choosing the right one matters" [5]. They are composed of the following parts, as shown in Figures (1-9) to (1-12):

1 Piston.
2 Main shaft.
3 Compression shims.
4 Rebound shims.
5 Hydraulic liquid (oil).
6 Nitrogen (used in some high-performance dampers).
7 Floating divider (used in dampers equipped with nitrogen or pressurized air).
8 Base valve compression shims (twin-tube and internal bypass dampers) as shown in Figures (1-10) and (1-11).
9 Electromagnetic coils (used in electromagnetic damper) as shown in Figure (1-12).

The monotube damper shown in Figure (1-9) is a single tube only filled with hydraulic fluid (oil) during the compression stroke to the left and at the rebound stroke to the right. The oil passes through the orifice hole and regulates fluid flow during extension in a monotube damper, affecting damping forces and suspension behavior.

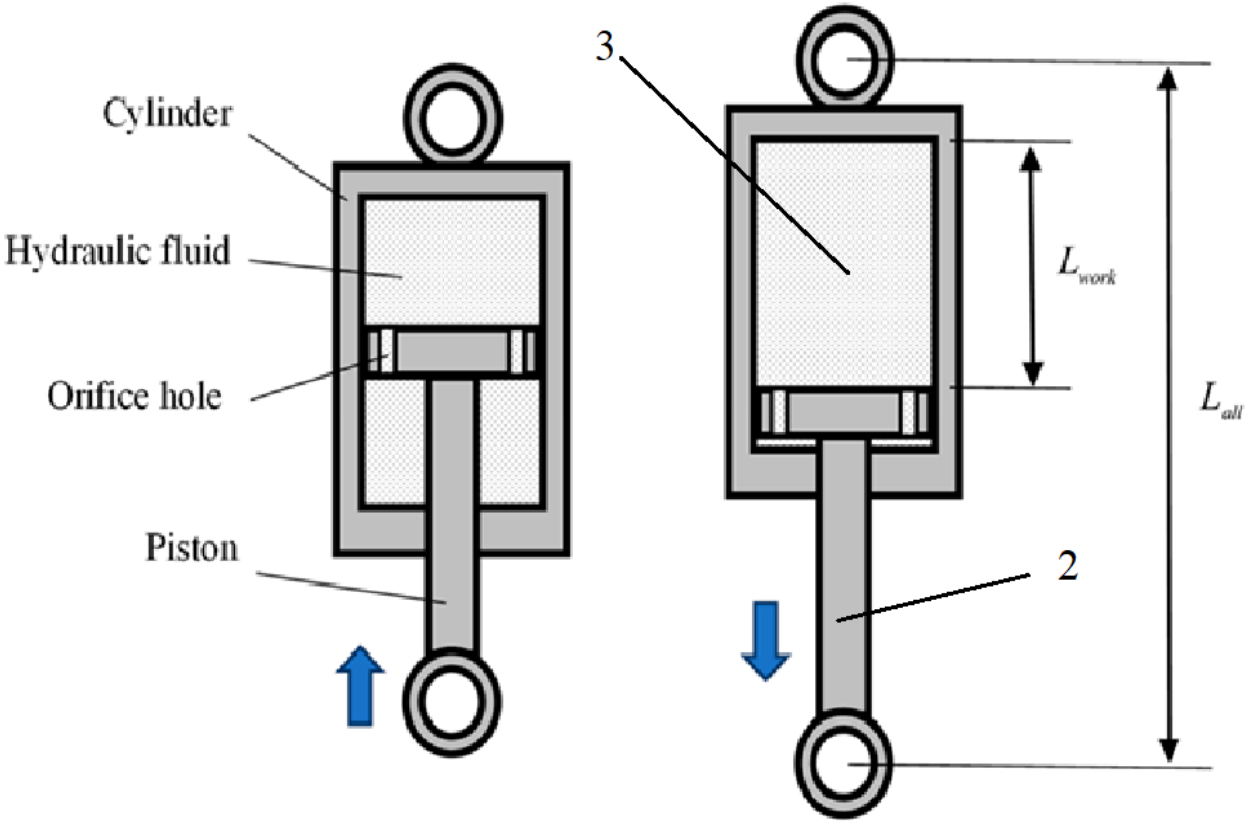

Figure (1-9): Monotube damper during compression and rebound strokes.

The twin-tube damper illustrated in Figure (1-10) has inner and outer tubes. The first one contains a piston, base valve shims, and fluid, and the outer acts as a fluid reservoir, improving heat transfer to the outside of the damper and prolonging its life.

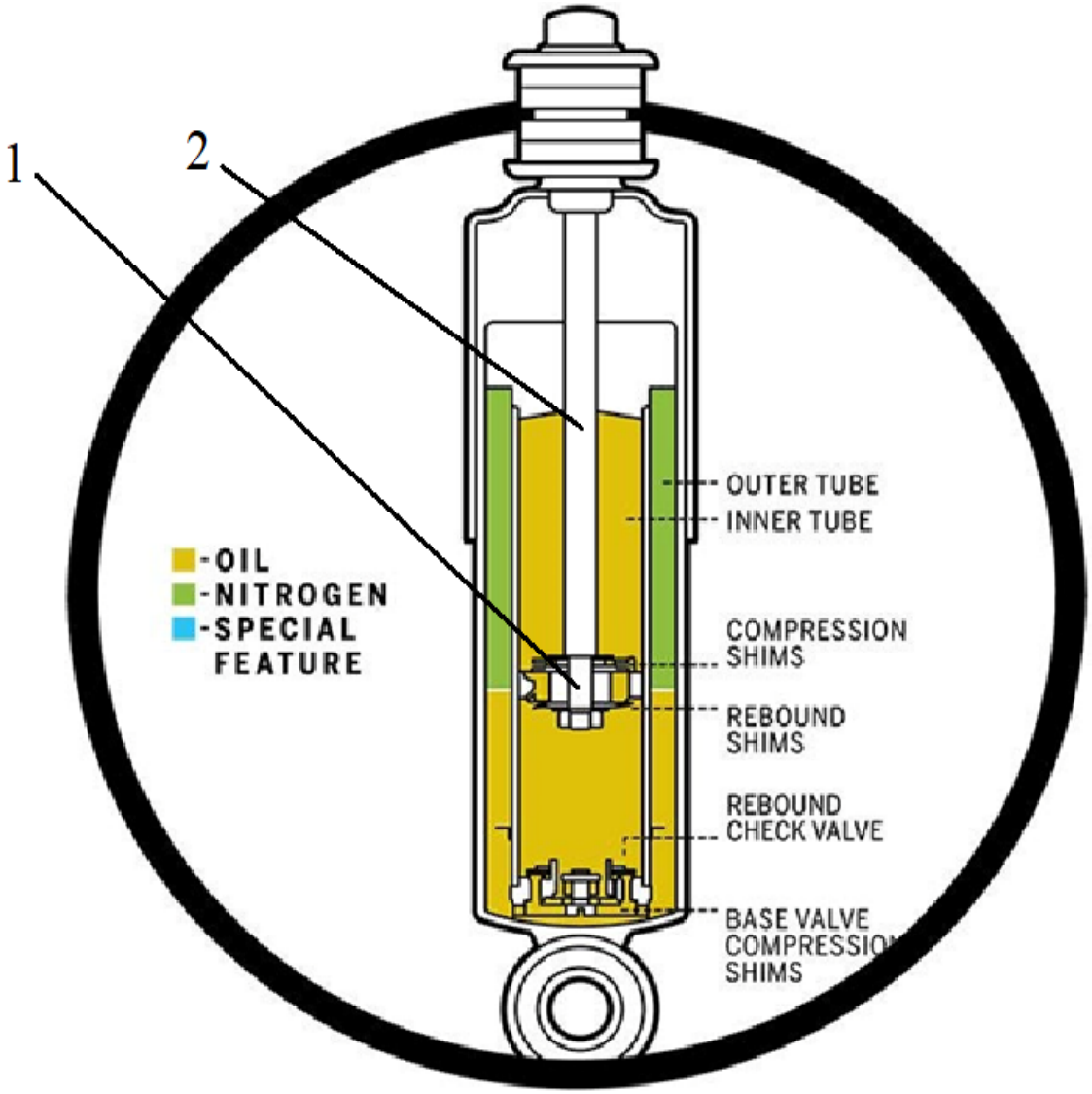

Figure (1-10): Twin-tube damper.

The Internal bypass damper illustrated in Figure (1-11) uses internal passages to control fluid flow, permitting variable damping rates without outside adjustments. The internal passages are configured and shaped to meet the required damping rate that gives needed handling and ride comfort.

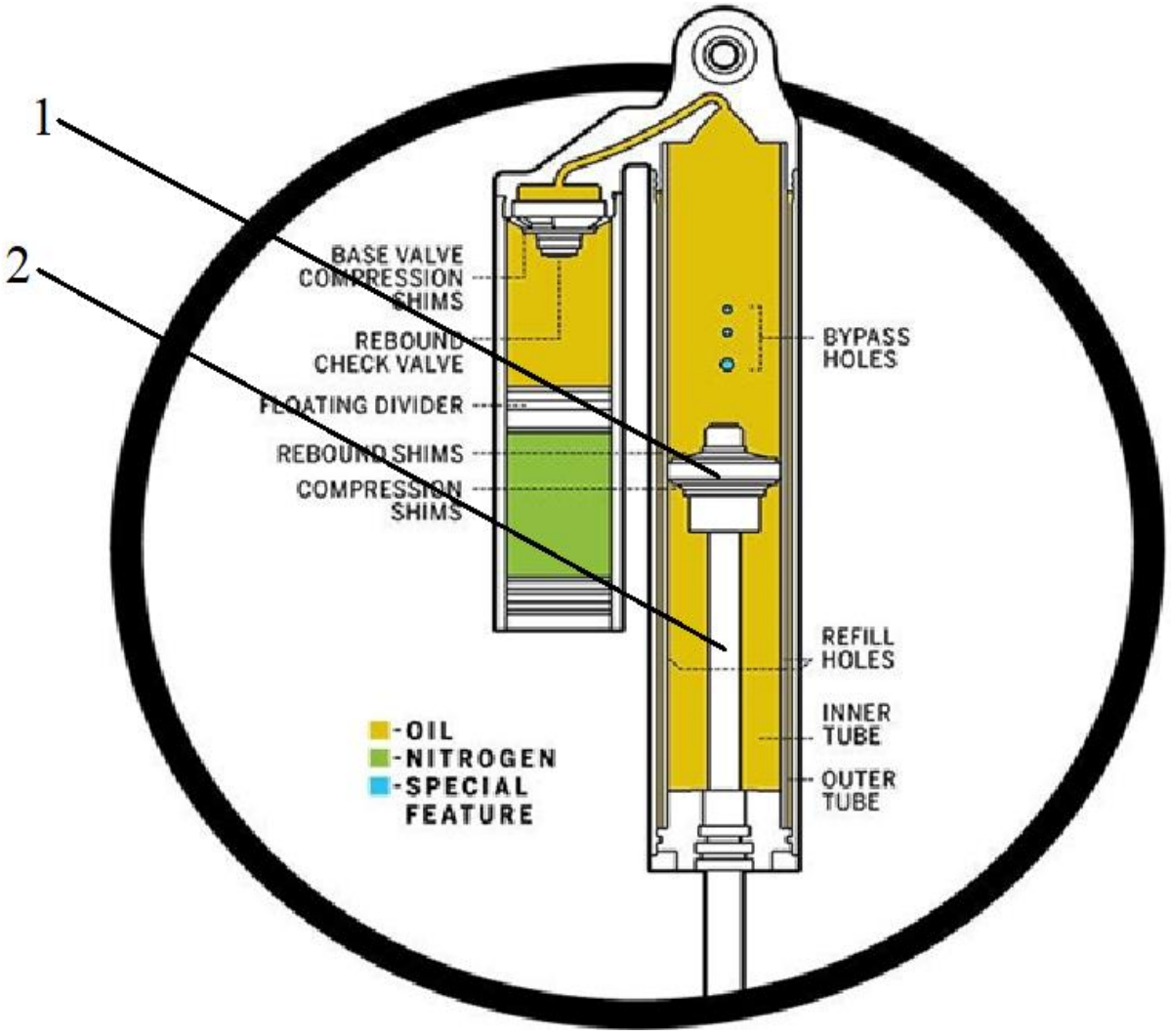

Figure (1-11): Internal bypass damper.

The magnetorheological damper shown in Figure (1-12) uses an electromagnetic coil to precisely adjust the vehicle's dynamic response and to deliver the appropriate damping rate for the required handling and ride comfort.

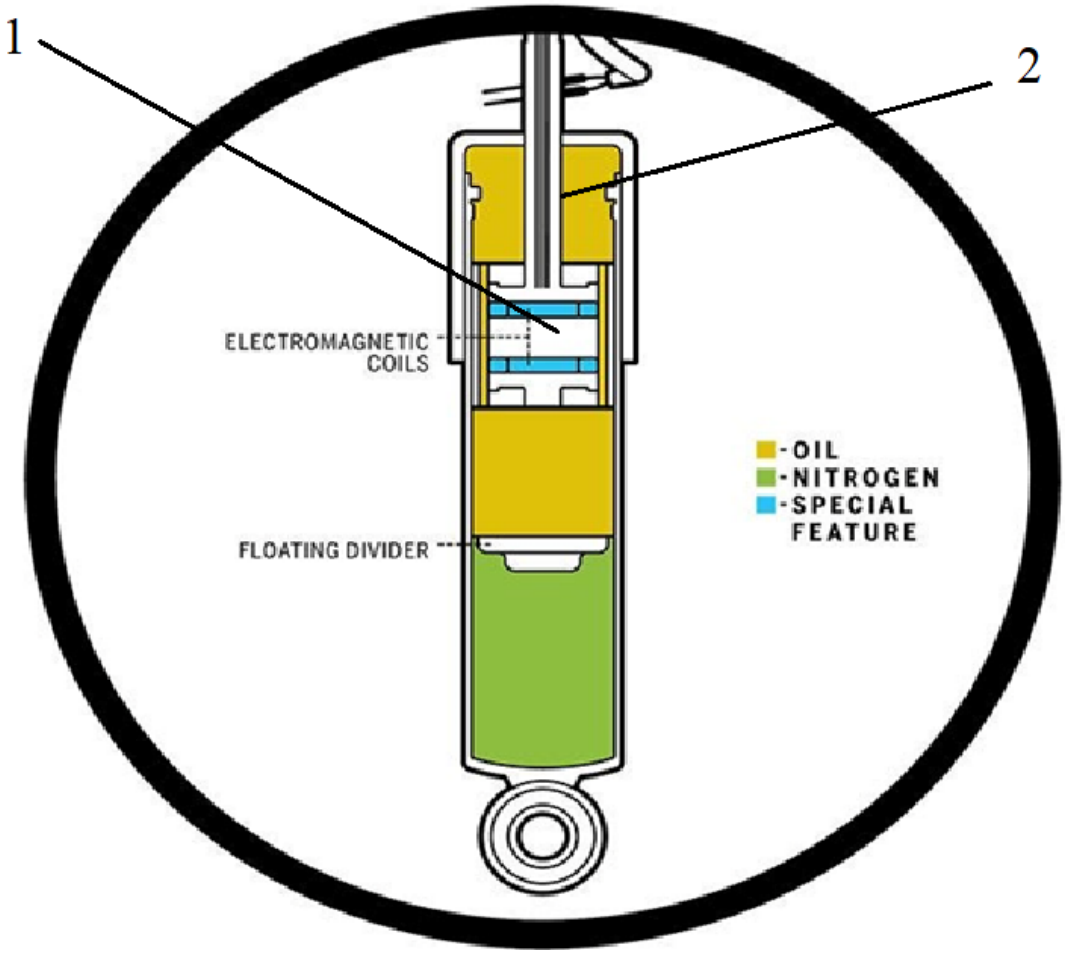

Figure (1-12): Magnetorheological Damper.

1.4 Vibration Control Techniques of Viscous Damper

Many techniques are used in the vibration control of viscous dampers, as below:

• Electronic Damping Control System: In this system, electronic components (Sensors and a control unit) vary the damper force according to the road profiles and driving conditions.

• Active Damping System: This system uses hydraulic or electric actuators to continuously vary the damper force based on road conditions and vibration data provided by sensors.

• Semi-active damping System: It uses wireless frequencies, electromagnetic valves, and coils to change the damper force in real time, but less than the active suspension system.

• Smart damping System: Mechanical control valves are added to a passive damper and transformed into a smart damper, enhancing both road handling and vehicle stability.

1.5 Ride Comfort

Vibrations, noise, acceleration, and other factors that impact people's comfort, activity, and health are experienced by both the driver and passengers in cars. Vibrations' impact on the human body depends upon their frequency, amplitude, duration, and direction of effect. Driver and passenger tiredness from prolonged vibration exposure impairs their performance and decreases their functional state. One of the primary needs for modern cars is to improve ride comfort because this can have an impact on traffic safety. When driving a car, the driver and passengers experience various conditions, effects, and experiences that make up the ride comfort. Measurement, assessment, and analysis of the several elements influencing ride comfort have been the focus of numerous research projects and scientific advancements. Numerous complex aspects that can be divided into the following categories influence how comfortable a car's passengers are: The microclimate in the vehicle's passenger compartment (cabin) (thermal comfort, air quality, atmospheric pressure, etc.); the mechanical comfort (vibrations with low and very low frequency, shocks, and accelerations); and

the factors based on the passengers' comfortable positions are all dynamic factors that affect ride comfort. The driver and passengers use their subjective judgments to rate the comfort of the trip. “The ride comfort depends on the characteristics of the forces that cause oscillations and vibrations, on the design of the car, the parameters of the suspension, the driving conditions, etc.”[6].

1.5.1 Human Body Vibration Acceptable Limits

Automobile vibration sources can be classified into onboard vehicle sources from the “engine, the driveline, and the wheels. These sources supply the vibration in the frequency region of 25-20000 Hz”[7], and road sources from road conditions. The human body can deal with vibration from rarely felt at $0.01\ \frac{m}{s^2}$ (at 1 HZ to 20 HZ)[7] to a hazardous peak value of $1\frac{m}{s^2}$ “depending on the frequency, direction, and duration of the vibration”[8]. The on-road acceptable vehicle vibration beginning from $0.1\ \frac{m}{s^2}$ for smooth riding to $0.2\ \frac{m}{s^2}$ r.m.s to $1\ \frac{m}{s^2}$ r.m.s for uncomfortable riding, while off-road vehicles can reach $2\ \frac{m}{s^2}$ r.m.s or more [8]. Figure (1-13) shows the natural frequency of human body parts [9]. Reaching a frequency equal to or near the natural frequency of any part caused a harmful issue.

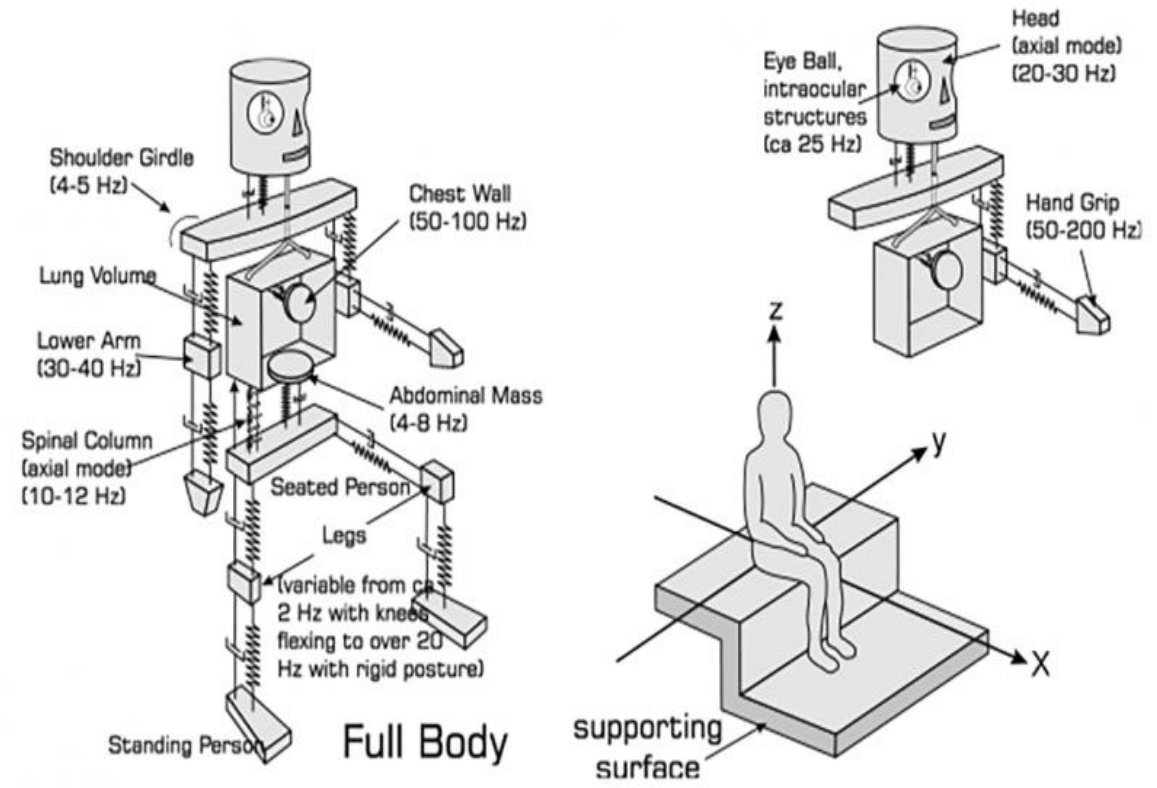

Figure (1-13): Natural frequencies of the human body[7].

1.6 Road Handling

The term "road handling" describes an automobile's ability to be stable and efficient on a variety of road conditions, including things like steering reaction, cornering ability, and stability at high speeds. Road handling quality depends on many variables, including tire setup, drivetrain type (front-wheel drive, rear-wheel drive, or all-wheel drive), and suspension system. The ultimate goal of improving road handling is to increase driver confidence and vehicle performance, which will ultimately guarantee passenger comfort and safety. Good road handling requires a balance between performance and comfort to provide drivers with a sense of security and control under a variety of driving circumstances. “The system

should be capable of switching safely and predictably between a stiff spring and high damping mode (for handling) as well as a soft spring and low damping mode (for ride comfort)" [9]. Figure (1-14) illustrates the relation between ride comfort and vehicle stability (road handling) when increasing damping leads to more road handling but low ride comfort. On the contrary, when decreasing damping leads to low vehicle stability but more ride comfort, a balance was chosen represented by the point of intersection between the two curves.

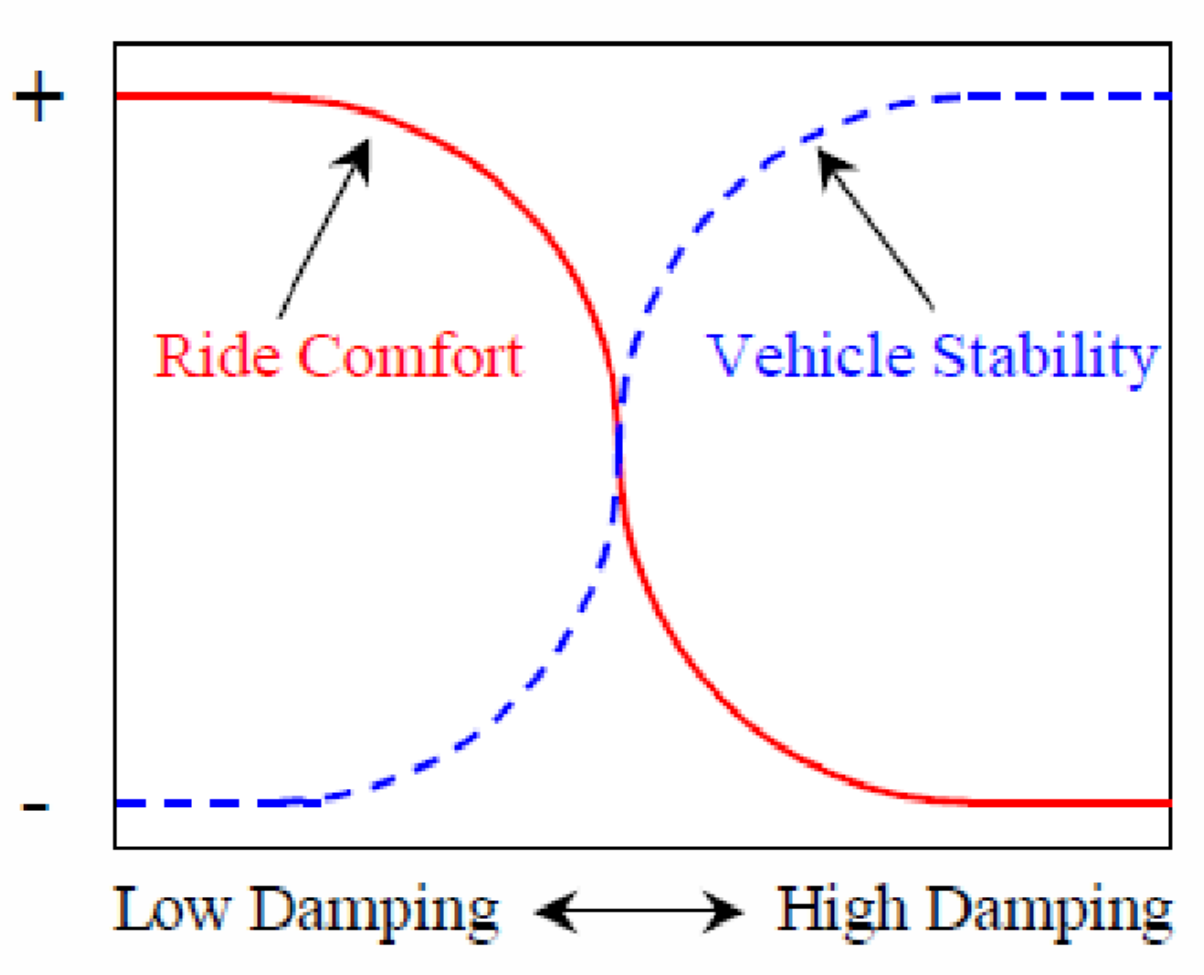

Figure (1-14): Road handling aginst ride cmfort.

1.7 Aim and object

The aims of this work can be summarised as:

1. Create and build a model of a half-car apparatus to test both passive (traditional) and smart dampers.
2. Developing and producing novel smart dampers.
3. Create a control plan for the suspension system with the proposed smart dampers that regulate vibration.
4. Assessing the vibration of the vehicle suspension system controlled by the two smart dampers by using several types of control valves.
5. Examining how the system response is affected by the damping change.
6. Evaluating the suspension system's responsiveness while utilizing the two smart dampers vs the two passive (conventional) dampers.
7. Examine how the two smart dampers respond in practice and contrast them with the two smart damper simulations.

Chapter Two

Literature Review

Chapter Two: Literature Review

2.1 Introduction

Automobiles passed through a revolutionary development, including all aspects like improving vehicle performance, comfort, and safety. Vibration control is one of the most significant matters that affects these aspects, leading to more passenger comfort and road handling. Controlling vibration prolongs the life of the automobile structure and ensures cargo transportation safety. Many studies were conducted in this field based on quarter and half-car models with advanced damper technology like smart, semi-active, and active dampers to vary damping rates according to road profiles and driving conditions. By uniting smart dampers with suspension systems, studies aim to enhance passenger comfort and/or stability. This literature review seeks to explain the efforts and challenges created through historical developments to recent studies focusing on researchers and technologies used in automobile vibration control.

2.2 Automobile Vibration Control Past Studies

Many researchers have studied the vibration control of automobiles to improve vehicle road handling, safety, and passenger(s) comfort, leading to the invention of passive, semi-active, and active suspension systems.

2.2.1 Passive Damper Studies

Goga, V., & Kľúčik, M. [10] presented a study focused on the potential of combined simulated modelling and evolutionary computation in the optimization process. A half-car mathematical model was developed using the MATLAB/Simulink package. The study optimized the stiffness and

damping coefficients of the passive suspension through evolutionary computation. Comparative analyses were conducted between the simulation results of the model using the original and optimized suspension parameters. As compared to the model with original parameters, the findings for the model with optimized parameters show a significant decrease in amplitudes and a faster stabilization of measured quantities.

Sharma, P. et al [11] presented a quarter-vehicle model with two degrees of freedom. For the overshoot and settling time of the sprung and the unsprung mass, the impact of a speed bump as a step function is examined. A MATLAB application was created for the state space model analysis. The program created here can be used to analyze vehicles' quarter automobile models with two degrees of freedom, which will help reduce the cost of test rigs and circuits.

The research presented by Shahriar, A. et al [12] investigates a half-car model with a passive damper experienced Road Humps, according to the 1999 Highways Regulations. The MATLAB numerical simulation program studied its effect on the separated front and rear suspension to obtain the best damper parameters.

2.2.2 Magneto-Rheological (MR) Damper Studies

Hassan Ahmed Metered [13] looked into magneto-rheological (MR) dampers. The features of these dampers were varied by controlling the voltage signals. The study found that the simulation results showed good dynamic performance, leading to enhanced ride comfort. Control algorithm development for MR-damped automobile suspensions is the

main focus of the research to increase cost-effectiveness and reliability while decreasing the use of sensors. Comparing the controlled system to the passive system, the former may lower the maximum RMS (root mean square) value of seat acceleration by 27% and seat travel distance by 67.64%, respectively.

Krauze, P., & Kasprzyk, J. [14] investigated automobile vibration with a four-degree-of-freedom (4-DOF) car model utilizing MR Dampers, taking its road roughness data from a sensor on the front axle to reduce vibrations in semiactive vehicle suspensions, minimizing the requirement for additional sensors. By using the Skyhook algorithm to control the front damper and another algorithm for the rear damper, the aim is to lessen the vehicle's body displacement. The study shows through simulations that vibration control in the suspension system progresses magnificently.

According to the work by Hemanth, Kumar, and Gangadharan [15], a half-car model with a magnetorheological (MR) damper under random stimulation is dynamically studied. A mathematical model for the prototype MR damper was proposed. The MR damper suspension system performs well when compared to passive suspension systems with proportional-integral-derivative (PID) control and the half-car model with semi-active suspension. The MR damper-based suspension system with the PID controller lowers the vibration amplitude by about 33% and indicates that the vehicle's road-holding performance is 40% better than when using a passive suspension system.

Ansari, M. A. et al [16] studied the effect of altering the geometry of the magnetorheological damper by changing its circular gap and piston

configuration. MRD1 to MRD6 are the names of the six distinct MRD (magnetorheological damper) models that have been designed with various configurations. Additionally, the magnetic flux density is computed using the MRD model's magnetic reluctance circuit. This procedure affects the magnetic flux density that makes (MR) fluid inside the damper more or less stiff accordingly. This results in choosing the best magnetorheological damper model concerning optimum magnetic force and decreased weight.

Yaghoubi, S., & Ghanbarzadeh, A. [17] provided a study to lessen vehicle vibrations by adding a magnetorheological damper (MR damper) to a half-car model with four degrees of freedom. The vehicle system has been modeled using MATLAB/Simulink software. The particle swarm optimization (PSO) technique has been used to optimize the suspension system variables to reduce vehicle vibrations and enhance passenger comfort. Vehicle vibrations have been found to decrease when the MR damper is integrated in any mode. In the first optimization mode, the objective function's greatest improvement was around 18%, whereas in the second optimization mode, it was approximately 32%.

2.2.3 Semi-active Damper Studies

The work done by Tyagi, S. R. [18] concentrated on testing a new semi-active damper. Initially, a 2-degree-of-freedom quarter-car model was used to simulate the damper. Detailed analyses were performed using a MATLAB/Simulink model to evaluate the physical and flow dynamics. A double damper was designed and tested against single semi-active and passive dampers of comparable dimensions to demonstrate much greater damping capabilities. Significant variations in the damping force were

shown by adding a low-power bidirectional valve as a bypass circuit for both dampers. Increased damping options and accurate controller integration were credited with the double damper's improved performance. The study sought to confirm the efficacy of the double damper prototype.

To enhance vehicle ride comfort, fuzzy logic control (FLC) was applied to a new, cost-effective, semiactive shock absorber by Mokhiamar, O. et al. [19]. A novel device, replacing the passive shock absorber, features a traditional hydraulic cylinder with a throttle valve positioned outside the cylinder between its ports. The proposed model of the semi-active shock absorber was developed using Simscape/MATLAB. A comparative analysis was conducted between the proposed semi-active shock absorber and the magneto-rheological (MR) suspension system. At a quarter of the price of the MR damper, the results showed that the FLC-controlled shock absorber performed better than the regular damper. The performance of the FLC at higher speeds (20, 30, 40 km/hr) shows notable enhancements in ride comfort and reduced overshoot compared to other suspension systems, at 20 km/h, the advised damper with FLC lowers overshoot by 60% when compared to the standard damper, 50% when compared to the MR damper. At 30 km/h, the overshoot was reduced by 50%. In contrast, the decrease was 30% at 40 km/h. The settling time of the FLC-controlled suspension system was notably lower. In addition, the valve's displacement frequency and amplitude increased with vehicle speed at a mean frequency of 40 Hz (25 millisecond response time). The system dynamically adjusts damping as vehicle speed changes, with the valve

stem movement reflecting compatible response times for effective control strategies.

Unnithan, A. R. R., & Subramaniam, S. [20] have developed a semi-active stability augmentation system (S-SAS). Controlled damping of suspension systems is achieved through the use of electrohydraulic (EH) dampers of the semi-active type. The algorithm is implemented in hardware based on microcontrollers, and its functionality is evaluated in outdoor settings under irregular road conditions at varying speeds. The fuzzy S-SAS (FS-SAS) is compared with passive suspension and normal S-SAS for various road inputs. Outdoor test results on a bumpy road at 5 km/h speed show a decrease in the heave acceleration and roll rate of 53.85% and 51.23%, respectively, compared to passive suspension. Simulation and experimental findings demonstrate that FS-SAS can provide improved road-holding, roll stability, ride comfort, and prevent untripped vehicle rollovers.

Zhang, B. et al [21] presented a paper that suggested an adaptive variable domain fuzzy PID control approach for a semi-active suspension. Additionally, a simulation model of the semi-active suspension was developed using bench testing of shock absorbers. By comparing the new approach to other control systems, it was shown to be more effective in lowering the maximum values of suspension dynamic deflection, vehicle body acceleration, and car body dynamic load under random road stimulation, specifically, peak values for suspension dynamic deflection, vehicle body acceleration, and car body dynamic load were decreased by 49.6%, 50%, and 50%, respectively, at 120 km/h using the adaptive variable domain fuzzy PID control. With a semi-active suspension that

uses CDC shock absorbers, this optimized design approach provides passengers with a more comfortable ride.

A paper about semi-active suspension systems was presented by Mohamad Haniff Bin Zamahsari, M. H. [22]. Systems provide a useful way to improve the ride quality of vehicles and are known for using less energy than active systems. Researchers are simulating a semi-active suspension system using Simulink and MATLAB based on the equation of motion. By adjusting many factors, the main goal of this simulation is to maximize vehicle performance on various road surfaces. A fuzzy logic controller is incorporated into the simulation framework. Starting with a basic quarter model and working its way up to a more complex half model. The study concluded that semi-active suspension systems significantly enhance ride comfort by reducing vehicle body acceleration by 23.93% compared to passive systems, making them a favorable choice for vehicle suspension enhancement.

2.2.4 Active Damper Studies

Ebrahimi [23] presented hybrid electromagnetic dampers integrated into automobile suspension systems. This investigation suggests two hybrid damper concepts—one employing hydraulic damping for passive control and the other utilizing eddy current damping effects to enhance effectiveness. Analytical modeling, numerical simulations, and experimental analyses on fabricated prototypes, including eddy current and electromagnetic dampers, are conducted to validate theoretical models and ensure the practicability of the proposed hybrid dampers. The study concluded that the suggested hybrid dampers maintain the benefits of

active damping performance while using 74% less power and about 55% less weight as compared with the active electromagnetic damper.

Mustafa, G. I. et al [24] examined a half-car model with an active suspension system controlled by a model-free adaptive fuzzy logic controller (MFAFLC) studied for three road profiles (classic bump road profile, sinusoidal road profile, and the random road profile), resulting in enhancing vehicle road handling, safety, and passenger(s) comfort. When compared to the passive system, the MFAFLC reduces the vertical body acceleration overshoot value by 61.1%, while PID and iPID reach 54.23% and 33.15%, respectively. When compared to the other controllers, it can be observed that the suggested controller's amplitude of the body's vertical and angular accelerations decreases far faster, guaranteeing much greater ride comfort.

Hamza, A., & Ben Yahia, N. [25] Discussed throughout this paper the significance of creating an artificial neural network-based intelligent control strategy for active truck suspensions. He developed a hydraulic model for active suspension control for trucks using an artificial neural network after obtaining a mathematical model for active suspension systems. The MATLAB Toolbox was used to create the model, and its data were calculated and verified using information gathered from vehicle tests in other research projects. When compared to an existing passive suspension, the findings demonstrate the ANN controller's notable advantages. In the B, C, and D road profile classes, the controller ANN implementation lowers the vehicle body acceleration levels by 59.5%, 75%, and 82.5%, respectively.

Rodriguez-Guevara, D. et al [26] presented a paper related to an active suspension system equipped with electro-hydraulic actuators controlled by a Model Predictive Control-Linear Quadratic Regulator (MPC-LQR). The suggested MPC-LQR-LPV strategy outperforms the other control strategies regarding ride comfort. Its RMS values are reduced by 72% and 54% in chassis and pitch acceleration, respectively, and its attenuation in peak values improves by 71% for chassis acceleration and 64% for pitch acceleration compared to the H2 controller. In addition, road-holding is maintained in both front and rear suspension units with lower peak values for the front and rear strokes, with the front stroke peak value reduced by 23% compared to the H2 controller method while keeping the RMS values for the front and rear strokes comparable.

Nguyen, D. N., & Nguyen, T. A. [27] examined and evaluated the models and control algorithms used in heavy-duty cars' active suspension systems. The study explored three popular dynamic models that are used to simulate vehicle oscillations: the completely dynamic model, the half-dynamic model, and the quarter-dynamic model. The importance of choosing the right control algorithm for the suspension system was highlighted. It is discovered that linear models correspond well with algorithms like LQR (linear quadratic regulator) and PID (proportional-integral-derivative), but nonlinear models do better with algorithms like ANN (artificial neural network), fuzzy logic, and SMC (sliding mode control). The findings ensure that vehicle oscillation control could be greatly improved by using an active suspension system.

2.2.5 Electromagnetic Damper (EMD) Study

Montazeri-Gh, M., & Kavianipour, O. [28] investigated an electromagnetic damper (EMD), which is made up of a nut, a ball screw, and a permanent-magnet DC motor, regarded as a passive damper. Then, it was tested to have good features that lead to comfort, safety, and stable riding. After that, it is examined how a spring placed in series with the EMD affects its performance. In the modified passive electromagnetic suspension system (PEMSS), to study energy regeneration, nonlinear equations are obtained. According to the simulation results, the designed passive EMD can regenerate and convert vibration energy from road stimulation into electric energy while maintaining the intended performance.

2.2.6 Electrically Interconnected Suspension System (EIS) Study

Liao, Y., et al [29] focused on an Electrically Interconnected Suspension (EIS) system. This novel method separates roll and heave motions through Electrical Networks (EN) and Direct Current (DC) motors, enabling independent vibration control via EN resistance modifications. To improve semi-active vibration control performance, a new closed-loop Current Control Unit (CCU) was developed to precisely modify EN resistance. The potential of EIS technology to increase ride comfort was highlighted by experimental validation on a half-car test rig, which demonstrated notable improvements in vibration control over conventional passive systems. The EIS with CCU significantly reduces vertical acceleration by 28.2% and angular acceleration by 34.9% when compared to passive systems in a series bump test.

2.2.7 Mechatronic Three-Setting Switchable Damper (SD) Study

Soliman, A. M. et al [30] submitted a paper compares the ride comfort of a mechatronic three-setting switchable damper (SD), which is chosen due to its cost-effectiveness when compared to active suspension and semi-active (SA) systems, and active suspensions, using fuzzy logic control (FLC) and linear quadratic regulators (LQR). For this investigation, a half-car model with four degrees of freedom is used. These systems incorporate a switchable inerter (SI) to examine its impact on ride quality. The ideal passive suspension characteristics are assessed. The fuzzy control method improves riding comfort, according to the results, greater than the LQR by up to 6.9% and 14%, for three-setting SD and active suspension systems, respectively. When compared to the same system without SI, the SD or active suspension systems with SI that use the fuzzy control technique provide a superior ride. Additionally, adding the SI enhances the vehicle's road holding and ride comfort.

2.2.8 Piezoelectric Actuator Damper Study

Knap, L. et al [31] present and examine a novel design for a vehicle vibration damper operated by a valve based on a piezoelectric actuator. By altering the size of the opening through which oil passes between the damper's chambers, the valve that is being described enables the damper's damping features to be controlled more quickly than in other systems. The experimental study's findings of the damper are also provided, demonstrating that by varying the voltage applied to the piezoelectric actuator, the damping force may be changed five times in around 10 ms.

2.2.9 Smart Damper Studies

Ali Al-ghiz'zy et al [7] studied the road profile effect on automobile vibration for a traditional damper based on a quarter-car model and then explored the findings after transforming the passive damper to a smart damper by externally adding control and check valves via hydraulic hoses to the passive damper to reduce vibrations. The proposed control valve parameters are optimized to minimize settling time and peak overshoot**.** Studying different conditions, the research presented how smart dampers adjust to control vibrations. The MATLAB Simulink computer program is used to solve the mathematical model, which saves time and reduces cost. When compared to a passive damper, the study indicates that the sprung mass utilizing a smart damper settled in a short amount of time (0.25 seconds). The passive damper settled in a longer time of (2.314) s, as compared to the first one, the settling time is reduced by 89.19%.

The study presented by Ahmed M.A. & Ahmed A. [32] focused on the theoretical analysis of the vibration control of an automobile due to different road irregularities. The analysis was based on the Half-car model with four degrees of freedom. The proposed smart damper is controlled by a hydraulic control valve. The values of the valve parts are optimized based on settling time and peak overshoot. He studied the response of the sprung mass when excited by step input at the front, rear, or consecutively at the front and rear wheels. The MATLAB-Simulink program was used to solve the model. The results show that the smart damper enhanced the whole dynamic system response compared with the traditional passive damper. In this study, a simple high-performance mechanical smart damper is proposed as an alternative option to the traditional damper or

the complicated active/or MR dampers. An experiment was performed to evaluate the performance of the proposed smart damper, as well as to improve the theoretical study done by [33] on the same smart damper.

The work done by Ahmed M.A. & Ahmed A. [32], [33] differs from the work done by Ali Al-ghiz'zy et al [7] is that the former uses a half-car model and electronic sensors connected to a computer with Ardunio program installed to evaluate displacements, while the latter used a quarter-car model with a roller with paper to measure vibration by a pen fixed to the quarter-car model's frame.

Throughout studying the available literature related to the vibration control of automobiles, it is found that the mechanical smart damper can be developed, and it is worth studying. The best parameters of the smart damper will be studied in this work, as well as the effect of the front and rear sides of the automobile on each other.

Chapter Three

Mathematical Modeling

Chapter Three: Mathematical Modeling

3.1 Introduction

This study studies the effect of the smart damper on automobile motion under road disturbances using a half-automobile model. In this model, the sprung mass is assumed to move vertically and rotate about an axis parallel to the wheel axes through its center of gravity. The front and rear suspension systems each contribute one degree of freedom, while the sprung mass contributes two degrees of freedom, resulting in a four–degrees–of–freedom system. The equations of motion for each model are derived using Newton's Second Law.

3.2 Half-Automobile Model

The Half-automobile model is more realistic than the quarter-automobile one because it simulates the automobile more realistically, since it depends on more degrees of freedom. In this model, the automobile is assumed to be supported by two suspensions, one in the front and one at the rear. The sprung mass can be moved vertically (translation) and can rotate about a horizontal axis passing through the mass center of gravity and parallel to the wheel's axes. The rotation motion of the sprung mass is known as pitching. Each of the front and rear suspensions is composed of an unsprung mass, spring, and damper. The suspension linkage is supported by the wheel-tire assembly. Figure (3-1) shows a Half-automobile model.

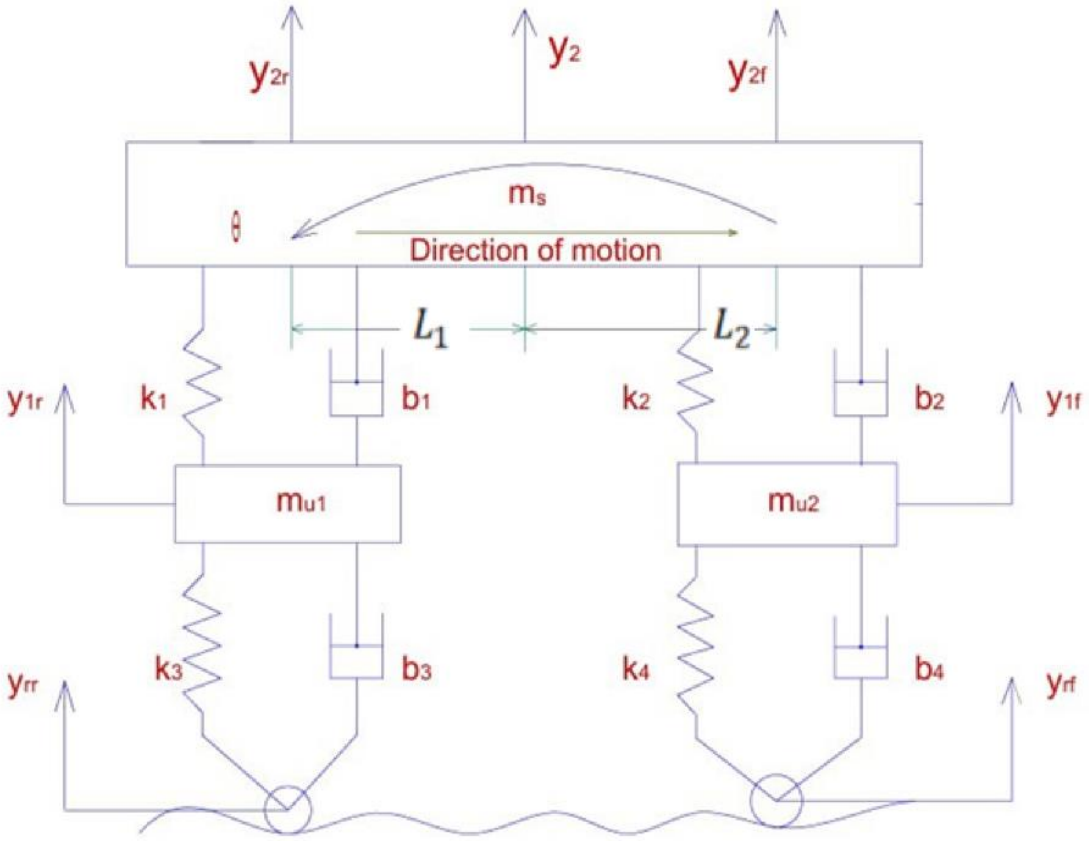

Figure (3-1): Schematic diagram of Half-automobile model.

The governing equation of the sprung mass for the Half-automobile model is derived following Newton's second law of motion. For the Half-automobile model, the sprung mass can rotate (pitching) and translate vertically. Therefore, there is an interaction (coupling) between the rotational motion and the vertical translation motion. The origin of the coordinates of the sprung mass is chosen at its center of gravity to eliminate the dynamic coupling and maintain the elastic coupling only [34]. Figure (3-1) shows a schematic representation of this model, illustrating all the required coordinates. Referring to figure (3-1) and assuming small motions, the front and rear displacements of the automobile are given by;

$$y_{2r} = y_2 - L_1\,\Theta \quad (3\text{-}1)$$

$$y_{2f} = y_2 + L_2\,\Theta \quad (3\text{-}2)$$

Where y_2 is the vertical motion of the sprung mass at its center of gravity, and $\Theta = \sin\Theta$ for small angle.

Following Newton's second law, the equation of motion of the sprung mass for the vertical motion is [35];

$$m_s\,\ddot{y}_2 = -k_1\,(y_{2r} - y_{1r}) - b_1\,(\dot{y}_{2r} - \dot{y}_{1r}) - \quad k_2(y_{2f} - y_{1f}) - b_2(\dot{y}_{2f} - \dot{y}_{1f})$$

Rearranging this equation and using equations (3-1) and (3-2), the equation of motion of the sprung mass in the translational mode is rewritten as;

$$m_s\,\ddot{y}_2 + k_1\,(y_2 - L_1\Theta - y_{1r}) + b_1\,(\dot{y}_2 - L_1\dot{\Theta} - \dot{y}_{1r}) + k_2(y_2 + L_2\Theta - y_{1f}) + b_2(\dot{y}_2 + L_2\dot{\Theta} - \dot{y}_{1f}) = 0 \quad (3\text{-}3)$$

The equation of motion which governs the rotational motion of the sprung mass is also derived by following Newton's second law by balancing the moments about the gravity center (CG) as;

$$J_c\,\ddot{\Theta} - L_1\left[k_1(y_2 - L_1\Theta - y_{1r}) + b_1(\dot{y}_2 - L_1\dot{\Theta} - \dot{y}_{1r})\right] + L_2\left[k_2(y_2 + L_2\,\Theta - y_{1f}) + b_2(\dot{y}_2 + L_2\dot{\Theta} - \dot{y}_{1f})\right] = 0 \quad (3\text{-}4)$$

Equations (3-3) and (3-4) govern the translational and rotational motions of the sprung mass coupled with both the front and rear unsprung masses.

The front and rear unsprung masses can be assumed to move in the vertical direction only, as shown in Figure (3-1). Both of them lie under two opposite dynamic forces, which are the force resulting from the motion of the tires from the lower side and that resulting from the motion of the sprung mass from the upper side. The balancing of forces acting on the front and rear unsprung masses results in the following two differential equations;

$$m_{u2}\ddot{y}_{1f} - k_2\left(y_2 + L_2\Theta - y_{1f}\right) - b_2\left(\dot{y}_2 + L_2\dot{\Theta} - \dot{y}_{1f}\right) + k_4\left(y_{1f} - y_{rf}\right) + b_4(\dot{y}_{1f} - \dot{y}_{rf}) = 0 \quad (3\text{-}5)$$

$$m_{u1}\ddot{y}_{1r} - k_1\left(y_2 - L_1\Theta - y_{1r}\right) - b_1\left(\dot{y}_2 - L_1\dot{\Theta} - \dot{y}_{1r}\right) + k_3(y_{1r} - y_{rr}) + b_3(\dot{y}_{1r} - \dot{y}_{rr}) = 0 \quad (3\text{-}6)$$

Equation (3-5) governs the motion of the front unsprung mass coupled with both the sprung mass and the front tire motions, while equation (3-5) governs the motion of the rear one also with the sprung mass and rear tire motions.

To find the State-Space method matrices, let's assume that:

$$\begin{bmatrix} X_1 = y_2 \\ X_2 = \dot{X}_1 = \dot{y}_2 \\ X_3 = \Theta \\ X_4 = \dot{X}_3 = \dot{\Theta} \\ X_5 = y_{1\mathrm{r}} \\ X_6 = \dot{X}_5 = \dot{y}_{1\mathrm{r}} \\ X_7 = y_{1\mathrm{f}} \\ X_8 = \dot{X}_7 = \dot{y}_{1\mathrm{f}} \\ \dot{X}_2 = \ddot{y}_2 \\ \dot{X}_4 = \ddot{X}_3 = \ddot{\Theta} \\ \dot{X}_6 = \ddot{X}_5 = \ddot{y}_{1\mathrm{r}} \\ \dot{X}_8 = \ddot{X}_7 = \ddot{y}_{1\mathrm{f}} \end{bmatrix} \quad (3\text{-}7)$$

Ordinary differential equations (3-3), (3-4), (3-5), and (3-6) can be solved by the State-Space method. To do this, the following assumptions are necessary;

$$\boldsymbol{\dot{X} = AX + BU} \quad (3\text{-}8)$$

$$\boldsymbol{Y = CX + DU} \quad (3\text{-}9)$$

The state-space representation for a half-automobile is:

$$\begin{bmatrix} \dot{X}_2 \\ \dot{X}_4 \\ \dot{X}_6 \\ \dot{X}_8 \end{bmatrix} = \boldsymbol{A} \begin{bmatrix} X_1 \\ X_2 \\ X_3 \\ X_4 \\ X_5 \\ X_6 \\ X_7 \\ X_8 \end{bmatrix} + \boldsymbol{B} \begin{bmatrix} y_{rr} \\ \dot{y}_{rr} \\ y_{rf} \\ \dot{y}_{rf} \end{bmatrix} \tag{3-10}$$

$$y_2 = \boldsymbol{C} \begin{bmatrix} X_1 \\ X_2 \\ X_3 \\ X_4 \\ X_5 \\ X_6 \\ X_7 \\ X_8 \end{bmatrix} + \boldsymbol{D} \begin{bmatrix} y_{rr} \\ \dot{y}_{rr} \\ y_{rf} \\ \dot{y}_{rf} \end{bmatrix} \tag{3-11}$$

Where;

$$\boldsymbol{A} = [\boldsymbol{A_1} \quad \boldsymbol{A_2} \quad \boldsymbol{A_3} \quad \boldsymbol{A_4} \quad \boldsymbol{A_5} \quad \boldsymbol{A_6} \quad \boldsymbol{A_7} \quad \boldsymbol{A_8}] \tag{3-12}$$

Where :

$$\boldsymbol{A_1} = \begin{bmatrix} -(k_1 + k_2)/m_s \\ (k_1 L_1 - k_2 L_2)/J_c \\ k_1/m_{u1} \\ k_2/m_{u2} \end{bmatrix} \tag{3-12-a}$$

$$\boldsymbol{A_2} = \begin{bmatrix} -(b_1 + b_2)/m_s \\ (b_1 L_1 - b_2 L_2)/J_c \\ b_1/m_{u1} \\ b_2/m_{u2} \end{bmatrix} \tag{3-12-b}$$

$$\boldsymbol{A_3} = \begin{bmatrix} -(k_2L_2 - k_1L_1)/m_s \\ k_2/J \\ -k_1L_1/m_{u1} \\ k_2L_2/m_{u2} \end{bmatrix} \quad (3\text{-}12\text{-c})$$

$$\boldsymbol{A_4} = \begin{bmatrix} (b_1L_1 - b_2L_2)/m_s \\ (b_2{L_2}^2 + b_1{L_1}^2)/J_c \\ b_2L_2/m_{u1} \\ b_2L_2/m_{u2} \end{bmatrix} \quad (3\text{-}12\text{-d})$$

$$\boldsymbol{A_5} = \begin{bmatrix} k_1/m_s \\ -k_1L_1/J_c \\ -(k_1 + k_2)/m_{u1} \\ 0 \end{bmatrix} \quad (3\text{-}12\text{-e})$$

$$\boldsymbol{A_6} = \begin{bmatrix} b_1/m_s \\ -b_1L_1/J_c \\ -(b_1 + b_3)/m_{u1} \\ 0 \end{bmatrix} \quad (3\text{-}12\text{-f})$$

$$\boldsymbol{A_7} = \begin{bmatrix} k_2/m_s \\ k_2L_2/J_c \\ 0 \\ -(k_2 + k_4)/m_{u2} \end{bmatrix} \quad (3\text{-}12\text{-g})$$

$$\boldsymbol{A_8} = \begin{bmatrix} b_2/m_s \\ b_2L_2/J_c \\ 0 \\ -(b_2 + b_4)/m_{u2} \end{bmatrix} \quad (3\text{-}12\text{-h})$$

$$\boldsymbol{B} = \begin{bmatrix} 0 & 0 & \frac{k_3}{m_{u1}} & 0 \\ 0 & 0 & \frac{b_3}{m_{u1}} & 0 \\ 0 & 0 & 0 & \frac{k_4}{m_{u2}} \\ 0 & 0 & 0 & \frac{b_4}{m_{u2}} \end{bmatrix} \quad (3\text{-}13)$$

$$\boldsymbol{C} = [1 \quad 0 \quad 0 \quad 0 \quad 0 \quad 0 \quad 0 \quad 0] \quad (3\text{-}14)$$

$$\boldsymbol{D} = [0] \tag{3-15}$$

In equation (3-15), the disturbance matrix equals zero because the output variable y_2 has no relation with the road input variables (y_{rr}, $\dot{y}_{rr}$, y_{rf} and $\dot{y}_{rf}$). By solving the above equations, the half-automobile model response will be found.

3.3 Hydraulic Control Valves

The hydraulic control valve can be considered the heart of damping the vibration of the automobile because it controls the flow rate of the damper hydraulic fluid during the rebound stroke. If the flow rate of the hydraulic fluid of the damper is controlled, then the required damping factor and damping coefficient are defined. Because the flow of the hydraulic fluid depends on the valve area, the motion of the valve nose controls the hydraulic flow rate. As a result, the damping factor and damping coefficient values are functions of the motion of the valve nose. The governing equation of the valve spool (valve moving mass) can be derived according to Newton's second law. Depending on the coordinates shown in Figure (3-2) and Figure (3-3), the force balance on the valve nose gives the valve equation of motion as[7];

$$m_v\ddot{y}_v + b_v\dot{y}_v + k_v y_v = F \tag{3-16}$$

Where F is the force resulting from the pressure of the damper hydraulic fluid during the rebound stroke due to the main spring expansion. Equation (3-16) is used to govern the motion of the valve nose at both the front and rear sides of the automobile according to the parameters at each side.

Assuming constant viscosity and no leakage of the hydraulic liquid, the flow rate of the hydraulic liquid leaving the damper during the rebound stroke

should be equal to that passing through the control valve. This equality of flow rates is given by ;

$$Q_p = Q_v \tag{3-17}$$

Equation (3-17) is applicable for the front and rear damper pistons and control valves.

The flow rate of the hydraulic liquid that leaves the damper during the rebound stroke equals the net area of the damper piston multiplied by its velocity, which can be written by the equation:

$$Q_p = c_f \, A_{net}(\dot{y}_2 - \dot{y}_1) \tag{3-18}$$

Where;

A_{net}; damper piston net area, which is given by the equation;

$$A_{net} = (A_{DP} - A_{DR}) \tag{3-19}$$

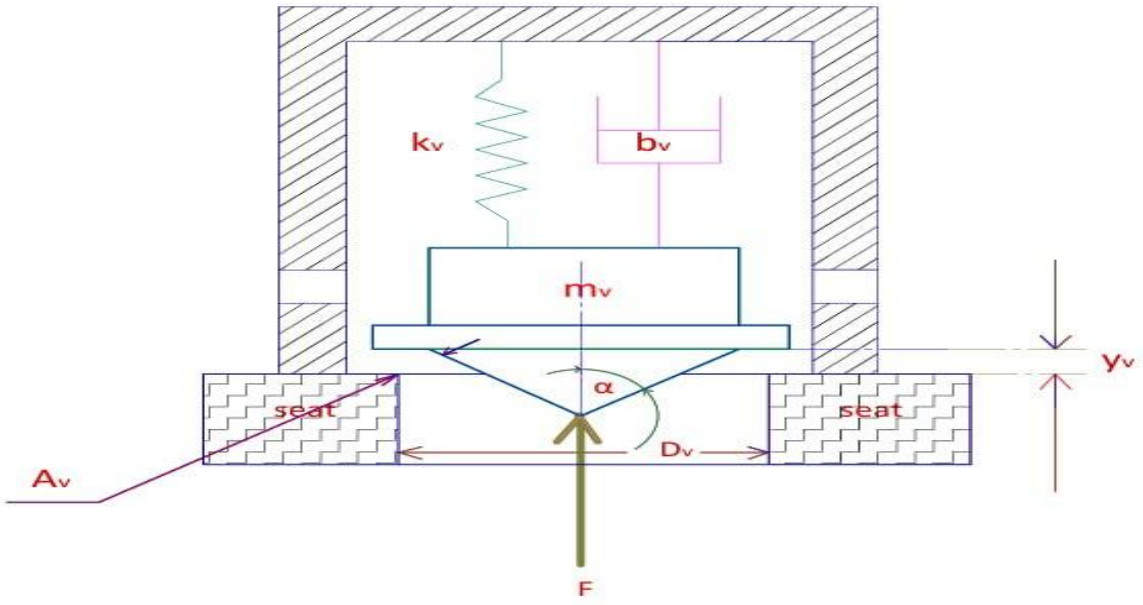

Figure (3-2): Control valve schematic diagram.

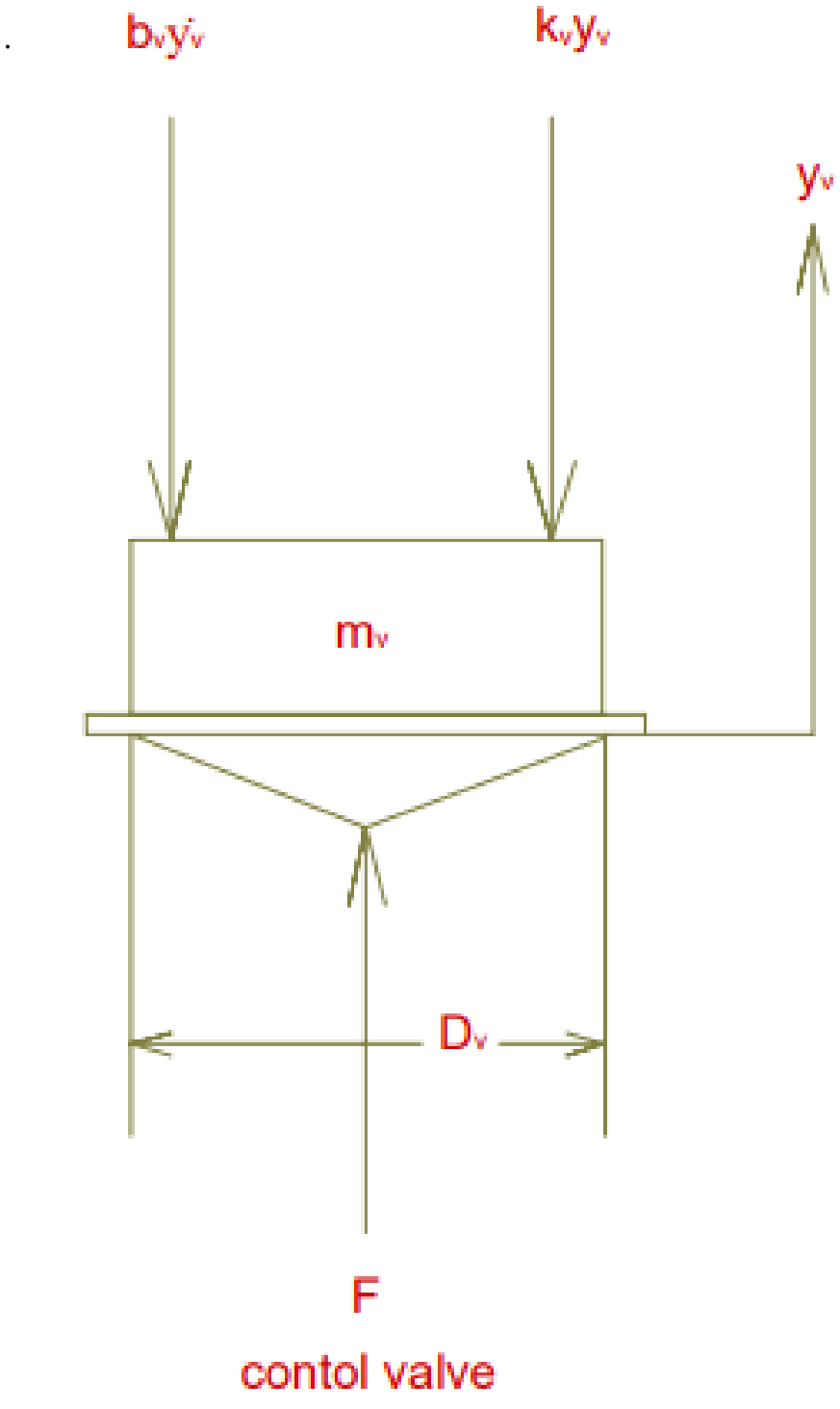

Figure (3-3): Control valve forces representation.

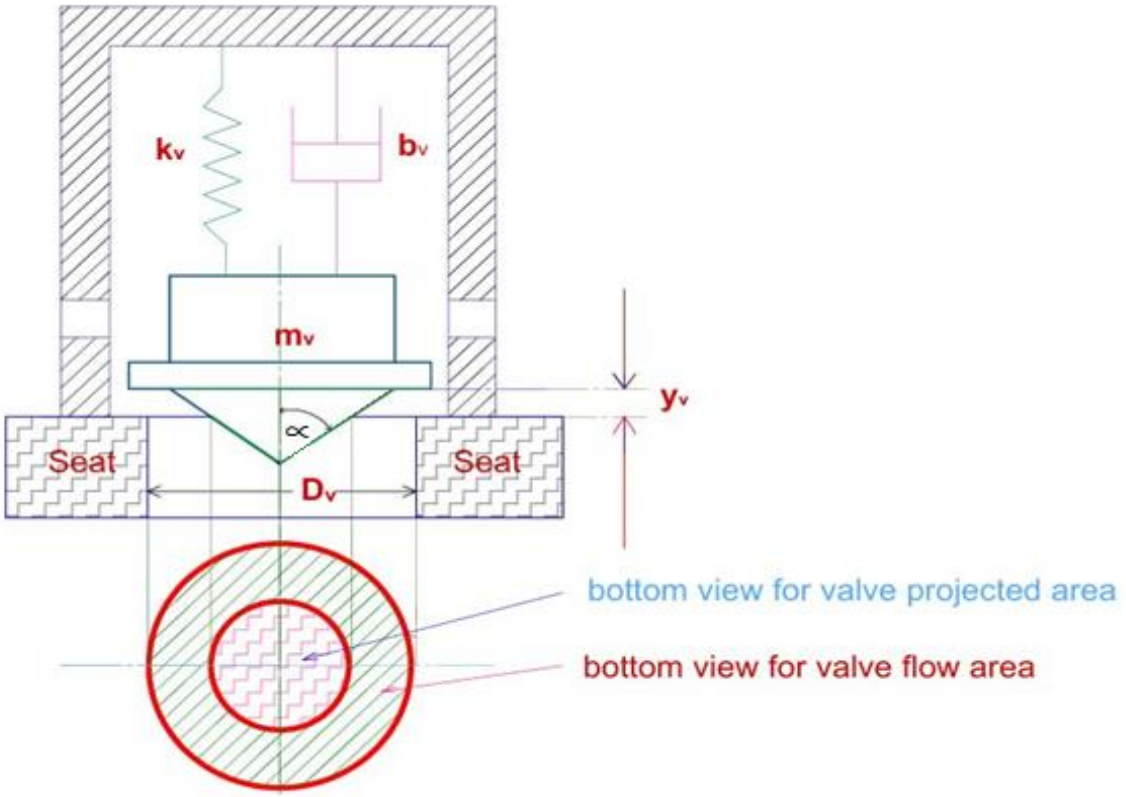

Figure (3-4): Proposed control valve cross-sectional area.

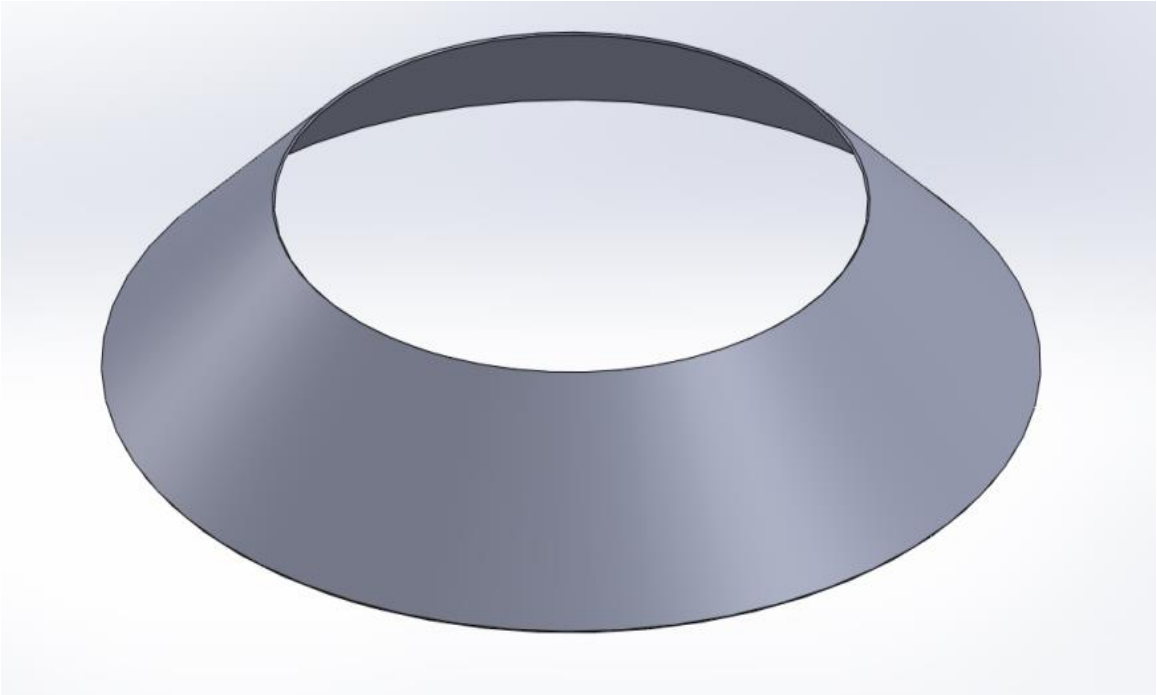

Figure (3-5): Three-dimension control valve flow area.

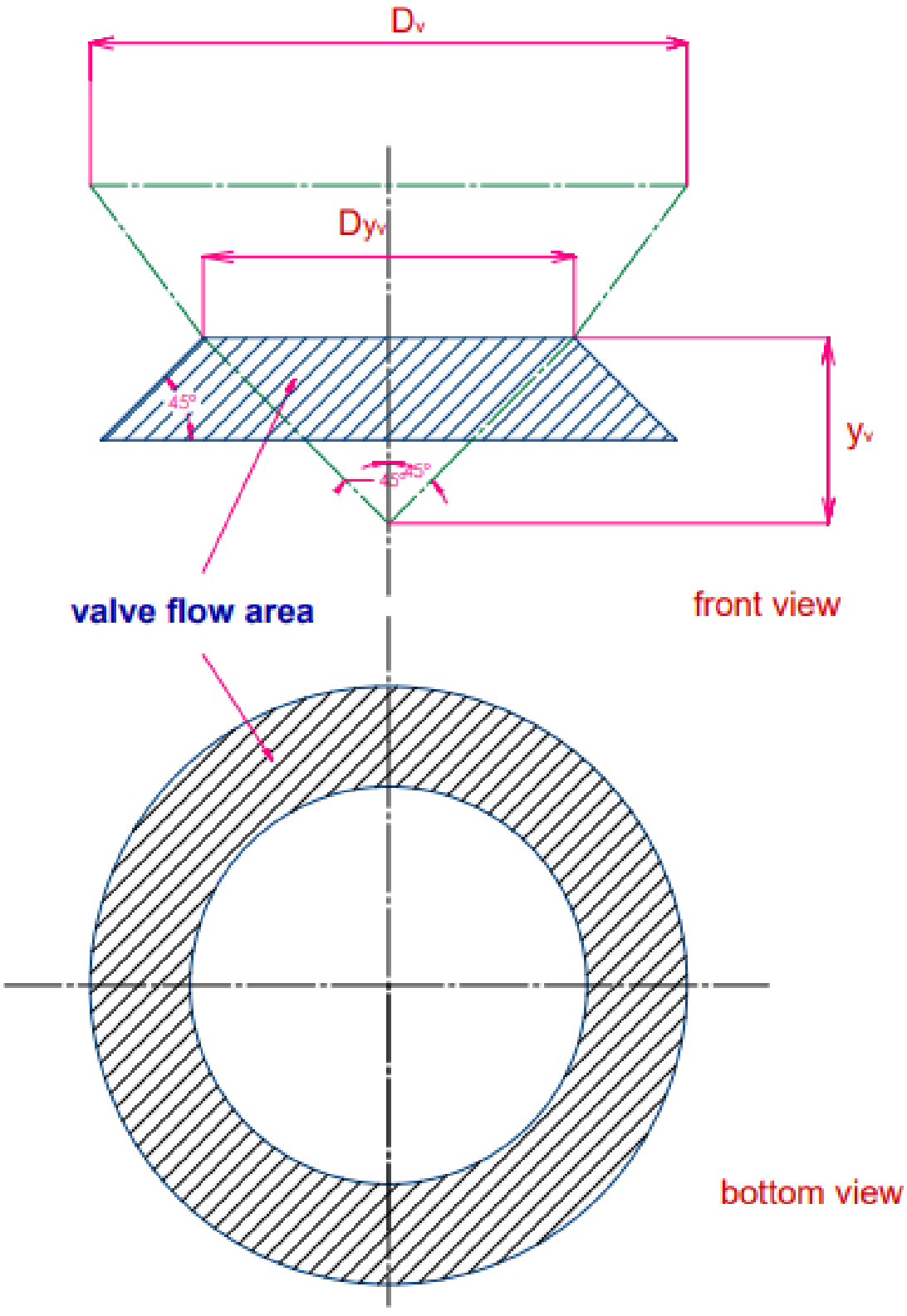

Figure (3-6): Control valve flow area from the front and bottom.

The hydraulic flow velocity through the control valve is given by [36];

$$U = Q_v/A_v \tag{3-20}$$

The valve flow area is given by [37]:

$$A_v = \pi D_v y_v \sin \propto \tag{3-21}$$

The valve projected area is shown in Figure (3-4), which represents the perpendicular area on the hydraulic flow rate direction, its derivation is illustrated in the appendices, and it can be given by the relation[7], page 37;

$$A_{vp} = \pi D_v y_v \tan \propto \tag{3-22}$$

The force exerted on the valve nose (moving mass) during the rebound stroke is composed of two components: the first is due to the pressure of the hydraulic liquid, and the second is due to the momentum of high-velocity liquid flow [7]. This can be described by the following form;

$$F = F_{vf} + F_{vP} \tag{3-23}$$

The momentum force due to the flow of hydraulic liquid is given by the equation, [38].

$$F_{vf} = \mathit{f} Q_v U \cos \propto \tag{3-24}$$

Substituting Equations (3-20) and (3-21) into (3-24) results in the following equation;

$$F_{vf} = {}^{\mathit{f} Q_v{}^2 \cos \propto}\Big/_{\pi D_v y_v \sin \propto} \tag{3-25}$$

The pressure of the hydraulic liquid is delivered from the spring force exerted on the suspension linkages during the rebound stroke at the front and/or rear sides. Mathematically, it can be written as:

$$P = k(y_2 - y_1)/A_{net} \tag{3-26}$$

In Equation (3-26), the parameters and variables are related to the front or rear sides of the Half-car model.

The valve hydraulic pressure force is given by the relation ;

$$F_{vp} = PA_{vp} \tag{3-27}$$

Where:

P; hydraulic pressure due to the main spring force.

Substituting Equations (3-22) and (3-26) in Equation (3-27), the valve pressure force can be written as;

$$F_{vp} = \frac{k(y_2 - y_1)}{A_{net}} \pi D_v y_v \tan \propto \tag{3-28}$$

Substituting Equations (3-25) and (3-28) into Equations (3-23), the total hydraulic force acting on the moving mass of the control valve is given by;

$$F = \frac{k(y_2 - y_1)}{A_{net}} \pi D_v y_v \tan \propto + \left. \rho Q_v{}^2 \cos \propto \right/ \pi D_v y_v \sin \propto \tag{3-29}$$

Substituting equation (3-29) into equation (3-16), one gets:

$$\ddot{y}_v = \left[\frac{k(y_2 - y_1)}{A_{net}} \pi D_v y_v \tan \propto - b_v \dot{y}_v - k_v \; y_v + \left. \rho Q_v{}^2 \cos \propto \right/ \pi D_v y_v \sin \propto \right] / \, m_v \tag{3-30}$$

Equations (3-16) to (3-30) can be used for the front and/or rear sides by using the corresponding parameters and variables for each side.

3.4 Smart Damper Damping Factor

In general, the damper works as a shock absorber to minimize the vibration of automobiles, which leads to ride comfort and road handling when the automobile passes through road disturbances. Increasing road handling causes less riding comfort, and increasing riding comfort causes

less road handling. Thus, the damper should satisfy both ride comfort and road handling instantaneously without magnifying one at the expense of the other.

The passive damper can withstand a constant damping factor for any road surface type, despite of the type of road disturbance or its hardness.

In this study, control valves are used, one at the front and the other at the rear sides of the automobile, to give a suitable damping factor proportional to the road disturbance. Figures (3-7) and (3-8) show the circuit of the flow of the hydraulic liquid during the compression and rebound strokes. This can be satisfied by controlling the flow rate of the hydraulic liquid during the rebound stroke. The flow rate of the hydraulic liquid through the control valve depends on the motion of the valve's moving mass. This can be done for the front and rear sides as shown in the following analysis;

As shown in Figure (3-7), during the compression stroke, the hydraulic liquid can flow through the check valve without significant impedance, while during the rebound stroke, it is restricted by the control valve.

The force balance in the damper is given by;

$$(P_1 - P_2)A_{net} = b(\dot{y}_2 - \dot{y}_1) \quad (3\text{-}31)$$

Where:

P_1; pressure below the damper piston.

P_2; pressure above the damper piston.

The difference between the upper and lower piston pressures and velocities during the rebound stroke is very high, so they can be represented mathematically:

$$P_1 - P_2 = P_1 = P \quad (3\text{-}32)$$

$$U_2 - U_1 = U_2 = U \quad (3\text{-}33)$$

Where:

$U_{1\ or\ 2}$; hydraulic liquid velocity above or below the damper piston sides, respectively.

Assuming no pressure losses occurred due to the connected hoses and fittings, the pressure in the damper during rebound is equal to that in the control valve pressure, namely, P.

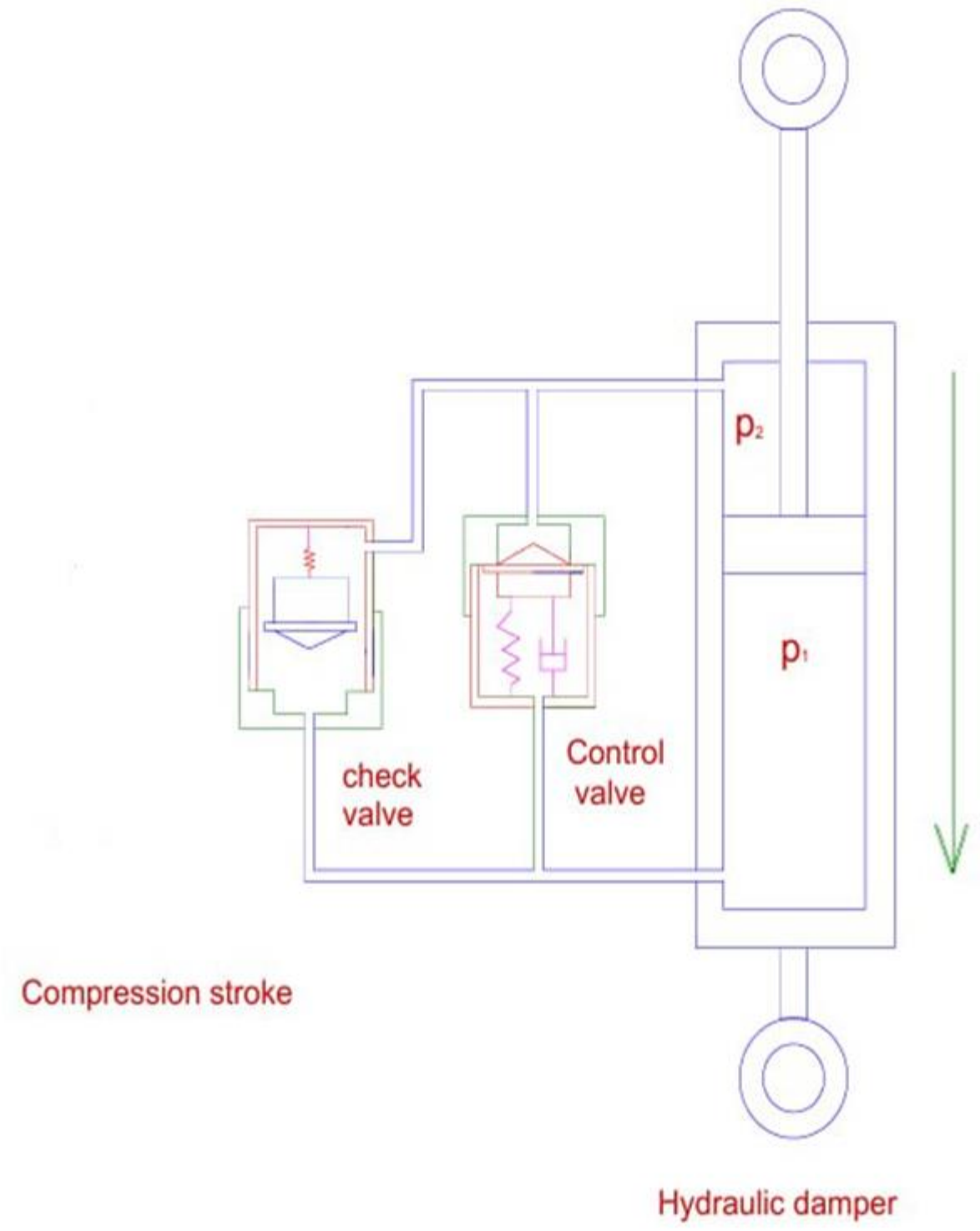

Figure (3-7): Schematic diagram of smart damper compression stroke.

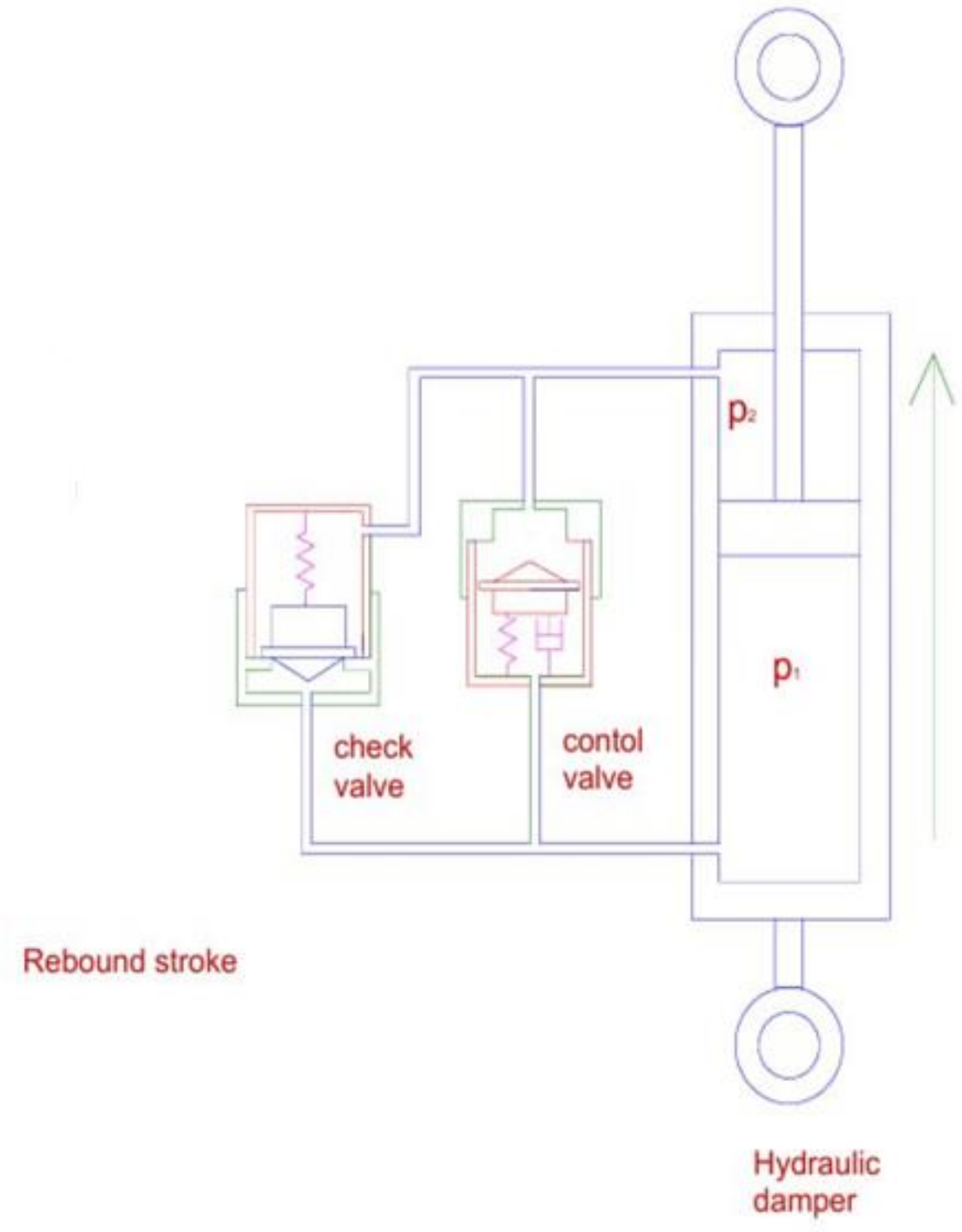

Figure (3-8): Schematic diagram of Smart damper rebound stroke.

From equations (3-20) and (3-21), the control valve hydraulic flow rate will take the form;

$$Q_v = U\pi D_v y_v \sin \propto \quad (3\text{-}34)$$

Applying Bernoulli's Equation for the top and bottom of the damper piston levels at the rebound condition, as follows:

$$P_1 + \frac{\rho {U_1}^2}{2} = P_2 + \frac{\rho {U_2}^2}{2} \quad (3\text{-}35)$$

Substituting equations (3-31), and (3-32) in equation (3-35) results in the form below;

$$\mathrm{P} = \frac{\rho U^2}{2} \quad (3\text{-}36)$$

After some steps:

$$U = \sqrt{(\frac{2\mathrm{P}}{\rho})} \quad (3\text{-}37)$$

The hydraulic pressures at the tip of the control valve mass are equal to the hydraulic force exerted on the damper net area. The hydraulic force can be obtained by multiplying the damping coefficient by the velocity difference for each side of the automobile, mathematically represented by;

$$\mathrm{P} = \mathrm{b}(\dot{y}_2 - \dot{y}_1)/A_{net} \quad (3\text{-}38)$$

Sub equation (3-37) into equation (3-38), one gets;

$$U = \sqrt{(\frac{2\mathrm{b}(\dot{y}_2 - \dot{y}_1)/A_{net}}{\rho})} \quad (3\text{-}39)$$

Substituting equation (3-39) into equation (3-34) results in the form below:

$$Q_v = \sqrt{(\frac{\mathbf{2b}(\dot{\mathbf{y}}_\mathbf{2} - \dot{\mathbf{y}}_\mathbf{1})/\boldsymbol{A_{net}}}{\boldsymbol{\rho}})}\pi D_v y_v \sin \propto \quad (3\text{-}40)$$

Referring to equation (3-17) and replacing equation (3-40) with equations (3-18), the following relation will be obtained:

$$c_f\, A_{net}(\dot{y}_2 - \dot{y}_1) = \sqrt{\frac{\frac{\mathbf{2b}(\dot{\mathbf{y}}_\mathbf{2} - \dot{\mathbf{y}}_\mathbf{1})}{\boldsymbol{A_{net}}}}{\boldsymbol{\rho}}}\pi D_v y_v \sin \propto \quad (3\text{-}41)$$

After squaring both sides of the equation (3-41) and some simplifications, the following form can be written as:

$$b = \left[\rho {c_f}^2 {A_{net}}^3\,(\dot{y}_2 - \dot{y}_1)\right]/[2(\pi D_v y_v \sin \propto)^2] \quad (3\text{-}42)$$

Where:

b is the front or rear smart damper damping factor in sequence with the corresponding parameters and values.

Chapter Four

Local Optimal Control Valve Solution and Computer Simulation

Chapter Four: Local Optimal Control Valve Solution and Computer Simulation

4.1 Introduction

In general, control valves are mechanical tools used to adjust the flow rate and/or pressure to maintain a required flow to carry out a specific process. In this chapter, the control valve under study is used to control the flow rate of the hydraulic fluid used in presenting the automobile's damper. Control of the hydraulic fluid flow means controlling the damping force, which is considered the main factor in controlling an automobile's vibration. The selection of the best values of the valve elements is known as the "optimization technique". The best values of valve elements, which will be studied here, affect the performance of the valve, which in turn affects the damping coefficient of the automobile's damper. This technique is carried out by using "computer simulation," in which a computer program is used to simulate the control valve response to a step input while varying its parameter values, saving time and costs.

4.2 Optimization Technique

The optimization technique can be defined as the mathematical procedure used to reach the best solution for a given problem. In this study, one variable is changed in magnitude with constantly increasing steps, starting with and ending with feasible values "constraints", and all other variables are set constant until the minimum objective function value occurs. Another variable is selected, and the same procedure is repeated above until reaching the minimum value of the objective function, and so on for all other variables. Finally, the values of the variables corresponding to the minimum

values of the objective functions are selected as an optimal solution for the given problem. This method is also known as the "Line search method". Figure (4-1) illustrates a flow chart for this method.

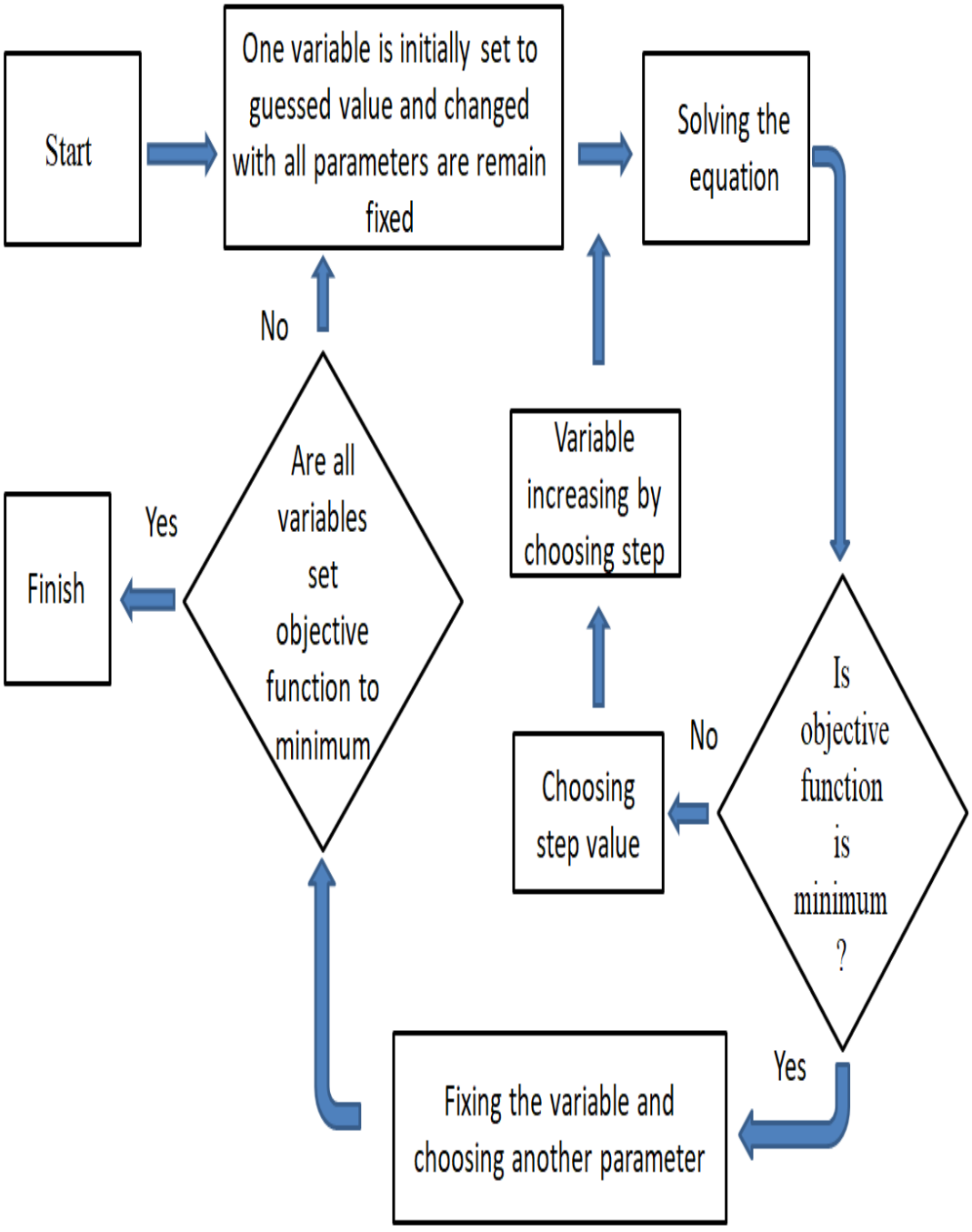

Figure (4-1): Line search optimization technique flow chart.

4.3 Optimization of Control Valve Elements

The equation of motion that describes the dynamics of the control valve is given by Equation (3-30). One of the methods to find the optimum valve parameter values is the Simulink included in the MATLAB package. Figure (4-2) shows a schematic diagram of the Simulink coding. To use the Simulink, Equation (3-30) should be transformed from the time domain to the s domain by the Laplace transform, assuming zero initial conditions as;

Let;

$$f = \frac{k(y_2 - y_1)}{A_{net}} \pi D_v y_v \tan\theta + \frac{\rho \cos\theta Q_v^2}{\pi D_v y_v \sin\theta} \quad (4\text{-}1)$$

Taking the Laplace transform of Equation (3-30) and rearranging results in the following transfer function;

$$\frac{Y(S)}{F(S)} = \frac{1}{(m_v s^2 + b_v s + k_v)} \quad (4\text{-}2)$$

The right side of Equation (4-2) is represented in the MATLAB Simulink program as a transfer function block “num(s)/den(s)” with the details shown in Figure (4-3). Figure (4-2) contains a step input, mathematical action “num(s)/den(s)”, scope, and simout blocks.

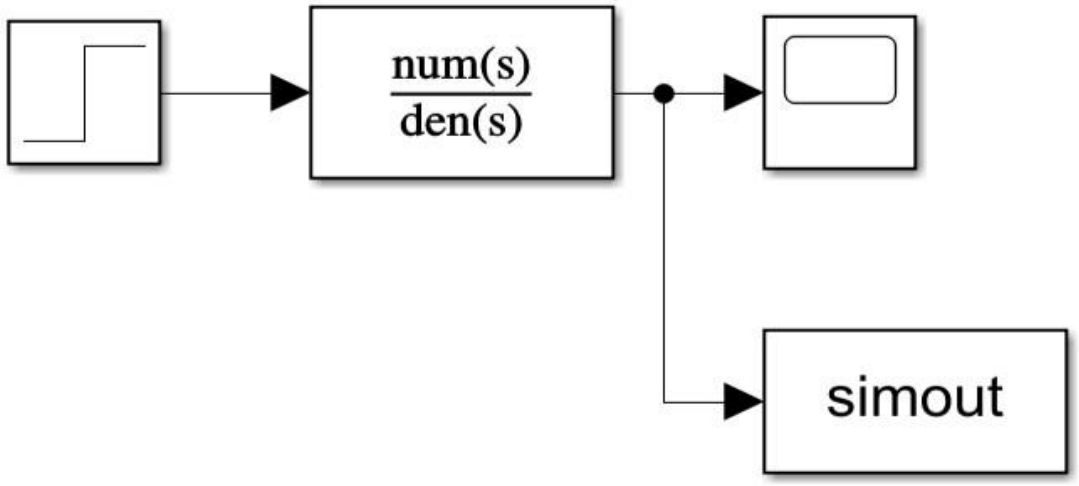

Figure (4-2): Schematic diagram of the MATLAB Simulink program for finding optimal control valve parameters.

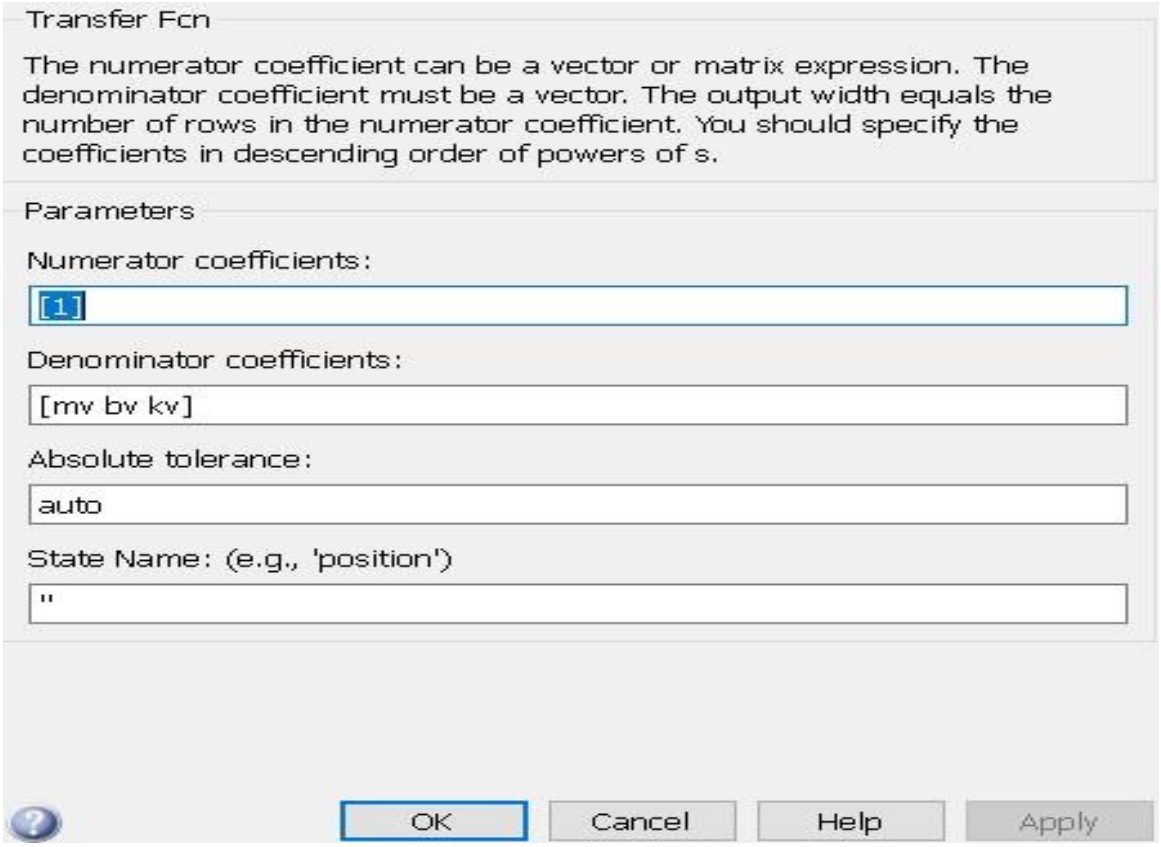

Figure (4-3): Transfer function block details for right side for Equation (4-2) in MATLAB Simulink program.

The force f in Equation (4-1) is to be calculated assuming initial values listed in Table (4-1), displacement and velocity difference values as described in Table (4-2) calculated after running the MATLAB program illustrated in Figure (6-3) by using values shown in the Table (4-1), the hydraulic flow rate can be calculated using equations (3-17), (3-18) and automobile linear velocity v.

Table (4-1): Assumed initial values of control valve parameters according to experience.

No.	parameter	Initial value	unit
1	y_v	0.001	m
2	D_v	0.01	m

Table (4-2): Extracted parameter values from simout, simout1, simout2, and simout3 are shown in Figure (6-3).

No.	Extracted parameter	Value	unit	Automobile side
1	$y_2 - y_1$	**0.0**63	m	Front
2	$\dot{y_2} - \dot{y_1}$	2.7333	m/s	Front
3	$y_2 - y_1$	0.0786	m	Rear
4	$\dot{y_2} - \dot{y_1}$	3.54	m/s	Rear

From the above parameter values that form Equation (4-1), assuming hydraulic density ($980\ kg/m^3$), damper piston net area A_{net} ($7 \times 10^{-4} m^2$) and the coefficient of discharge c_f (0.62) [7], the force f is calculated for the front and rear automobile sides as shown below;

For the front automobile side:

$$f_f = 42.4\, tan\, \theta + 48.24\, cot\, \theta \qquad (4\text{-}3)$$

For the rear automobile side:

$$f_r = 59.968\,tan\,\theta + 80.929\,cot\,\theta \qquad (4\text{-}4)$$

4.3.1 Optimization of Rear Control Valve Nose Angle

The best angle of the control valve nose is calculated such that the force acting on the valve nose is minimum for the required flow rate of the hydraulic oil through the control valve. The required flow rate is estimated by Equations (3-17) and (3-18). The force exerted on the rear valve nose is calculated from Equation (4-4). By changing the value of the angle θ for the range, 10^{o}-80^{o} gives the results shown in Figure (4-4). From this figure, the best nose angle of the rear control valve can be selected when the minimum force (f) is achieved (139.38 N), which is found to be 50°.

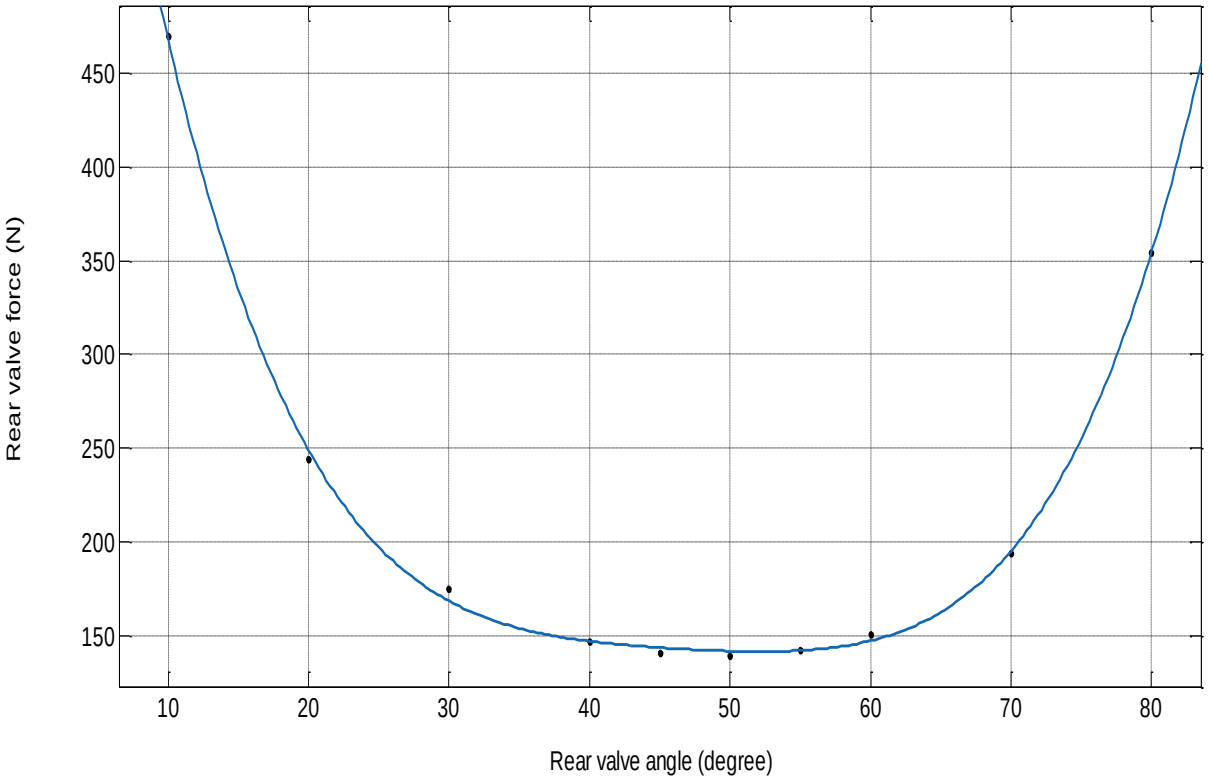

Figure (4-4): Rear valve force is minimum at valve angle equals 50 degrees.

4.3.2 Optimization of the Rear Control Valve Orifice Diameter

As for the angle of the control valve nose, the best diameter of the valve orifice is calculated such that the force acting on the valve nose is minimum for the required flow rate of the hydraulic oil through the control valve. Also, the required flow rate is estimated by Equations (3-17) and (3-18) with hydraulic density $\rho = 980\ kg/m^3$, damper piston area $A_{net} = 7 \times 10^{-4} m^2$, coefficient of discharge $c_f = 0.62$) [7]. The nose angle is taken as the best value obtained in section 4.2.1, which is 50°. The force exerted on the rear valve nose is calculated from Equation (4-1) and is simplified to the following form after using the above values;

$$f = 7146.769 D_v + \frac{0.679}{D_v} \qquad (4\text{-}5)$$

Changing the orifice diameter, D_v For the range 5 to 30 mm, the relation between the force, f, and D_v It was found that the best value of the rear valve orifice is 10 mm, corresponding to the lowest force (139.38 N).

4.3.3 Optimization of Rear Control Valve Moving Mass

The value of the valve moving mass is affected by three criteria, which are the settling time, peak overshoot, and the steady state displacement of the mass. When studying the effect of any one of the three criteria, the other two are taken as constant at a certain value. If the settling time is taken as the affecting criterion, the best value of the valve moving mass can be evaluated by starting with the initial guessed value, which is set at 0.1 grams in this study, and calculating the settling time. The valve moving mass is increased by steps from 0.05, 0.25, 0.5, 3, 5, and 10 grams, and the settling time is recalculated for each mass value. The relation between the value of the moving mass and the settling time is presented in Figure (4-5). The best value of the valve moving mass is selected when the settling time is minimal, and can be applicable for Manufacturing processes and durability. Therefore, the lowest value (0.15 to less than 2) grams, as shown in Figure (4-6) was not suitable. The results are based on a hydraulic oil pressure of 19 bar: (this pressure is obtained from the rear damper force, which equals the multiplication of rear damper stiffness 17000 N/m [41] by its displacement

0.0786 m (from Table (6-3), divided by the damper net area $7e^{-4}$ m^2[7]. From Figure (4-5), the best value for the valve moving mass, according to the settling time, is 2 grams.

When the peak overshoot is taken as the affecting criterion, the value of the moving mass is also started with an initial guessed value, such as 2 grams, and determining the peak overshoot. The initial guessed value is increased by steps, and the overshoot is calculated for each step. The relation between the valve moving mass and the peak overshoot is shown in Figure (4-7). From this figure, it is found that 2 grams is the best according to the peak overshoot criterion.

The same procedure is used for the settling time, and the peak overshoot is repeated for the steady-state displacement criterion. The result of this relation is shown in Figure (4-8). It shows that 2 grams of the valve moving mass is related to the minimum peak overshoot, which represents the best value of the valve moving mass.

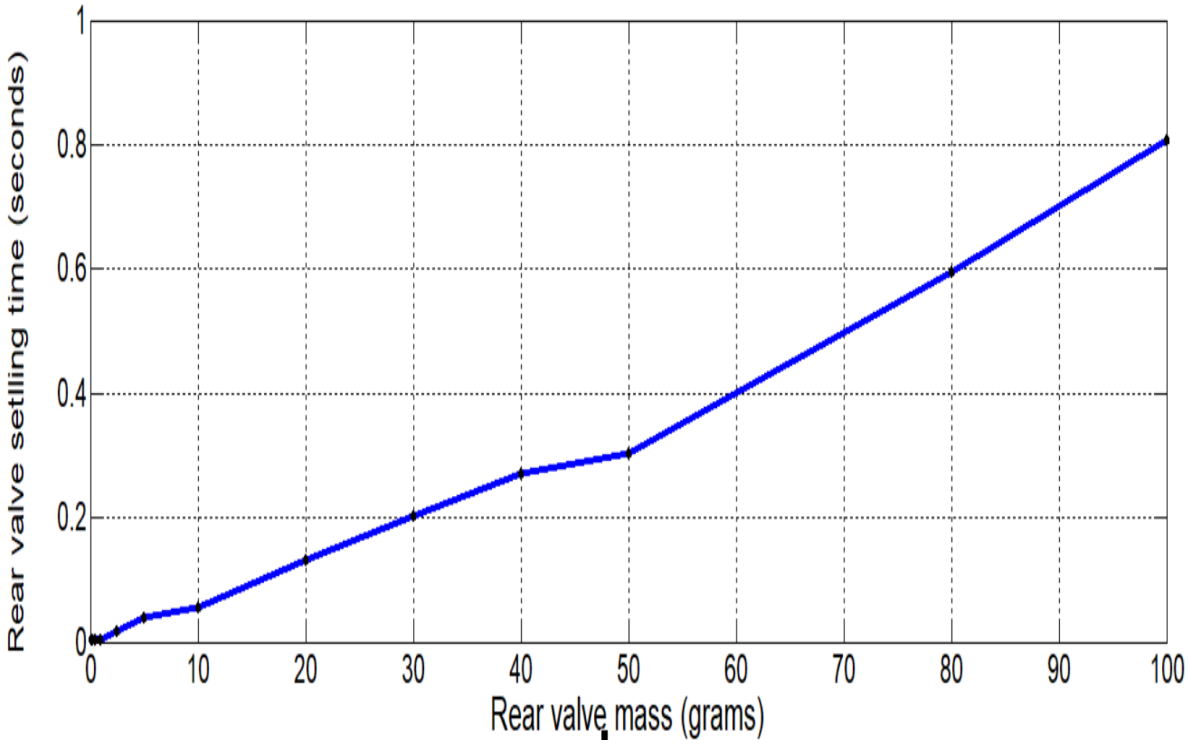

Figure (4-5): Effect of valve moving mass (0.1-100) grams on settling time, p=19 bar.

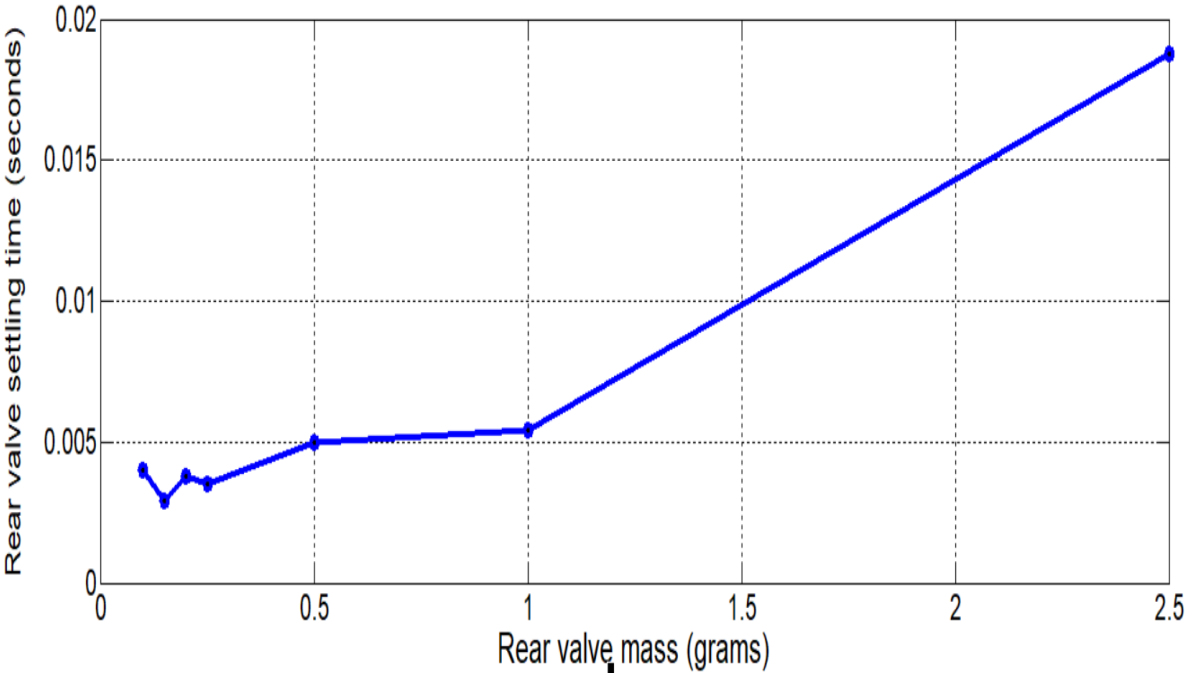

Figure (4-6): Effect of valve moving mass (0.1-2.5) grams on settling time, p=19 bar.

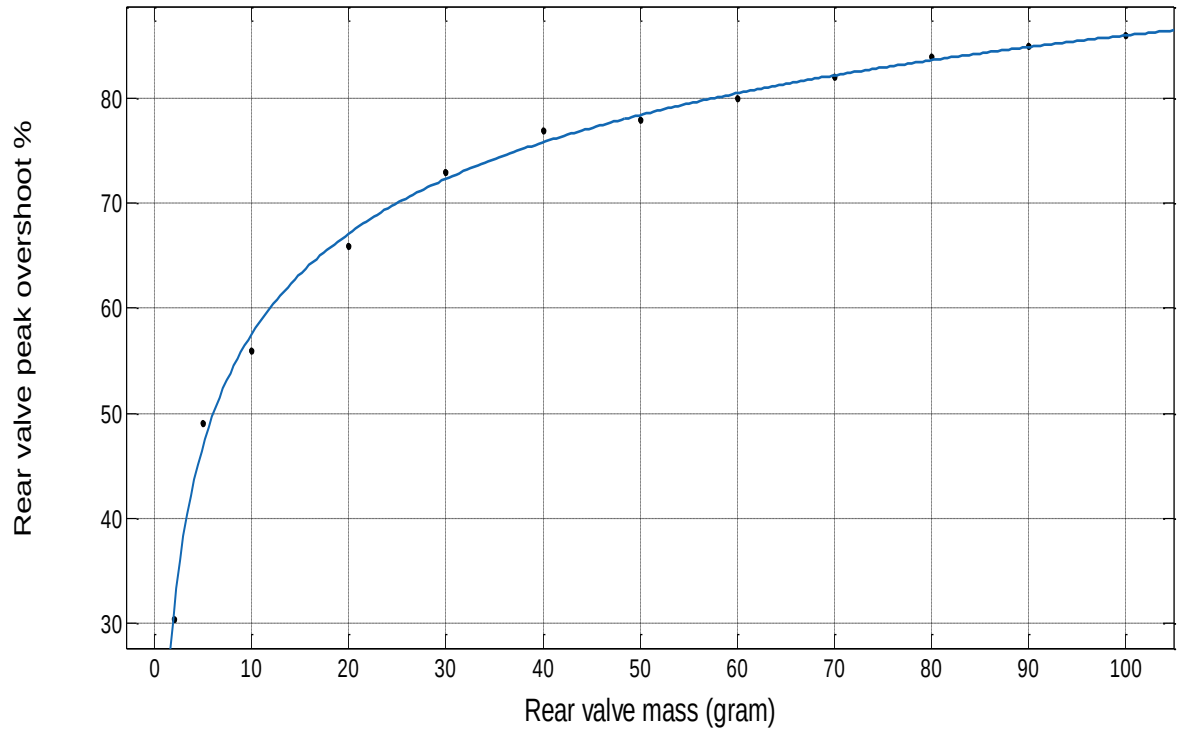

Figure (4-7): Effect of valve moving mass on peak overshoot, p=19 bar.

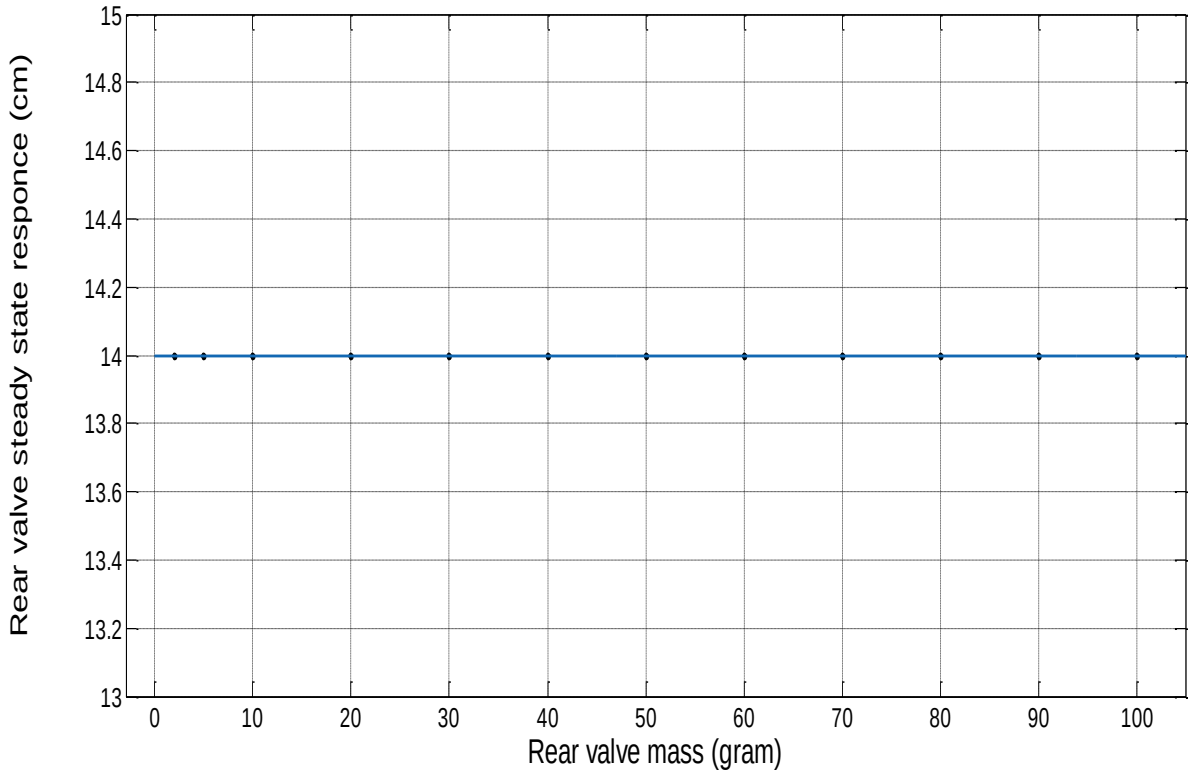

Figure (4-8): Effect of valve moving mass on the steady-state displacement of the moving mass, p=19 bar.

4.3.4 Optimization of Rear Control Valve Damping Factor

The damping factor depends on three criteria, such as valve moving mass, settling time, peak overshoot, and steady-state displacement. To investigate the variation of the settling time with the damping factor, it started from the guessed value for the damping factor as 0.25N.s/m. The damping factor varies from 0.25 N.s/m to 10 N.s/m with a step of (0.25, 0.5, and 1) N.s/m as presented in Figure (4-9). This figure shows that the best value of the damping factor is 1.5 N. s/m.

The dependence of the valve damping factor on the peak overshoot criterion is given in Figure (4-10) for the same above range, from 0.25 N.s/m to 10 N.s/m in (0.25, 0.5, and 1) N.s/m step increasing value. The best value of the moving mass that is taken from Figure (4-5) is used to calculate the results of this figure. The best value of the valve damping factor is taken when satisfying the minimum overshoot, which is found to be 10 N.s/m, as shown in this figure.

The variation of the peak overshoot of the valve moving mass displacement is presented in Figure (4-11) for the damping factor range also from 0.25 N.s/m to 10 N.s/m in (0.25, 0.5, and 1) N.s/m steps. The trend of this figure shows that the mass displacement is still at the same value of 13.94 cm for all the peak overshoot value ranges; therefore, 1.5 N.s/m can be selected as the best value of this factor according to the settling time criterion.

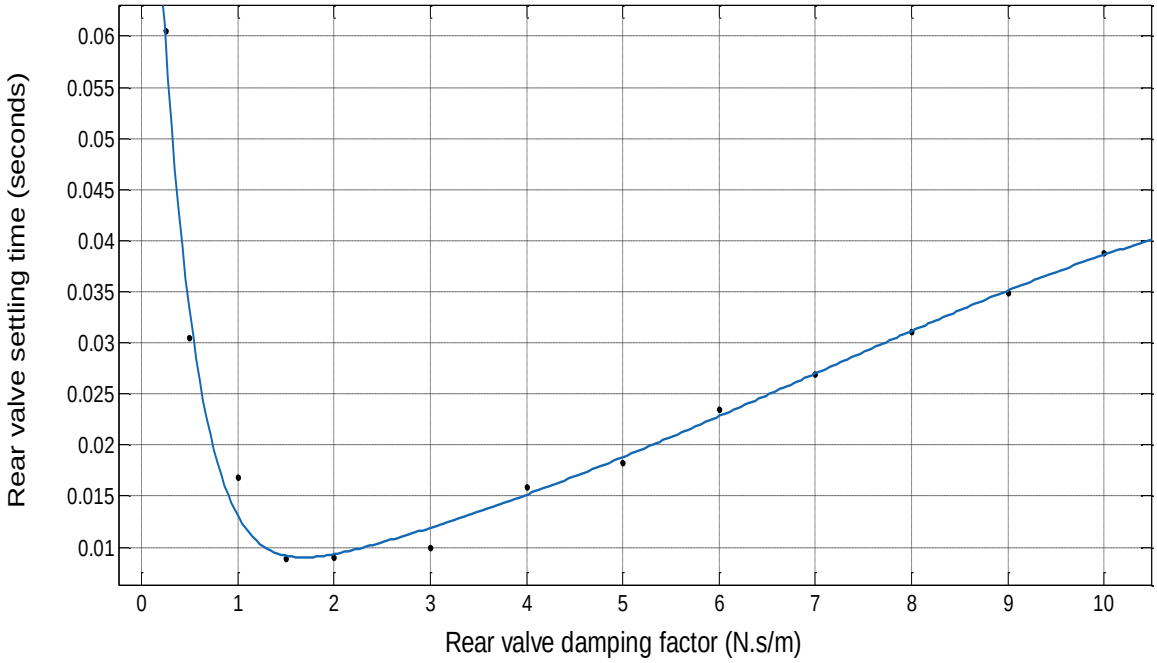

Figure (4-9): Effect of valve damping factor on the settling time of the moving mass, p=19 bar, m_v=2 g.

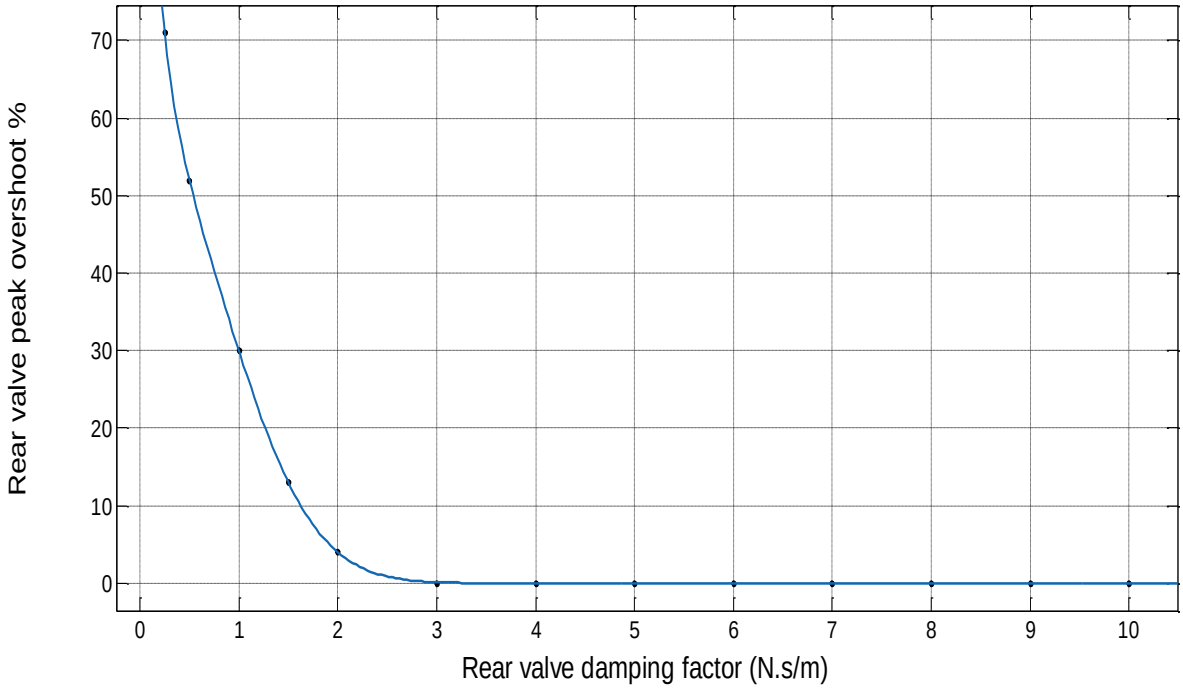

Figure (4-10): Effect of valve damping factor on peak overshoot, p=19 bar, m_v=2 g.

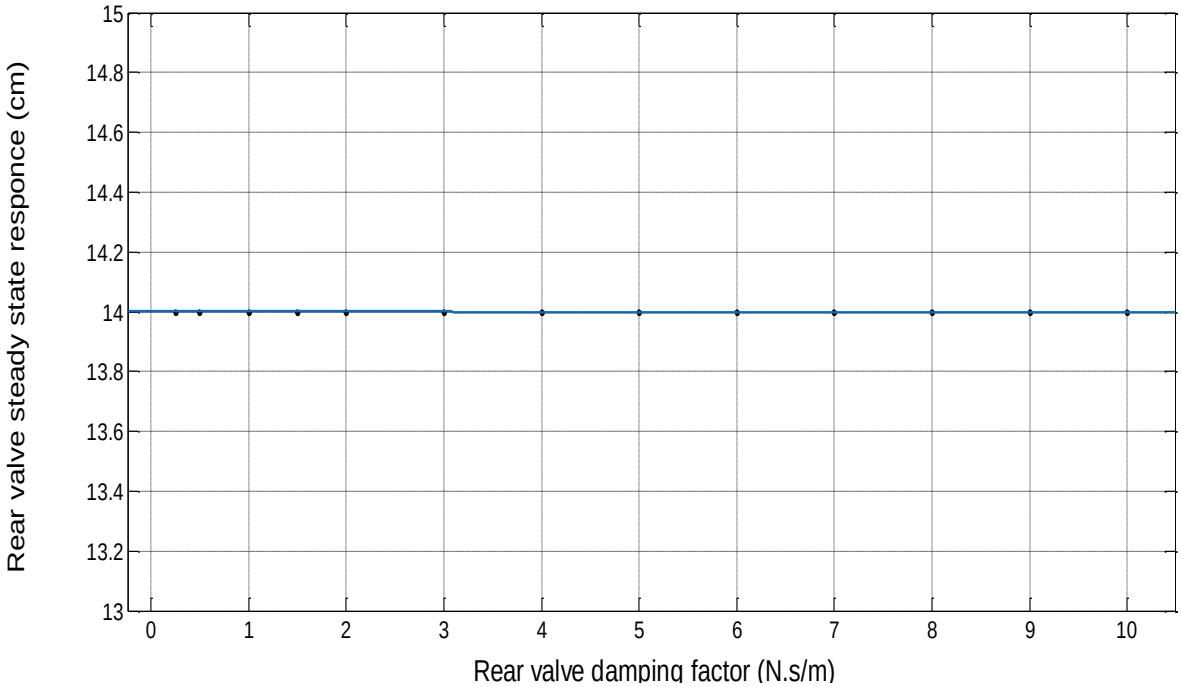

Figure (4-11): Effect of valve damping factor on the steady-state displacement of the moving mass, p=19 bar, m_v=2 g.

4.3.5 Optimization of Rear Control Valve Spring Stiffness

Optimizing control spring stiffness is crucial for enhancing the performance of control valves in control applications. This section aims to explore how adjusting spring stiffness can improve valve dynamics and overall control efficiency, addressing key challenges in fluid control systems [7]. Also, the three criteria, settling time, peak overshoot & steady state displacement of the valve moving mass, are followed here to adjust the value of the spring stiffness. This can be done by fixing the valve moving mass at 2 g and its damping factor at 1.5 N.s/m, which is taken from Figures (4-5) and (4-8), respectively, then varying the spring stiffness from 1000-10000 N/m in 1000 N/m steps. The results of this criterion are illustrated in Figure (4-2). The relation between the settling time and spring stiffness is given in Figure (4-12). From this figure, one can adjust the spring stiffness to 4000 N/m.

The other criterion that is dependent here is the peak overshoot. The effect of this criterion on the spring stiffness is determined by varying the spring stiffness and calculating the peak overshoot for each stiffness value. The results of this criterion are presented in Figure (4-13) for the range from 1000

N/m to 10000 N/m. The results presented in this figure show that the spring stiffness can be adjusted to 1000 N/m.

The variation of the steady state displacement of the valve moving part with the spring stiffness is shown in Figure (4-14) for a stiffness range the same as that taken in the above two criteria. From this figure, one can adjust the value of spring stiffness to 10000 N/m.

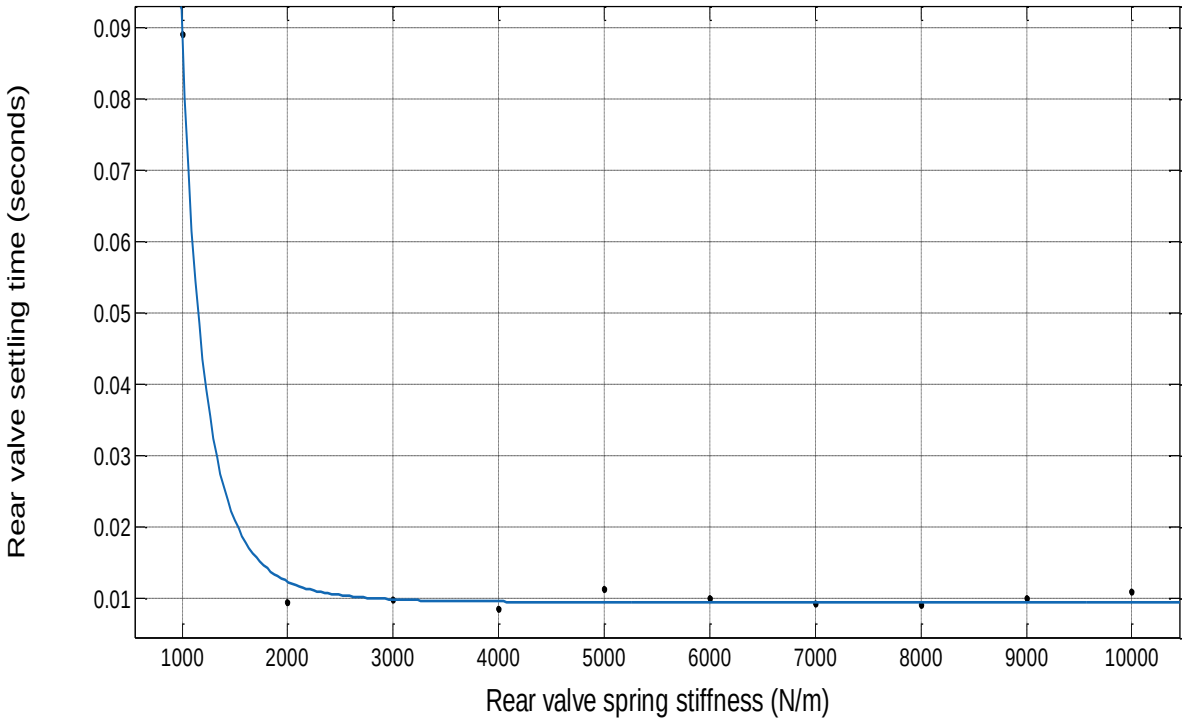

Figure (4-12): Variation of settling time as a function of the valve spring stiffness, p=19 bar, m_v=2 g, damping=1.5 N.s/m.

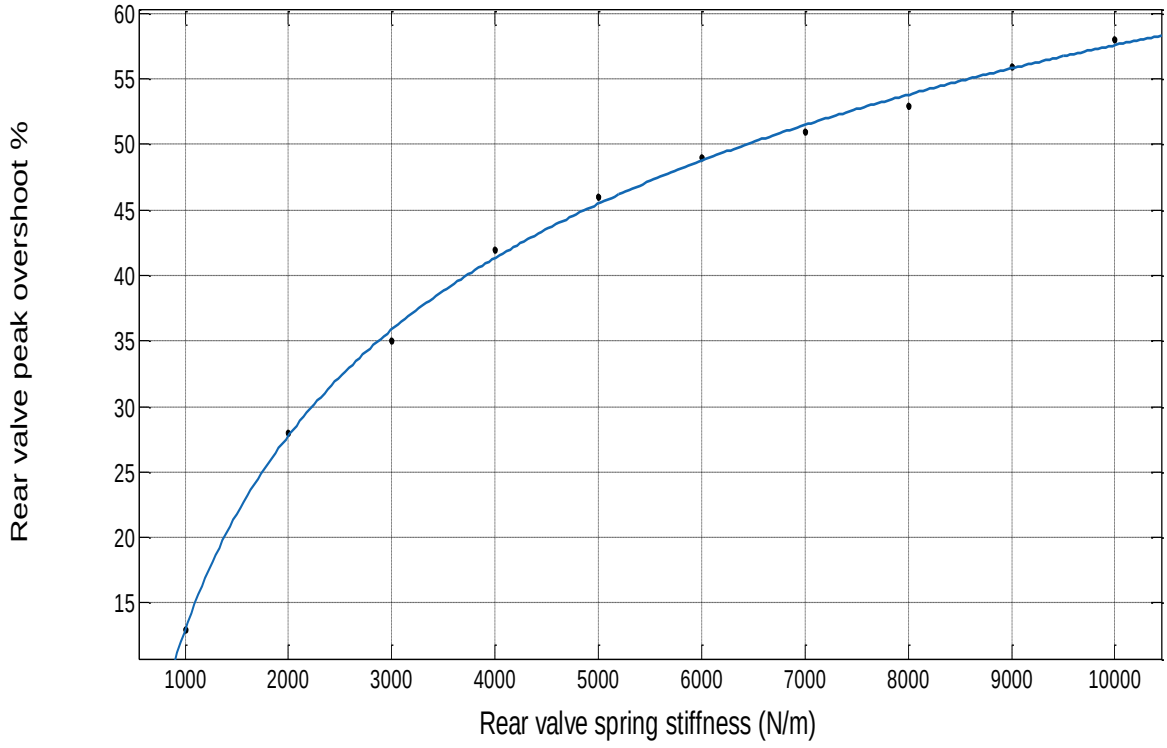

Figure (4-13): Variation of peak overshoot as a function of the valve spring stiffness, p=19 bar, m_v=2 g, damping=1.5 N.s/m.

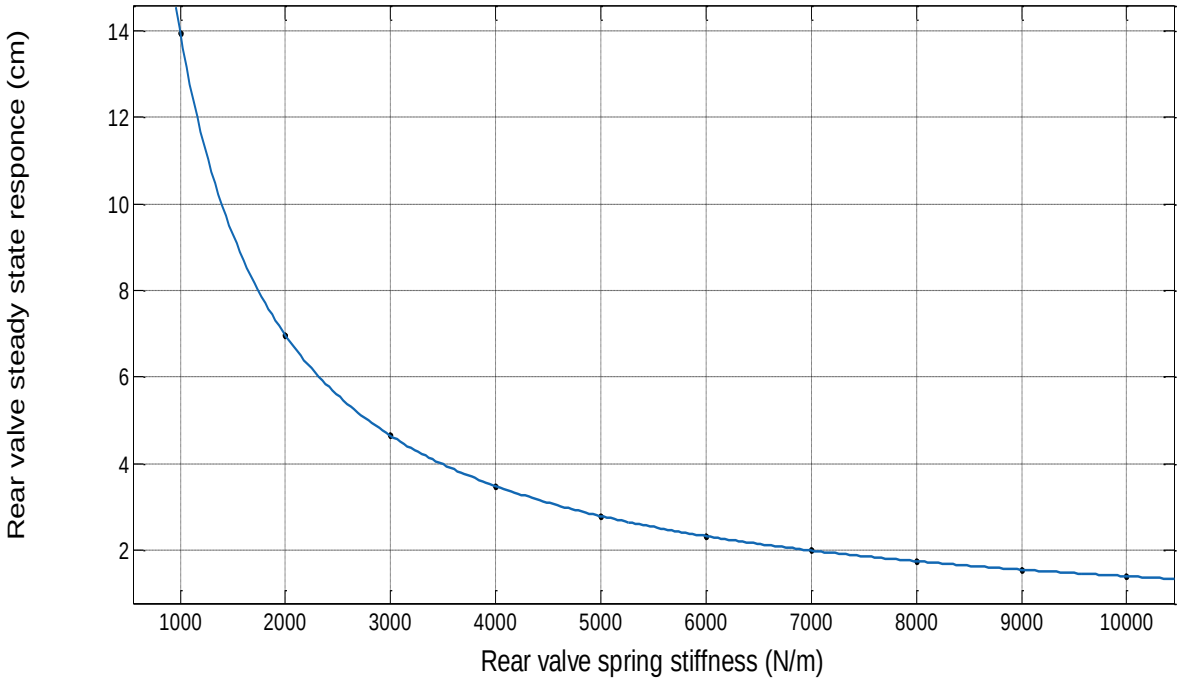

Figure (4-14): Variation of valve steady state displacement as a function of the valve spring stiffness, p=19 bar, m_v=2 g, damping=1.5 N.s/m.

4.3.6 Overall Optimal Values of Rear Control Valve Parameters

The final values of the control valve parameters are evaluated by taking into account the effect of each parameter on the others, according to the three criteria, which are the settling time, peak overshoot, and the steady state of the displacement of the valve moving mass. The final values of the control valve parameters are calculated by repeating the process given in subsections (4.2.3, 4.2.4, 4.2.5) many times (iterations). The values of the parameters that cause convergence are dependent on the final values. The final values are listed in Table (4-3).

4.4 Response of the Rear Control Valve

The optimal values of control valve parameters can be set in Table (4-3) as:

Table (4-3): Optimal rear control valve parameters.

moving mass (Kg)	spring damping factor (N.s/m)	spring stiffness (N/m)	mass angle (degree)	Orifice diameter (m)
0.002	8	13000	50	0.01

These values listed in Table (4-4) are used to calculate the response of the valve moving mass (valve nose) by using the MATLAB Simulink program shown in Figure (4-2). The response results of the valve nose are shown in Figure (4-15). Figure (4-15) shows that the settling time is 1.6 milliseconds, and the steady-state response is 1.07 cm.

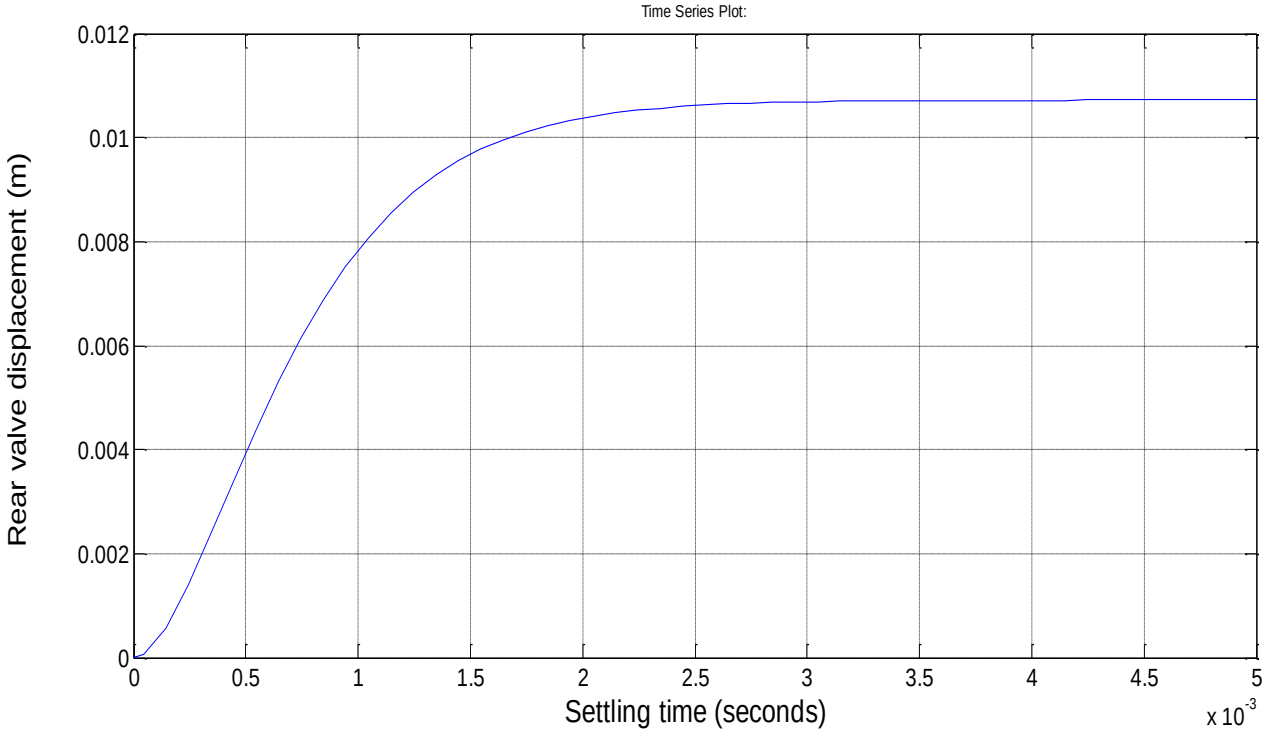

Figure (4-15): Optimal rear control valve response.

4.5 Optimization of the front control valve parameters

The same procedure used for evaluating the best values of the parameters of the rear control valve is used for the front one. The final dependent values of the front control valve parameters are listed in Table (4-4).

Table (4-5): optimal front control valve parameters.

moving mass (Kg)	spring damping factor (N.s/m)	spring stiffness (N/m)	mass angle (degree)	Orifice diameter (m)
0.002	7	9000	45	0.01

These values listed in Table (4-6) are used to calculate the response of the valve moving mass (valve nose) by using the MATLAB Simulink program shown in Figure (4-2). The response results of the valve nose are shown in Figure (4-16):

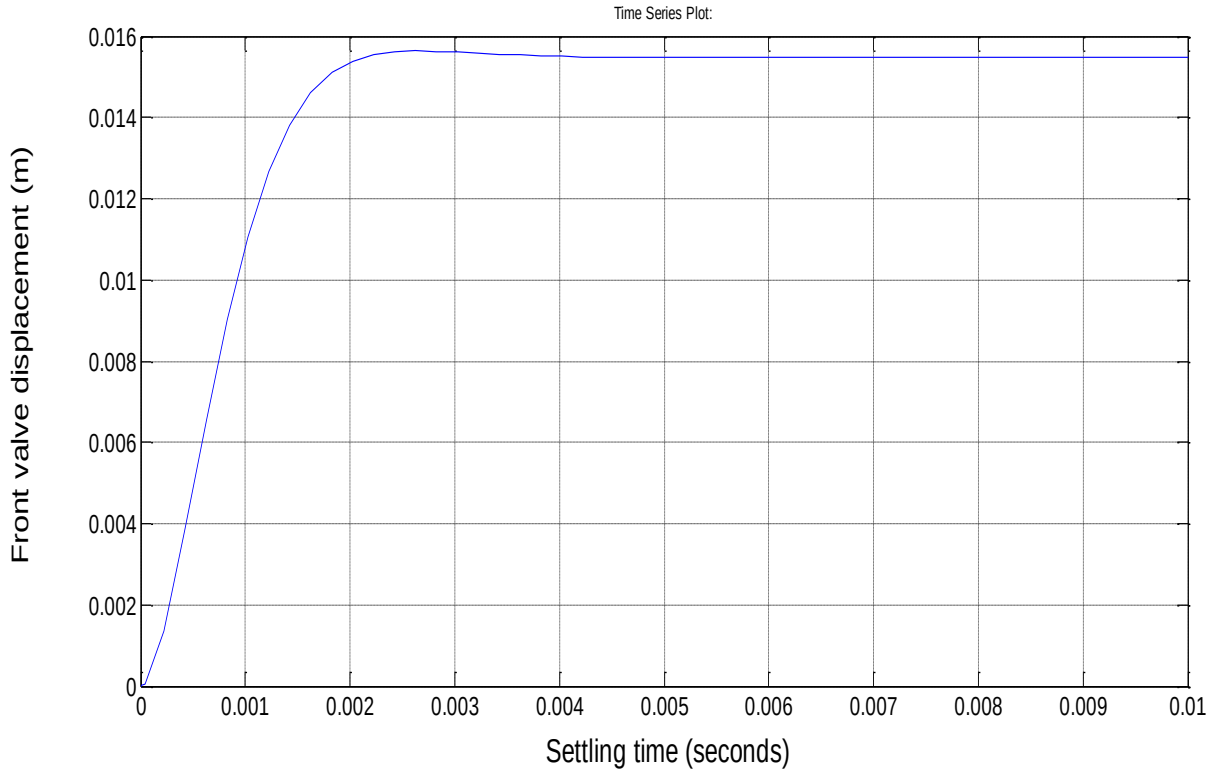

Figure (4-16): Optimal front control valve response.

From Figure (4-16), it is shown that the settling time is 2.3 milliseconds and the steady-state response is 1.55 cm.

Chapter Five

Experimental Work

Chapter Five: Experimental Work

5.1 Introduction

An experimental rig is manufactured to improve the theoretical results related to both the traditional passive damper and the proposed smart damper. The road profile is modelled by an artificial bump tightened to a belt that moves under the tires of the half-automobile model. The bump represents an impulse excitation of 6 cm in height and 34 cm in length, with rounded ends to be close to a half sine wave. The moving belt is driven by an AC electric motor of variable speed through pulleys. The displacement of the sprung mass is measured by an ultrasonic sensor type US-100 connected to an Arduino UNO connected by jumper wires. The measured values are saved by the computer. The parts of the suspension system are for the Saipa automobile model 2011.

5.2 Testing Rig

The testing rig, as shown in Figures (5-1) and (5-3), consists of the following parts;

1. The main frame is constructed from a rectangular cross-sectional area of 8.9 cm by 3.8 cm in dimensions, an iron c-channel of 10 cm by 3.8 cm, and four iron 90-degree angled channels of 3.8 cm by 3.8 cm to allow vertical and rotational movement only for the sprung mass.
2. Sprung mass constructed from steel of 200 kg.
3. Suspension linkages
4. AC Electrical motor.
5. Pullies.
6. Three shafts.
7. Flat belt of 10 cm in width and 5 m in length.

and a chain to transmit motion.

8. Two Mac Pherson suspensions and flanges.
9. Two wheels with two R13 165/65 tires fitted.
10. Two-passive damper with two coil springs.
11. Two displacement measurement devices come with a breadboard, UNO, USB cable for computer connection, jumper wires, and an ultrasound sensor as shown in Figure (5-4).

Figure (5-1): A half-automobile model test rig with a single displacement measuring device.

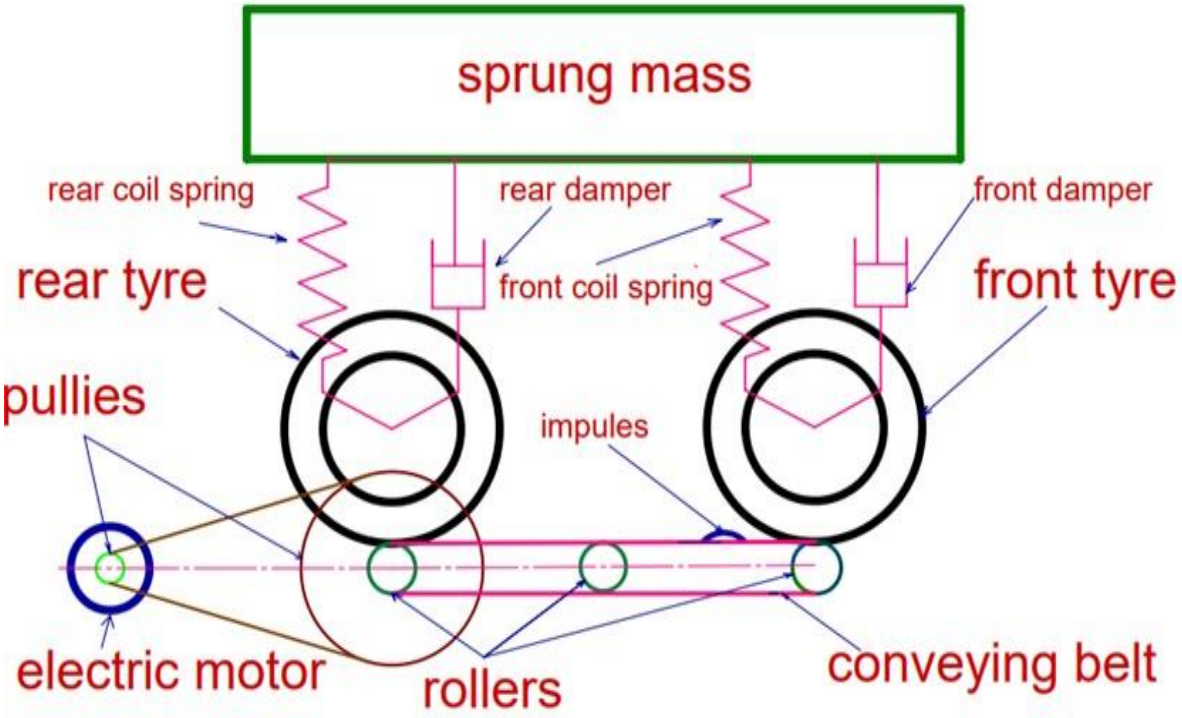

Figure (5-2): Schematic diagram of the experimental work parts.

Figure (5-3): The rig assembly declears the bump.

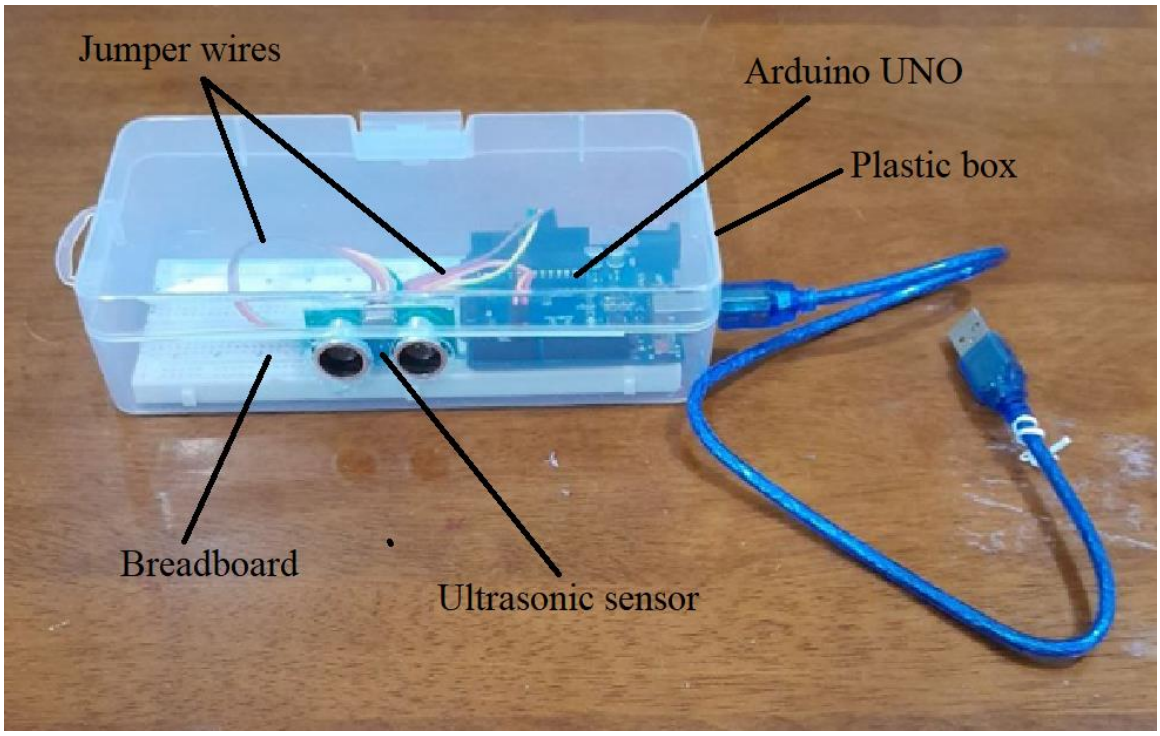

Figure (5-4): Displacement measuring device

5.2.1 Steps of the experiments

The experimental work is performed through the following steps.;

1-Utilizing the displacement-measuring device in the middle of the sprung mass, as shown in Figure (5-1), to measure the response of the sprung mass centre using passive or smart dampers. The displacement measuring device is connected to a PC for saving and plotting results.

2-Starting the AC motor for 1.5 seconds is controlled by using a timer and a contactor.

3-Repeat step 2 for the passive damper, smart damper, excitation at front tire, excitation at rear tire, and excitation at both front and rear tires, respectively.

4-Registering the data collected by the Excel program, saving it on the computer or an external storage unit, and plotting the results.

5.3 Smart Damper Construction

Each of the smart dampers, as shown in Figure (5-5), has two openings in the upper and lower sides, a hydraulic control valve, as illustrated in Figure (5-6), a non-return check valve, hydraulic hoses, and closed piston orifices. Figure (5-7) illustrates the two smart dampers installed in a test rig.

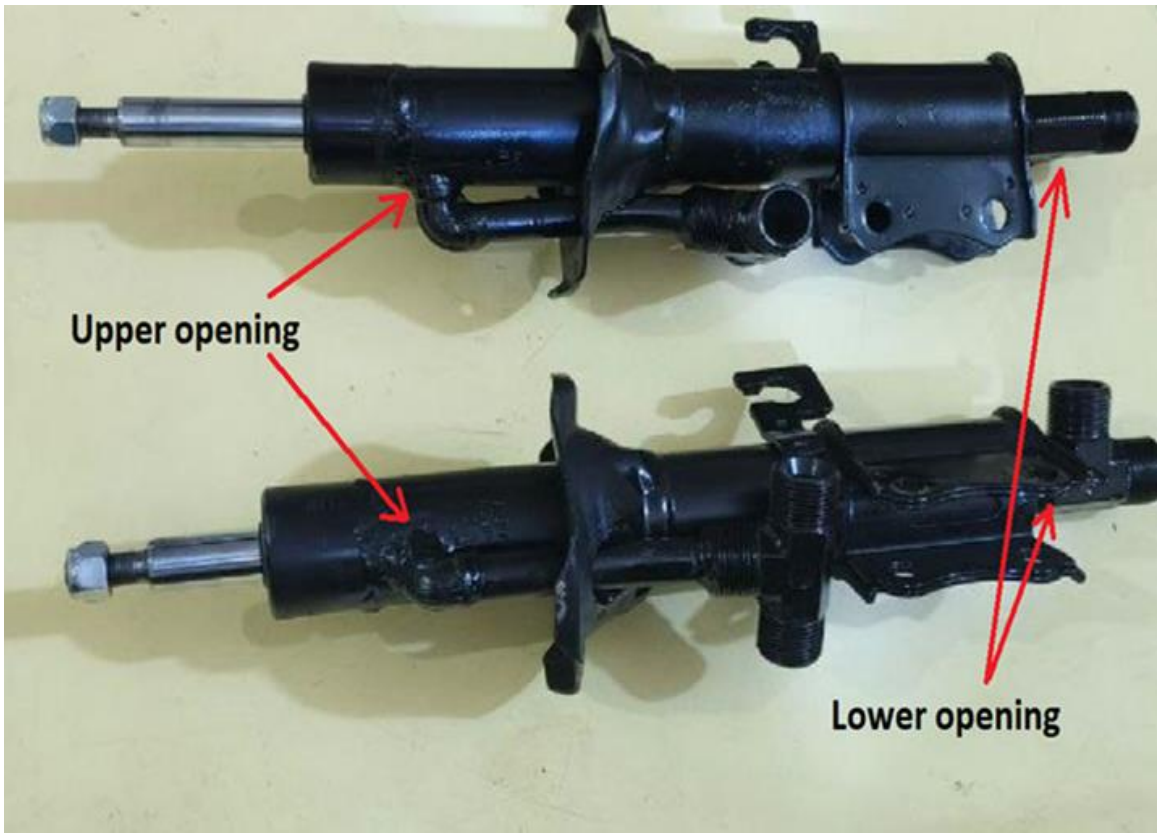

Figure (5-5): Two dampers with openings faces the top and bottom of the internal damper piston

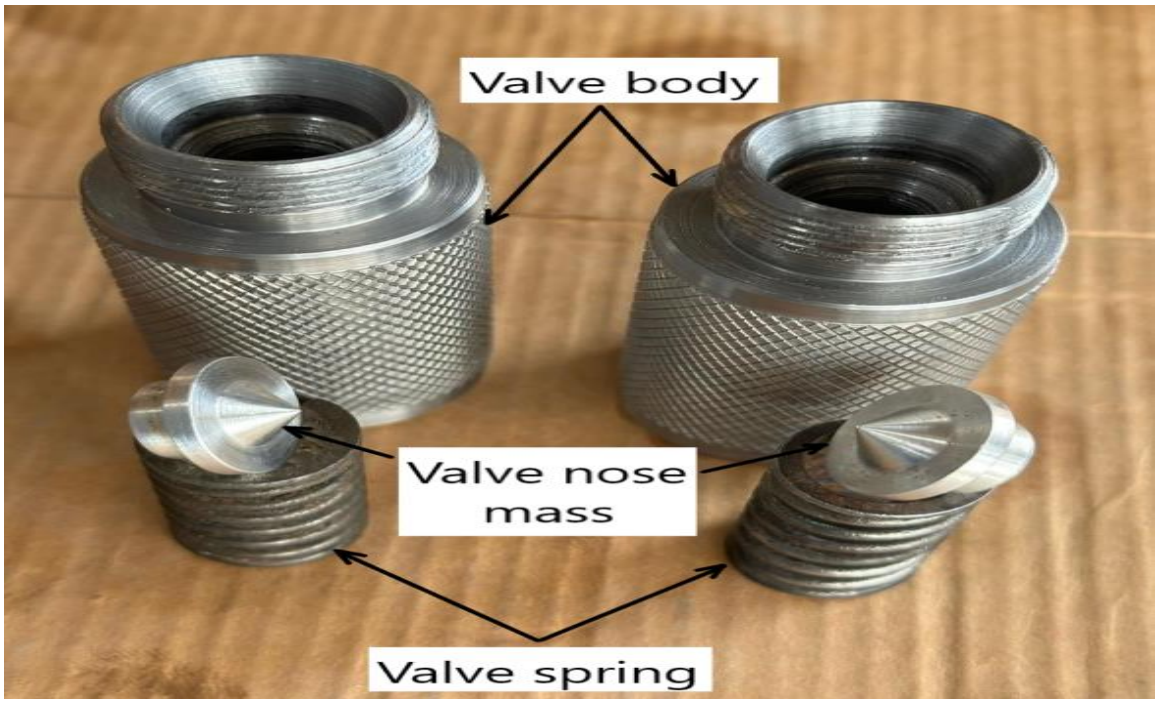

Figure (5-6): Hydraulic Control valves parts.

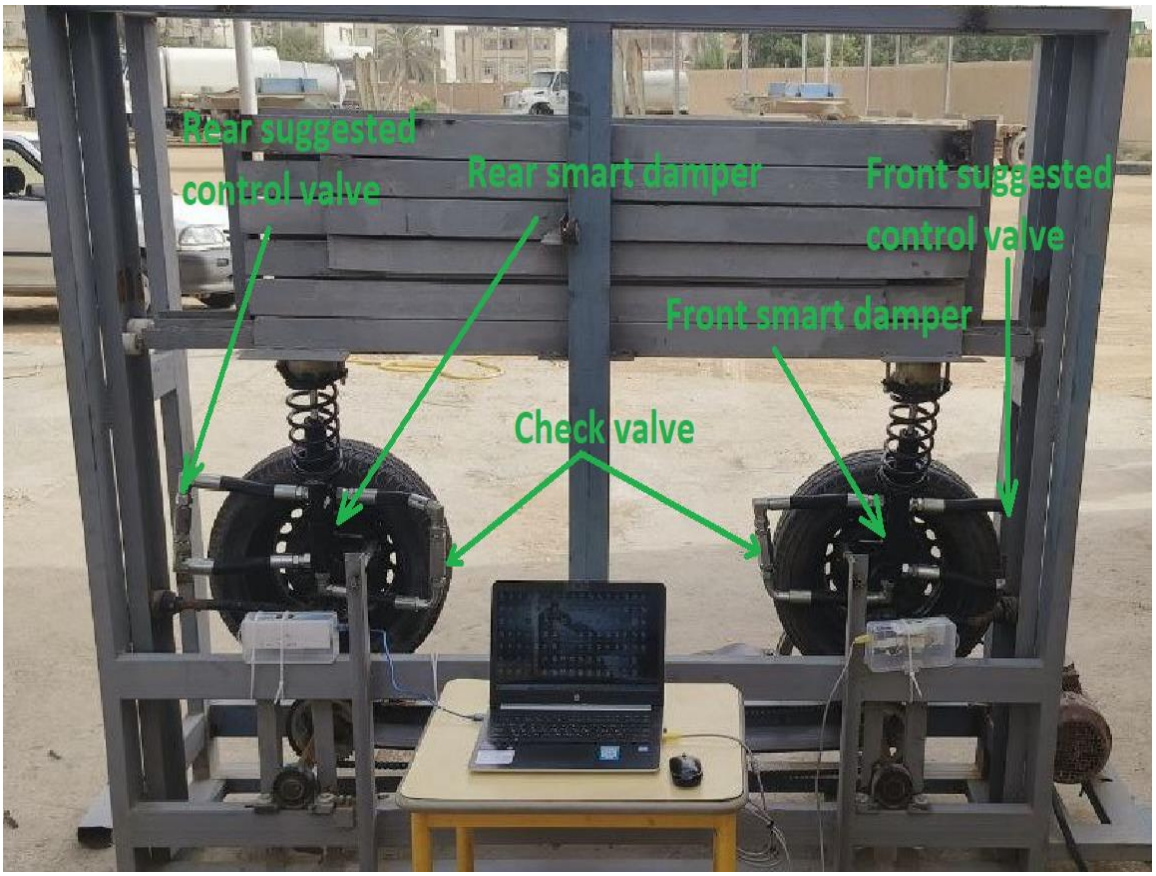

Figure (5-7): Half-automobile test rig with two smart dampers installed.

5.4 Testing Rig Parameter Values.

The test rig parameters were obtained as follows:

- The coil spring stiffness was tested by an SM1000 universal testing device, shown in Figure (5-8). The SM1000 universal testing machine is a hydraulic press coupled to a manual or electrical hydraulic pump with load and displacement gauges. It was found that the coil spring had a stiffness of 50 kN/m. Figure (5-9) illustrates the coil spring change in length due to the applied forces by the SM1000 universal testing machine.

- The passive damper was tested by the half-automobile test rig. The damper damping constant was found to be 1814 N.s/m by plotting the results for the passive case. This empirical value is discussed in Chapter 6, Section 6.2.2.

- The stiffness of the tire is measured by applying a load to the tire in the test rig several times and taking the average value. The tire stiffness is found by dividing the loading force by the vertical deformation, using the average values. It is found to be 151500 N/m.The tire air pressure was 35 PSI at 24 ℃.

- The tire damping constant is assumed to be 1400 N.s/m; this number is considered from a similar research, Reference [39].

- The weight scale measured the sprung and unsprung masses' weights as 200 kilograms and 19 kilograms in sequence.

- The sprung mass, mass moment of inertia, was found to be 26.042 kg. m^2 for a sprung mass of 200 Kg and a length of 1.25 m by the following relation below[40] :

$$J_c = \frac{m \times l^2}{12} \qquad \textbf{(5-1)}$$

Where: J_c ; the sprung mass, mass moment of inertia, rotating around a horizontal axis passing through its center,

m ; the mass of the rectangular plate, and l; the length of the plate.

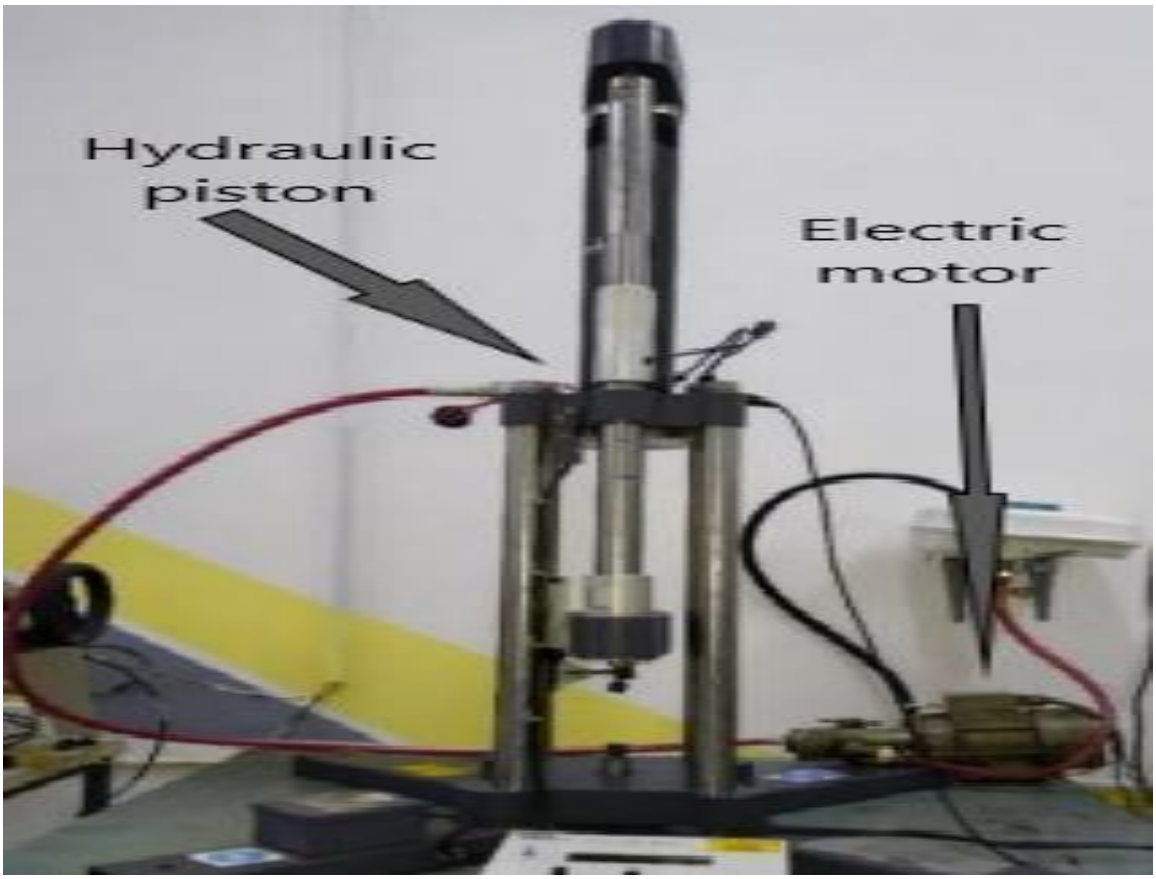

Figure (5-8): A duplicate image of the Universal testing machine SM1000.

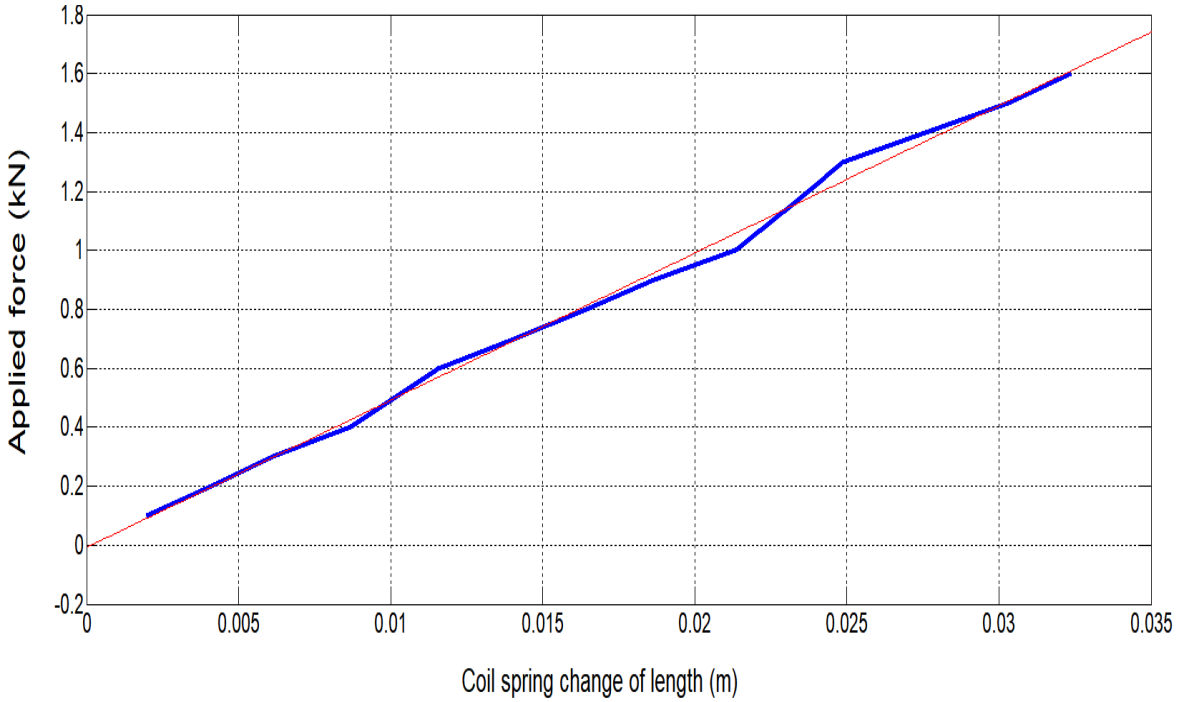

Figure (5-9): Applied forces by the Universal testing machine SM1000 against coil spring change of length.

5.5 Calibration of the Ultrasound US-100 Sensor

The ultrasound US-100 sensor is calibrated using a Vernier of 15 cm full range, as shown in Figure (5-10). Figure (5-10) explains the calibration process by comparing the distance measured by an electronic screen Vernier with the distance obtained from the US-100 ultrasound sensor. It is found that the percentage error for the front and rear sensors equals 0.953 % .

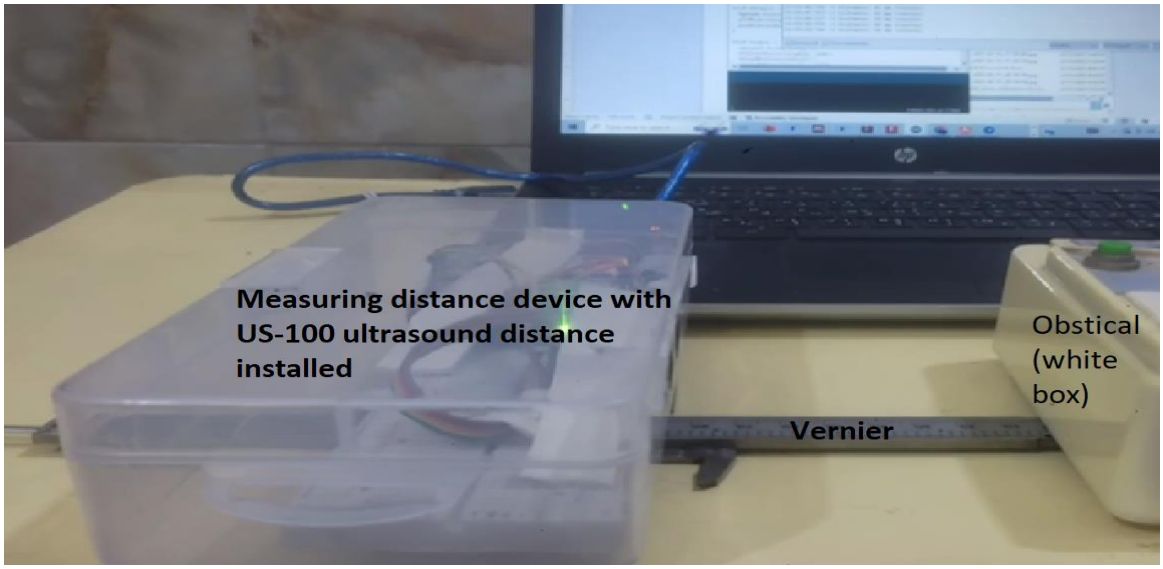

Figure (5-10): US-100 ultrasonic sensor calibration by a vernier and rigid Obstical (white box).

5.6 Calibration of SF-400 Scale

The suggested control valve conical mass of 2 grams was measured using the scale (balance) SF-400. The calibration process was carried out by comparing the scale weight measurement for standard weights with its results. This process is shown in Figure (5-11), where the scale registers 596 grams when 600 grams are placed on it, and all standard weights are measured. It was discovered that the average measuring error percentage was 0.37585%. Figure (5-12) illustrates the SF-400 Scale data against the standard weights.

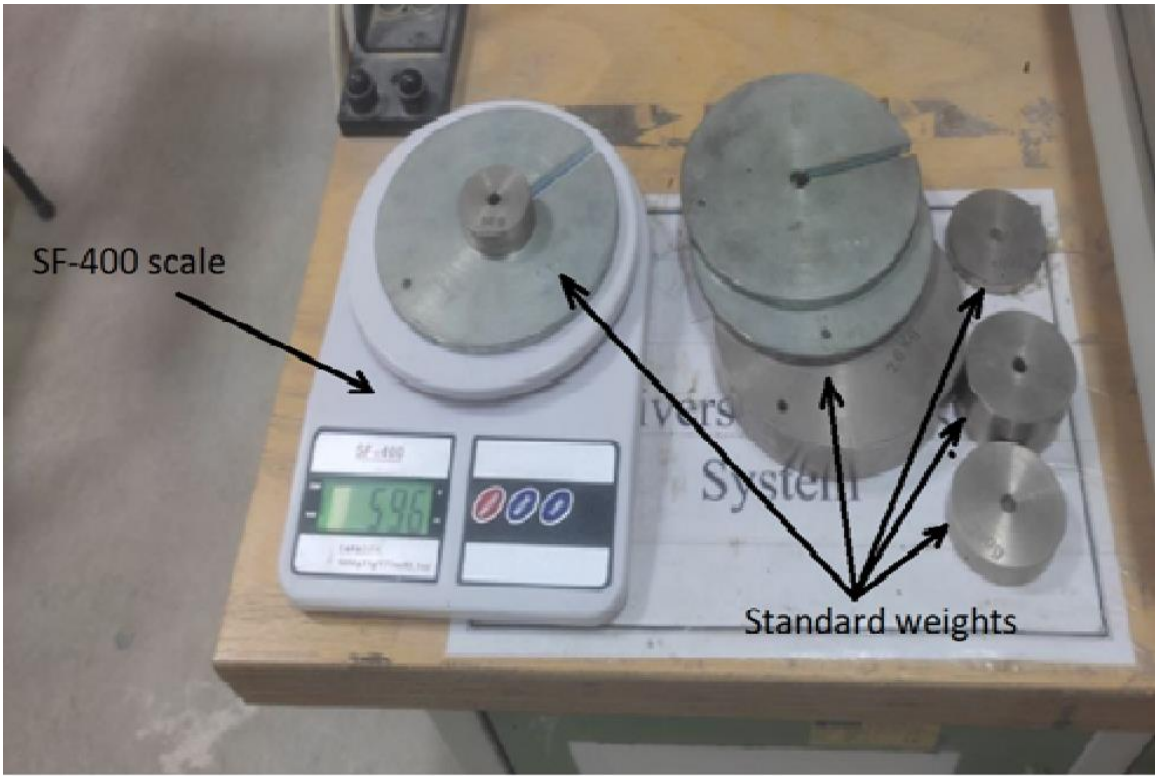

Figure (5-11): SF-400 scale calibration by using different standard weights.

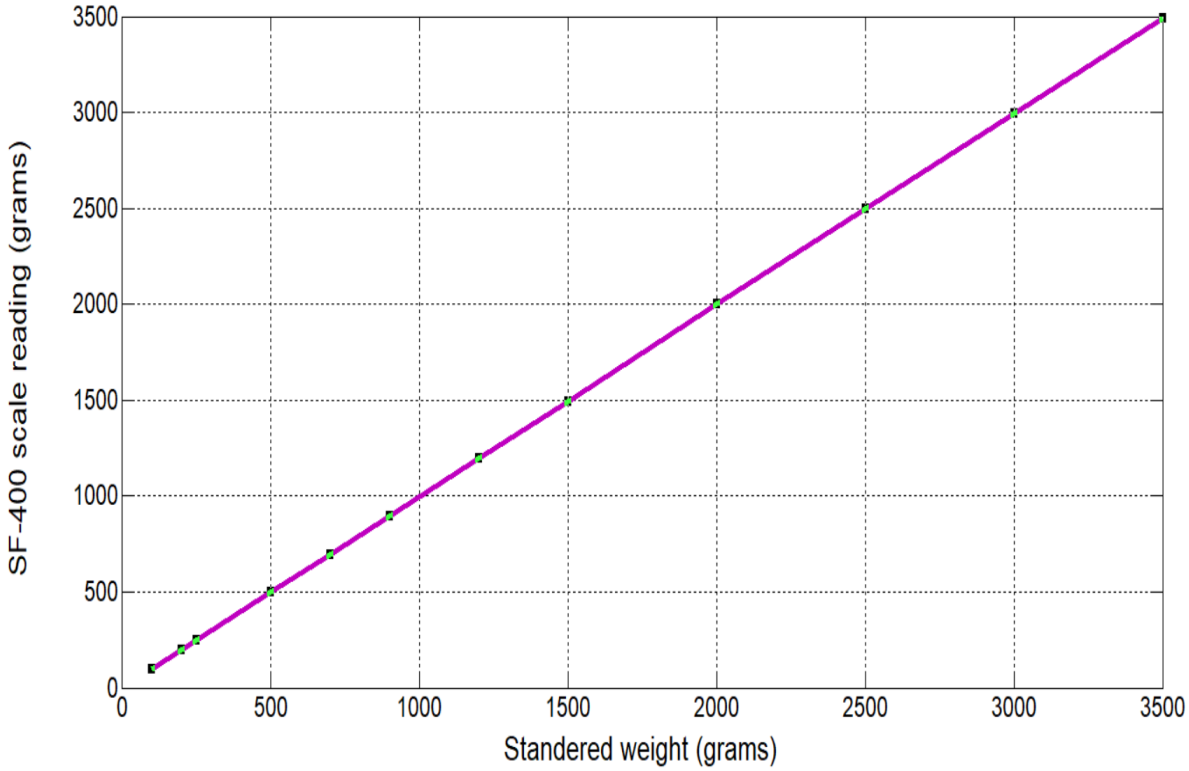

Figure (5-12): Standard weights against SF-400 scale readings in grams.

5.7 Stiffness of the Spring of the Hydraulic Control Valve

In Chapter 4, it is found that the optimal spring stiffness for the front and rear control valves is 13000 N/m and 9000 N/m, respectively. The stiffness of each of the springs is tested by a heavy-duty bench vise to record the force-displacement values using an SF-400 scale. This procedure is repeated three times for various applied forces. Figure (5-13) illustrates this procedure.

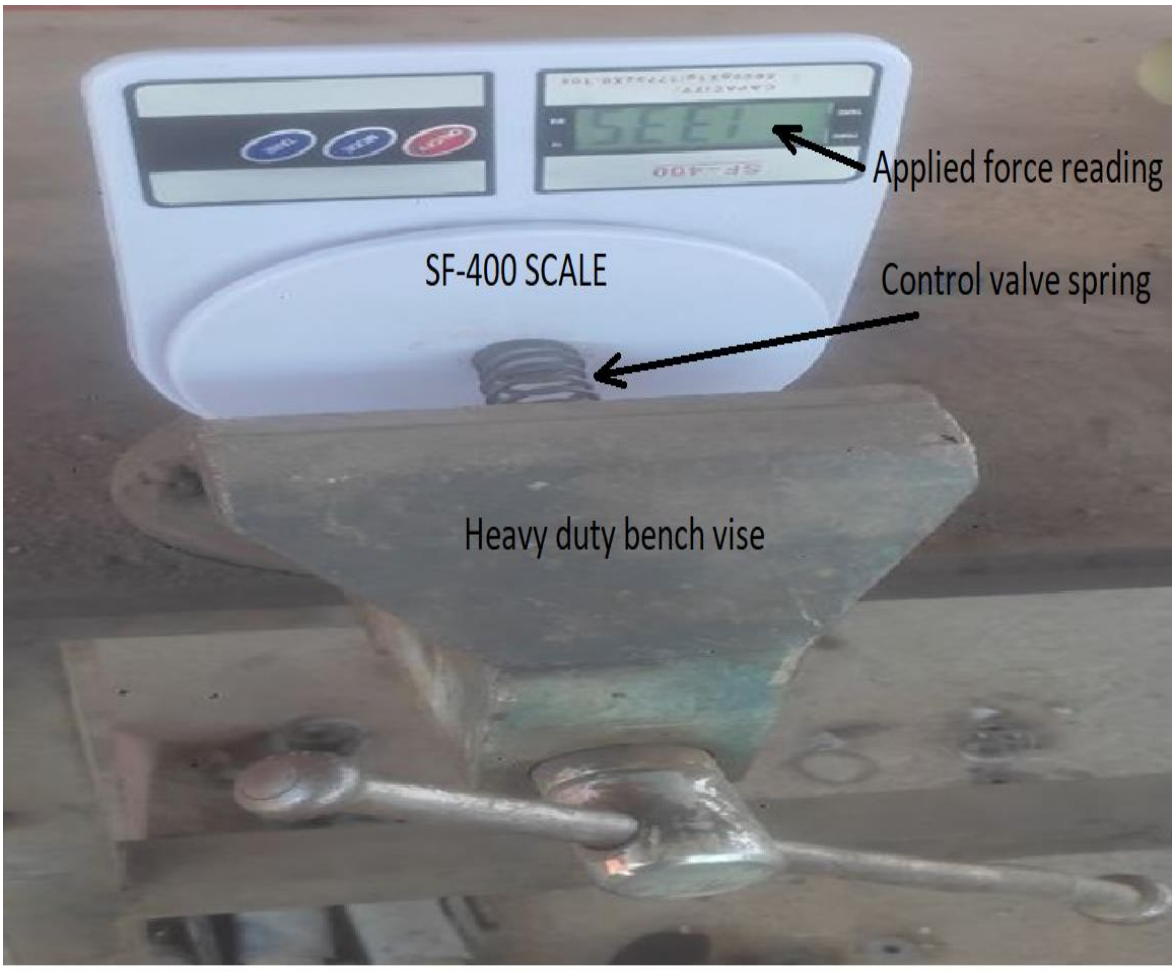

Figure (5-13): Measuring the stiffness of the Control valve spring.

Chapter Six

Results and Discussion

Chapter Six: Results and Discussion

6.1 Introduction

This chapter presents the results of both the theoretical work discussed in chapters three and four and the experimental part presented in chapter five. The theoretical results are determined by solving the mathematical relations of the control valve and those related to the half-automobile model using the Simulink package. Both the theoretical and experimental results include the passive damper and the suggested smart damper to show the difference in performance between the two types of dampers. The results related to the suggested smart damper are based on the control valve's parameters, which are taken according to the optimal values examined in Chapter 4. The step and impulse inputs are used as standard inputs to assess how well the suspension system isolates the sprung mass from road excitations.

6.2 Results and Discussion

The theoretical response of the sprung mass to a step input at the front tire is shown in Figure (6.1) for both the passive and the smart dampers of the Half-automobile model. The results given in this figure are based on the data given in Table (6-1) shown in Figure (6.1). The MATLAB Simulink construction is illustrated in Figures (6-2) and (6-3). The results of Figure (6-1) are due to the effect of a 0.1 m step input excitation on the front side of a half-automobile model. The response of the sprung mass damped by passive dampers approaches rest at about 2.6323 s, while the sprung mass damped by the smart damper approaches rest after 1.7539 s. The settling time in the case of the smart damper is reduced by about 67% of that related to the passive one. This behavior is because the damping of the passive one is constant, while the damping of the smart one is non-constant but is

controlled by the control valve. The damping of the suggested smart damper is proportional to the speed of the wheel rebound, as well as the other parameters of the control valve. The main difference between Figures (6-2) and (6-3) is that Figure (6-2) solves the response of the sprung mass damped by the traditional passive damper, while Figure (6-3) treats the same problem when the sprung mass is damped by the suggested smart damper.

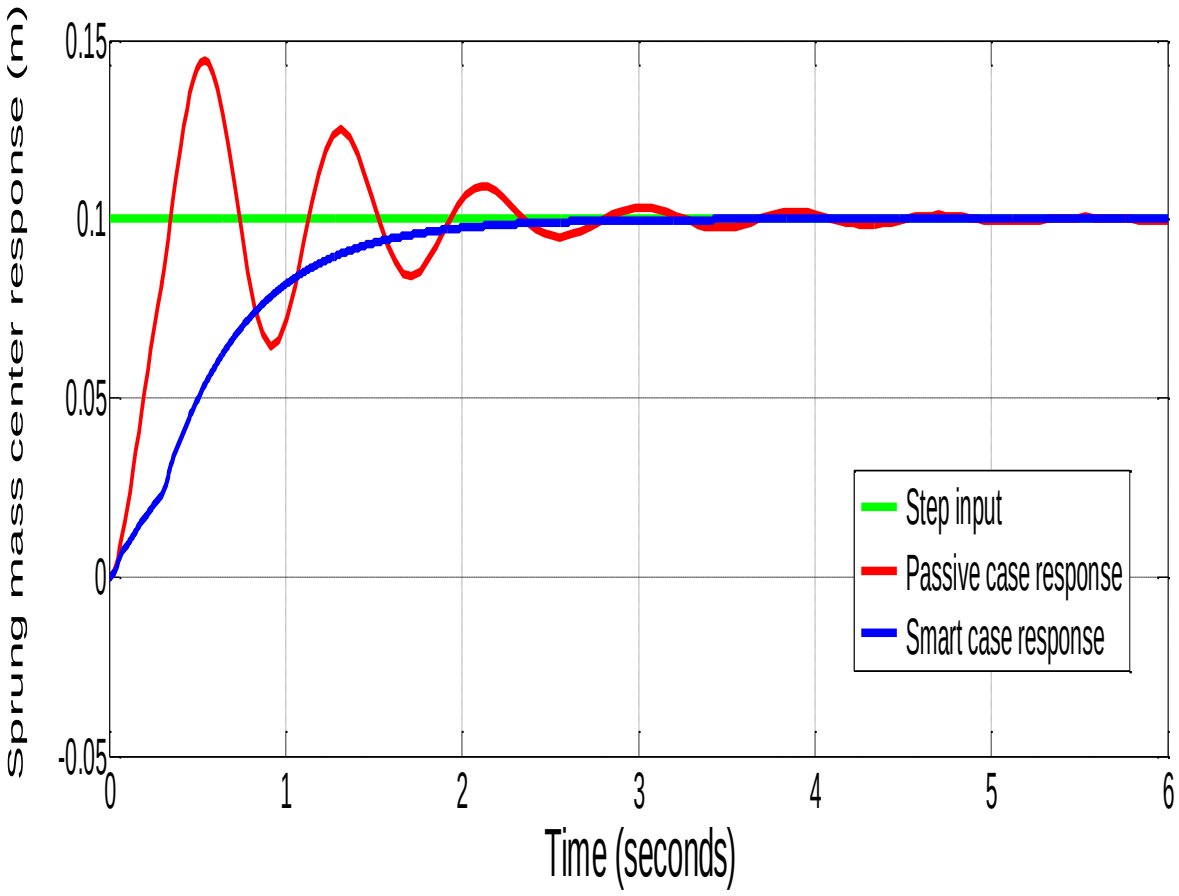

Figure (6-1): Sprung mass center theretical response (passive & smart damper case) due to step impulse input excitation at the front tire.

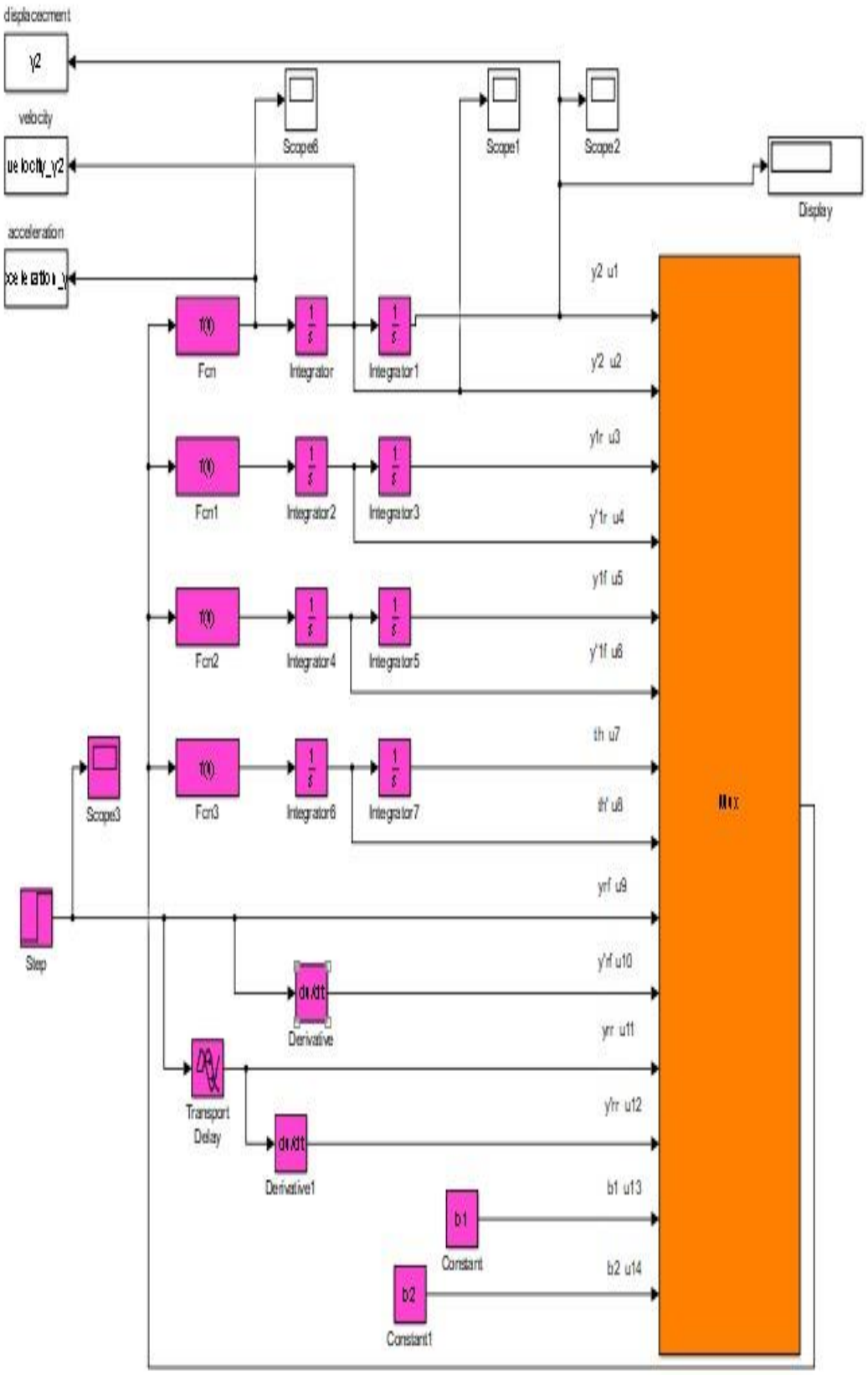

Figure (6-2): Simulink program for the passive damper case Half-automobile model.

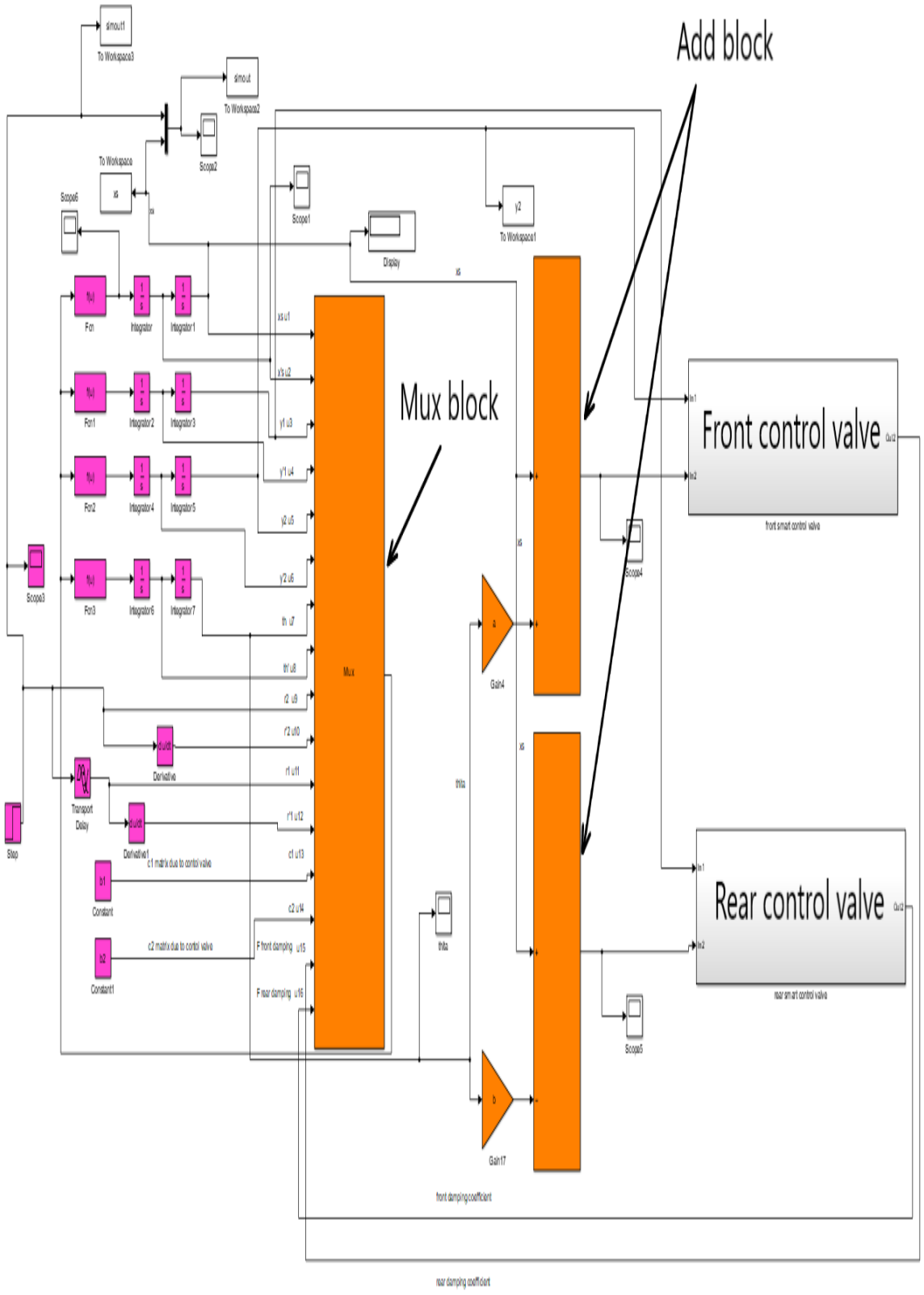

Figure (6-3): Simulink program for the smart damper case Half-automobile model.

Table (6-1): Passive suspension system data [41].

Parameter	Value	Unit
a	1.5	m
b	1.8	m
b_3	1000	$N.s/m$
b_4	1000	$N.s/m$
b_1	500	$N.s/m$
b_2	500	$N.s/m$
H	0.297	s
J_c	1000	$kg.m^2$
k_1	17000	N/m
k_2	15000	N/m
k_3	220000	N/m
k_4	220000	N/m
m_s	500	Kg
m_{u1}	50	Kg
m_{u2}	50	Kg
V	11.111	m/s

Figure (6-4) shows the theoretical response of the sprung mass center in the case of using a passive damper when the impulse excitation is supplied by the front tire at different excitation speeds, in which the excitation duration takes 0.103 s, 0.037 s, 0.0143 s, and 0.0102 s. Figure (6-5) reflects Figure (6-4) when the model is excited at both the front and rear tires with the same speeds of excitation used in Figure (6-4). Both Figures (6-4) and (6-5) show

that the amplitude of the response of the sprung mass decreased with increasing speed of excitation (decreasing the period of excitation). This behavior is attributed to the control forces in the system. When the duration of the excitation is large (soft impulse), the force of the suspension spring is the control one because the acceleration of the sprung mass is low, which induces a low inertia force by the sprung mass, and the compression of the spring is low. When the time of excitation is low (hard impulse), the control force is the inertia one because the acceleration of the sprung mass is high, which causes high compression to the spring of the suspension system.

Figures (6-6) and (6-7) deal with the same input excitations related to Figures (6-4) and (6-5), respectively, but for the case of using the smart damper instead of the traditional passive damper. The same trend shown in Figures (6-4) and (6-5) is repeated in these two figures, but the settling time is reduced by about 65% compared to the passive damper. Also, the same elaboration for the effect of time duration can depend on.

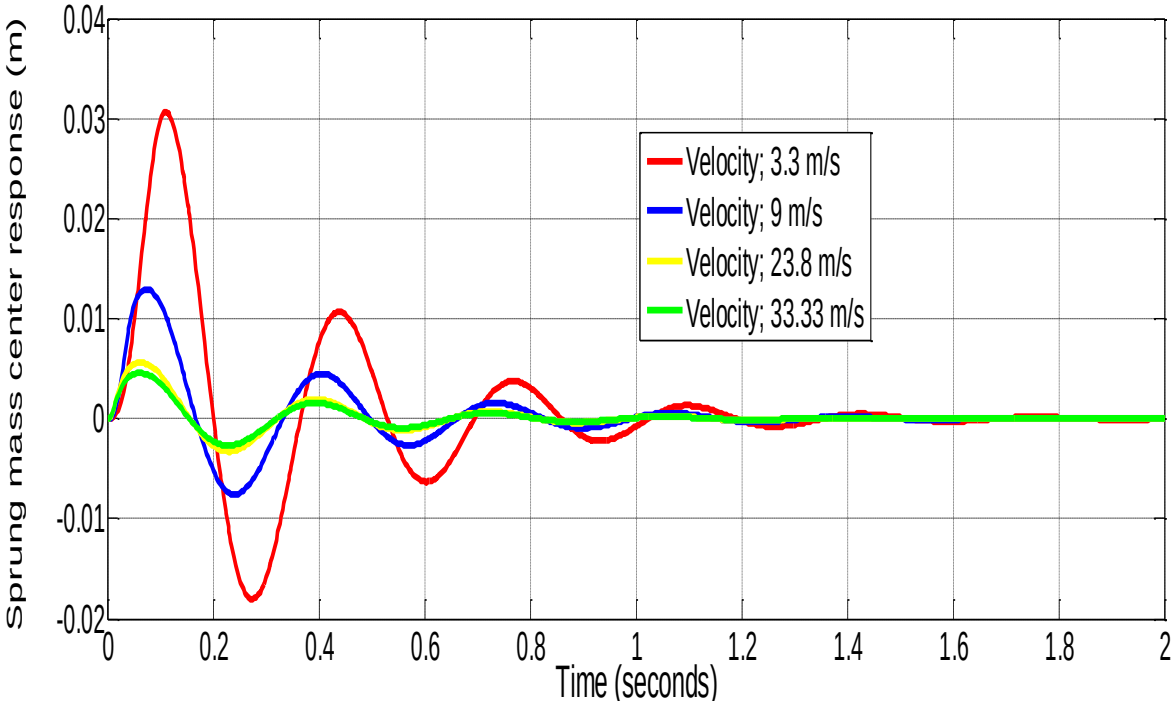

Figure (6-4): Sprung mass center passive theoretical response for different velocities, due to impulse excitation at front tire of 0.34 m in lenght and 0.06 m in amplitude, the excitation takes 0.103 s, 0.037 s, 0.0143 s, 0.0102 s duration in sequense.

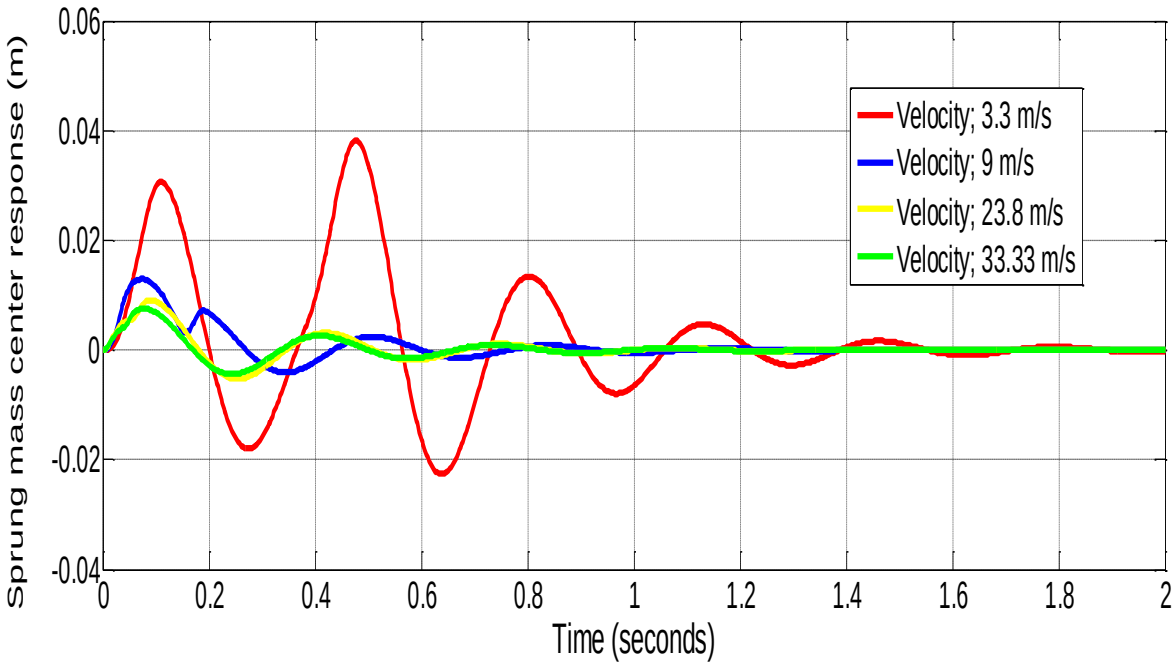

Figure (6-5): Sprung mass center passive theoretical response for different velocities, due to two impulse excitation at front and rear tires respectivelly of 0.34 m in length and 0.06 m in amplitude, the excitation takes 0.103 s, 0.037 s, 0.0143 s, 0.0102 s duration in sequense.

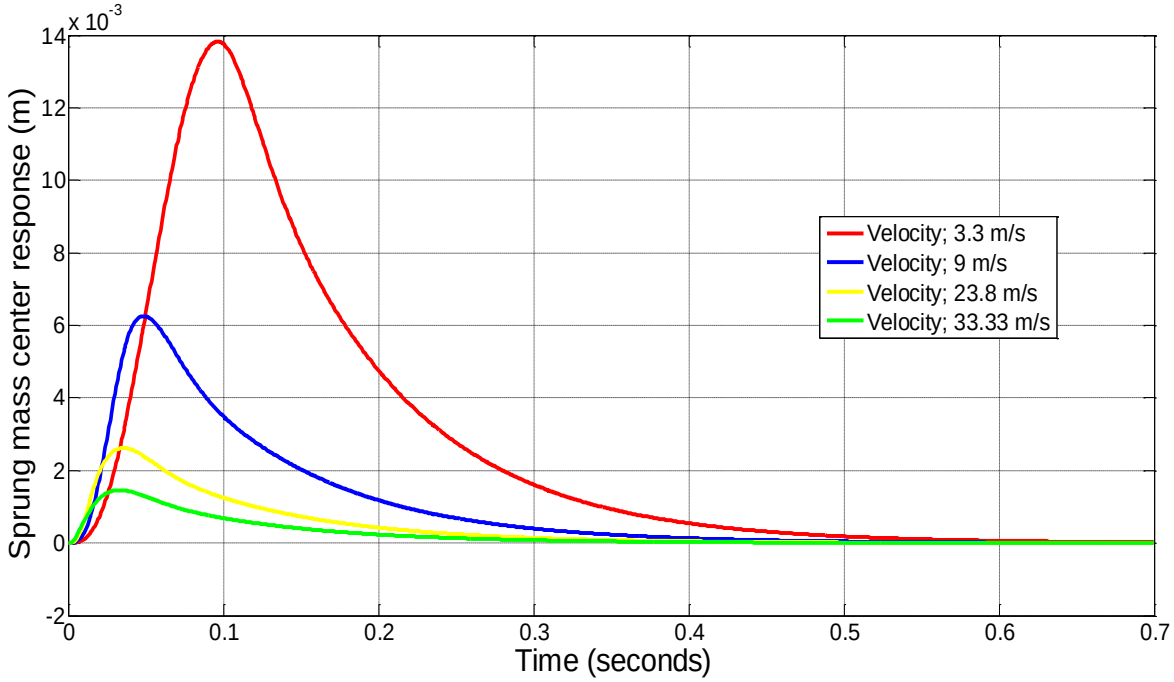

Figure (6-6): Theoretical response of sprung mass center to impulse input at front tire using smart damper, using different velocities. The impulse is of 0.34 m in lenght and 0.06 m in amplitude, the excitation takes 0.103 s, 0.037 s, 0.0143 s, 0.0102 s duration in sequense.

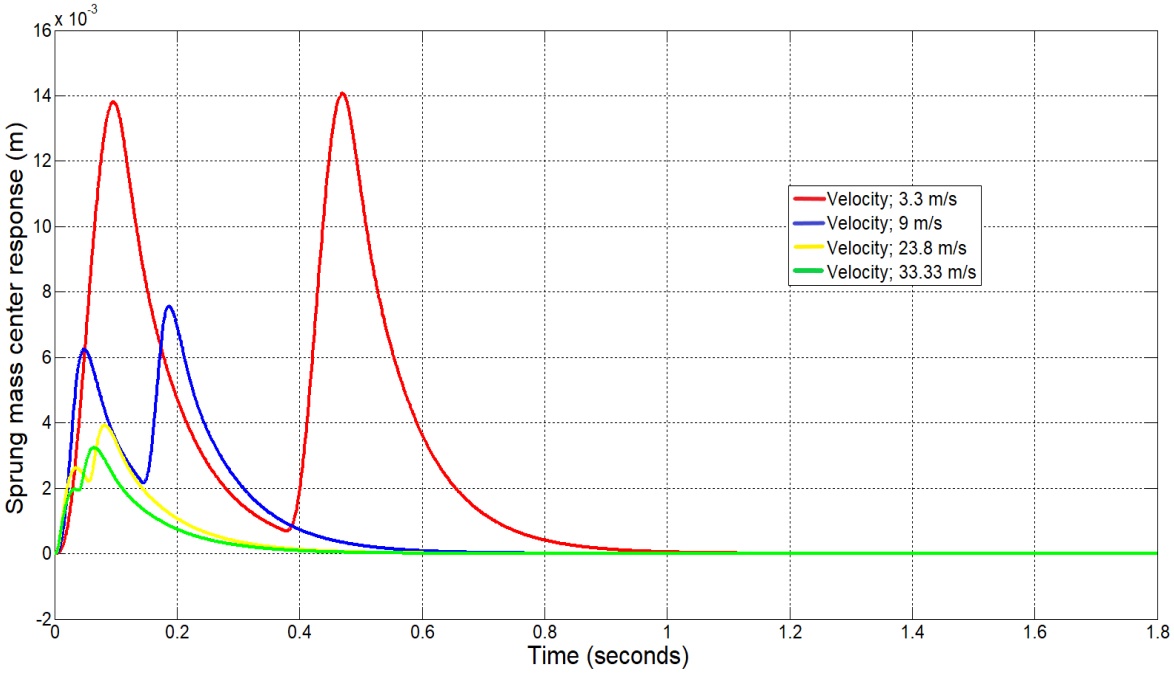

Figure (6-7): Sprung mass center smart theoretical response for different velocities, due to two impulse excitation at front and rear tires respectivelly of 0.34 m in lenght and 0.06 m in amplitude, the excitation takes 0.103 s, 0.037 s, 0.0143 s, 0.0102 s duration in sequense.

6.2.1 Matlab-Simulink Program Structure

The Matlab-Simulink program illustrated in Figures (6-2) and (6-3) used in this chapter is constructed from a function, scope, mux, step input source, integral, constant, display, derivative, delay, and simout blocks. These blocks stand for a mathematical operation that simulates the real response of each part of the targeted model. Scope blocks are frequently used to monitor changes every time the program runs with different parameter values while approaching acceptable results. The transport delay block in each figure was to give a delay time for the rear tire excitation from the front one, according to the belt speed and obstacle bump width described in Chapter 5.

6.2.2 Determination of the damping constant

The rate at which a system loses energy over time is described by the damping constant. This constant is commonly represented by the letter "c". System stability is accelerated by a greater damping constant, which denotes a faster oscillation decay. Plotting the experimental oscillatory motion for the passive case, the data was collected from the US-100 ultrasonic front sensor, as demonstrated in Chapter 5, and measuring the amplitude of the first and second peaks, x_1 and x_2. As seen in Figure (6-8), the damping constant may then be empirically estimated using the formulae (6-1) to (6-4)[42] given below.

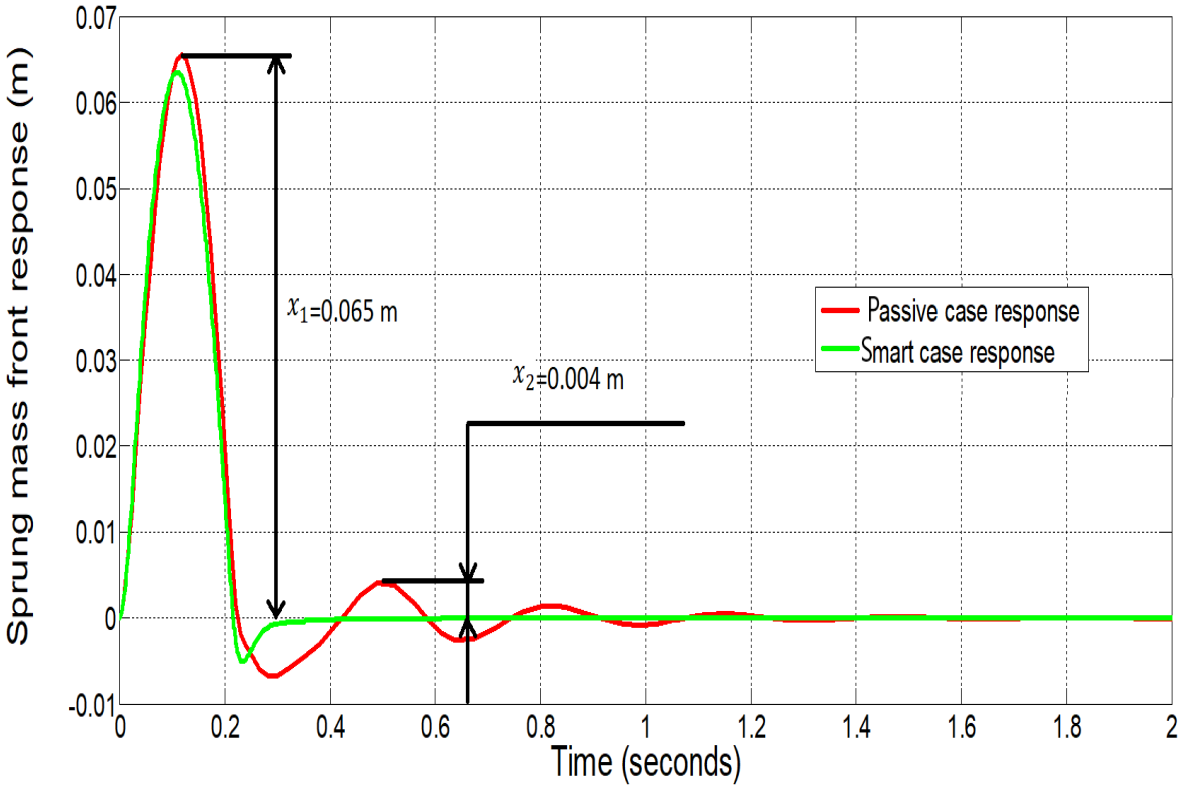

Figure (6-8): Experimental response of sprung mass at front side due to impulse excitation at front tire of 0.34 m in lenght and 0.06 m in amplitude at a speed of 1.6 m/s, the excitation takes 0.2125 s duration, with two first peaks measured for the passive response.

$$\delta = \ln \frac{x_1}{x_2} \quad \textbf{(6-1)}$$

$$\zeta = \frac{\delta}{\sqrt{(\delta^2 + 4\pi^2)}} \quad \textbf{(6-2)}$$

$$c_{cr} = 2\sqrt{(k \times m)} \quad \textbf{(6-3)}$$

$$\therefore c = 2\zeta\sqrt{(k \times m)} \quad \textbf{(6-4)}$$

After substituting the corresponding experimental values, x_1; 0.065 m, x_2; 0.004 m, k; 50000 N/m and m; 100 kg because each tire is located at the same distance from the experimentally half-automobile model center, in the above equations, the damping constant was found to be equal to 1814 N. s/m.

6.2.3 Experimental Results

The experimental results are based on the parameters given in Table (6-2) which are measured, calculated, or taken from references.

The experimental results are performed using the manufactured apparatus using a passive damper or a smart one. The apparatus, as shown in chapter five, is constructed as a Half-automobile model. The experimental response of the sprung mass center due to an impulse excitation at the front tire having 0.34 m in length and 0.06 m in amplitude at a speed of 1.6 m/s, and 0.2125 seconds duration is shown in Figure (6-9). From this figure, it is found that for the passive pamper, the settling time was 1.3 seconds, while for the smart one it was o.455 seconds. The suggested damper reduces the settling time by about 65% compared to the traditional passive damper. The reduction in the settling time that is related to the smart damper is attributed to the control valve, which gives a non-constant damping. This result leads

to the conclusion that the suggested smart damper gives more riding comfort and automobile stability.

Figure (6-10) illustrates the response of the sprung mass center excited by the front and rear tires, respectively, in which the duration time of excitation is 0.2125 s at each tire. The data of this figure shows that the total settling time of the sprung mass due to the two excitations was 2 seconds for the case of passive damper, while for the case of smart one, there are two periods of settling time, the first related to the excitation at the front tire which takes 0.2125 seconds. The second settling time is due to the excitation at the rear tire (which takes 0.78 seconds after the front tire). The total settling time of the sprung mass due to the two excitations takes 1.25 seconds. From this figure, it was found that the suggested smart damper reduces the total settling time due to the excitations at both the front and rear tires was found to be 37%.

In Figure (6-11), the experimental response of the sprung mass at the front side due to impulse excitation at the front tire of 0.34 m in length and 0.06 m in amplitude at a speed of 1.6 m/s. The period of this excitation is 0.2125 s. The time required for the front side of the automobile to settle out takes 1 second when using the passive damper, while it takes 0.35 seconds in the case of using the smart damper. This result shows that the settling time is reduced by about 65% when using the smart damper compared to that of the passive damper for the response of the sprung mass at its front side when excited by the front tire.

The experimental response of the sprung mass at its front side to excitation by both the front and rear tires consecutively is presented in Figure (6-12). The settling time for the case of a passive damper takes 2 seconds to settle

out, while it takes 1.1 seconds to settle out totally. The smart damper caused a 55% reduction in settling time.

Figures (6-13) and (6-14) show the response of the sprung mass at its rear side when the automobile is excited by an impulse caused by the front and rear tires, respectively. Both of these figures show a clear reduction in settling in the case of using the smart damper compared to that when using the traditional passive damper.

Table (6-2): Experimental and assumed parameter values for the test rig.

Parameter	Value	Unit
a	0.625	m
b	0.625	m
b_3	1400	$N.s/m$
b_4	1400	$N.s/m$
b_1	1814	$N.s/m$
b_2	1814	$N.s/m$
H	0.7813	s
J_c	26.042	$kg.m^2$
k_1	50000	N/m
k_2	50000	N/m
k_3	151000	N/m
k_4	151000	N/m
m_s	200	Kg
m_{u1}	19	Kg
m_{u2}	19	Kg
v	1.6	m/s

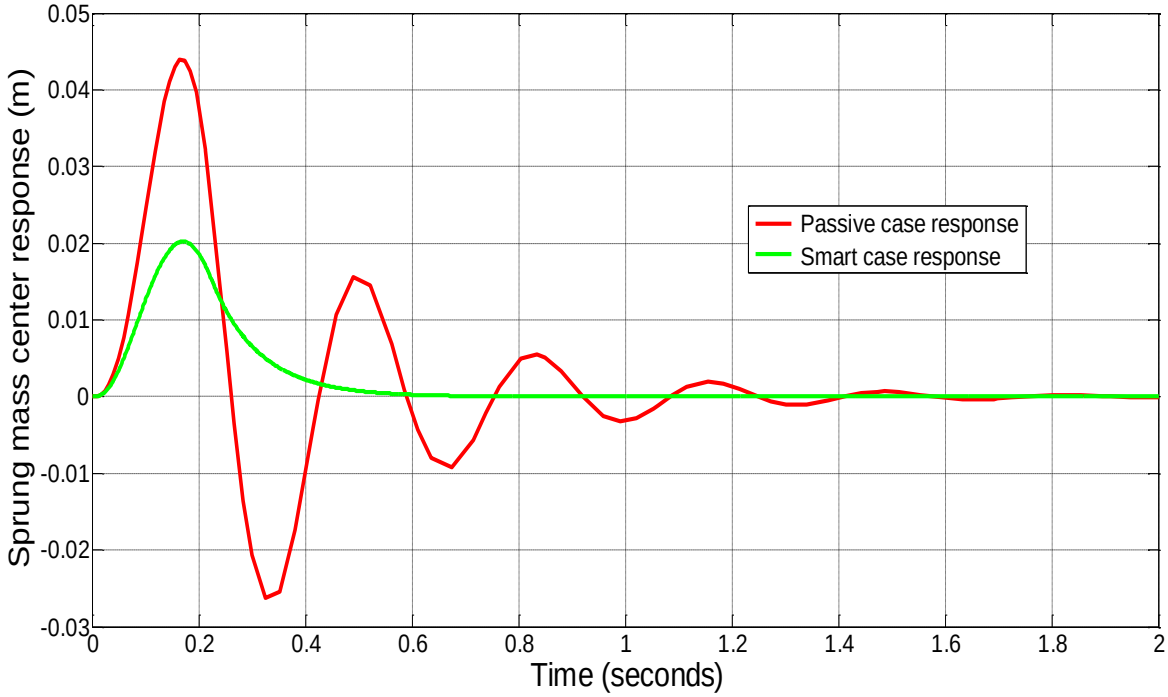

Figure (6-9): Experimental response of sprung mass at the center due to impulse excitation at front tire of 0.34 m in lenght and 0.06 m in amplitude at a speed of 1.6 m/s,the excitation takes 0.2125 s duration.

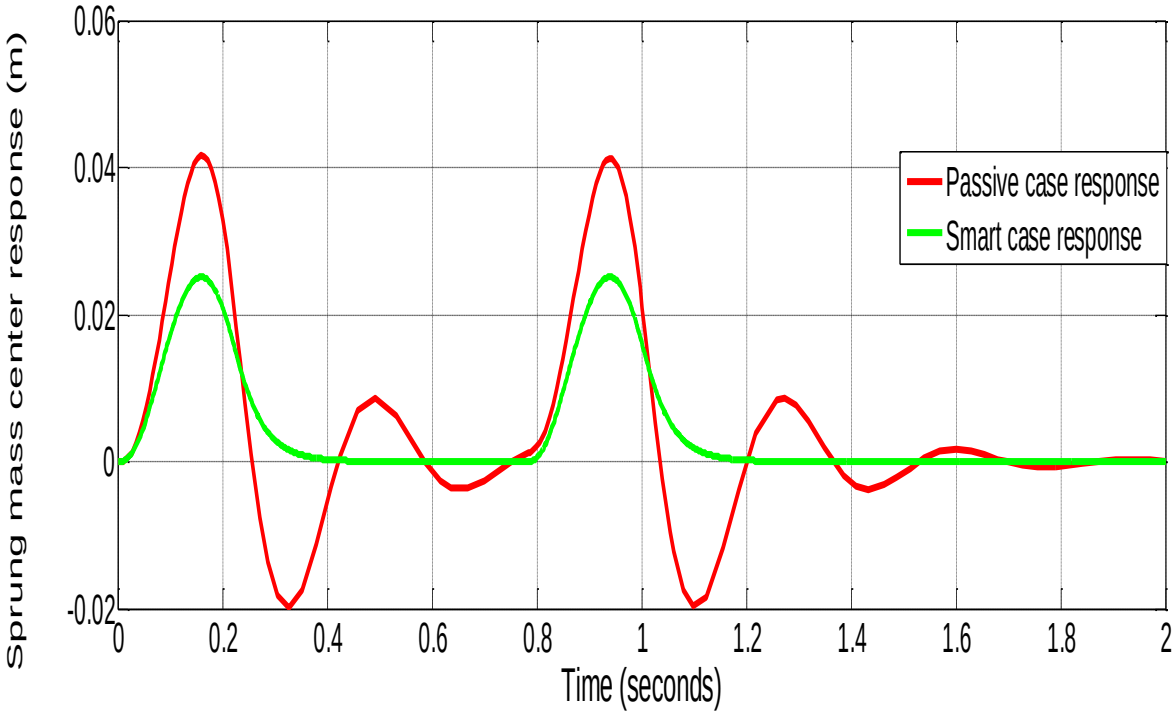

Figure (6-10): Experimental response of sprung mass at the center due to two impulse excitation at front and rear tires respectivelly of 0.34 m in lenght and 0.06 m in amplitude at a speed of 1.6 m/s, the excitation takes 0.2125 s

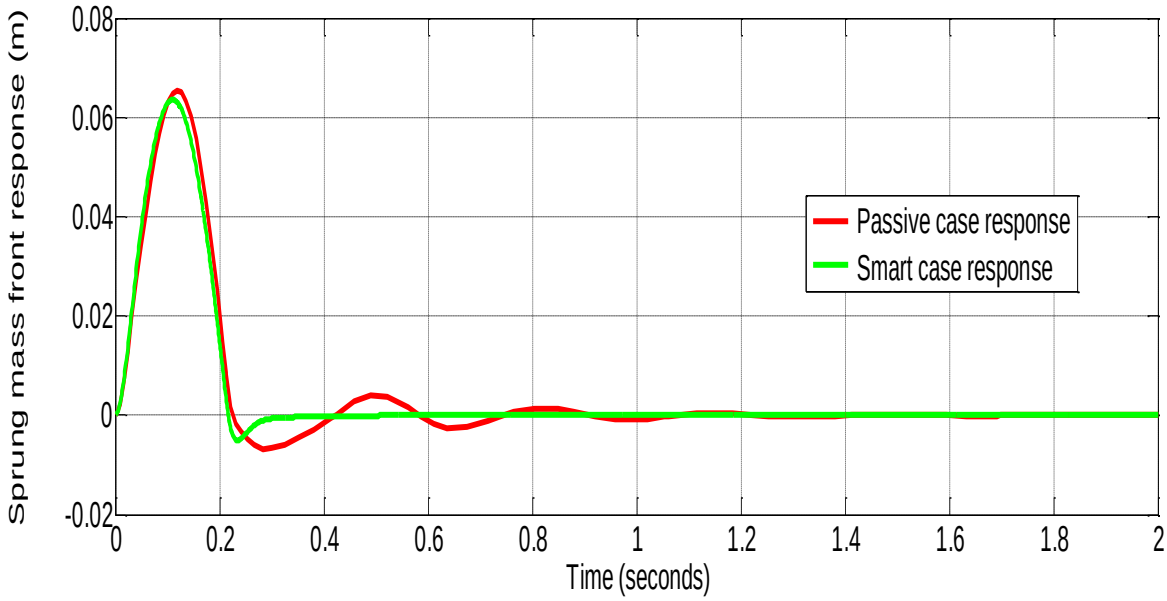

Figure (6-11): Experimental response of sprung mass at front side due to impulse excitation at front tire of 0.34 m in lenght and 0.06 m in amplitude at a speed of 1.6 m/s.the excitationtakes 0.2125 s duration.

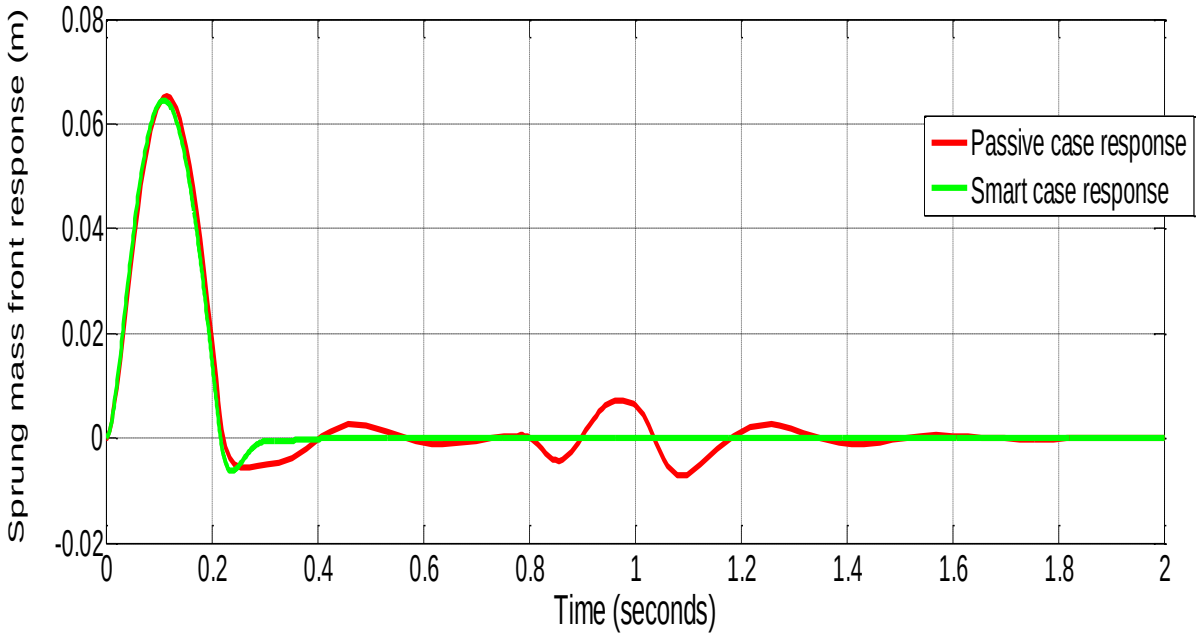

Figure (6-12): Experimental response of sprung mass at front side due to two impulse excitations at front & rear tires respectively of 0.34 m in lenght and 0.06 m in amplitude at a speed of 1.6 m/s. The excitation takes 0.2125 s

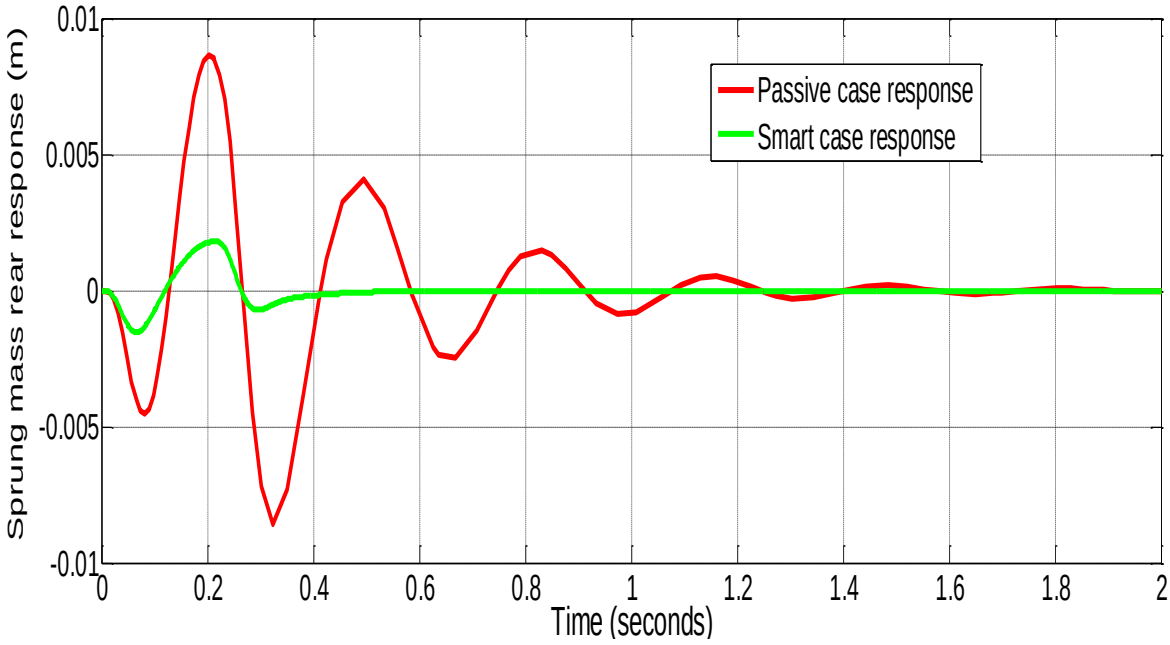

Figure (6-13): Experimental response of sprung mass at rear side due to impulse excitation at front tire of 0.34 m in lenght and 0.06 m in amplitude at aspeed of 1.6 m/s. The excitation takes 0.2125 s duration.

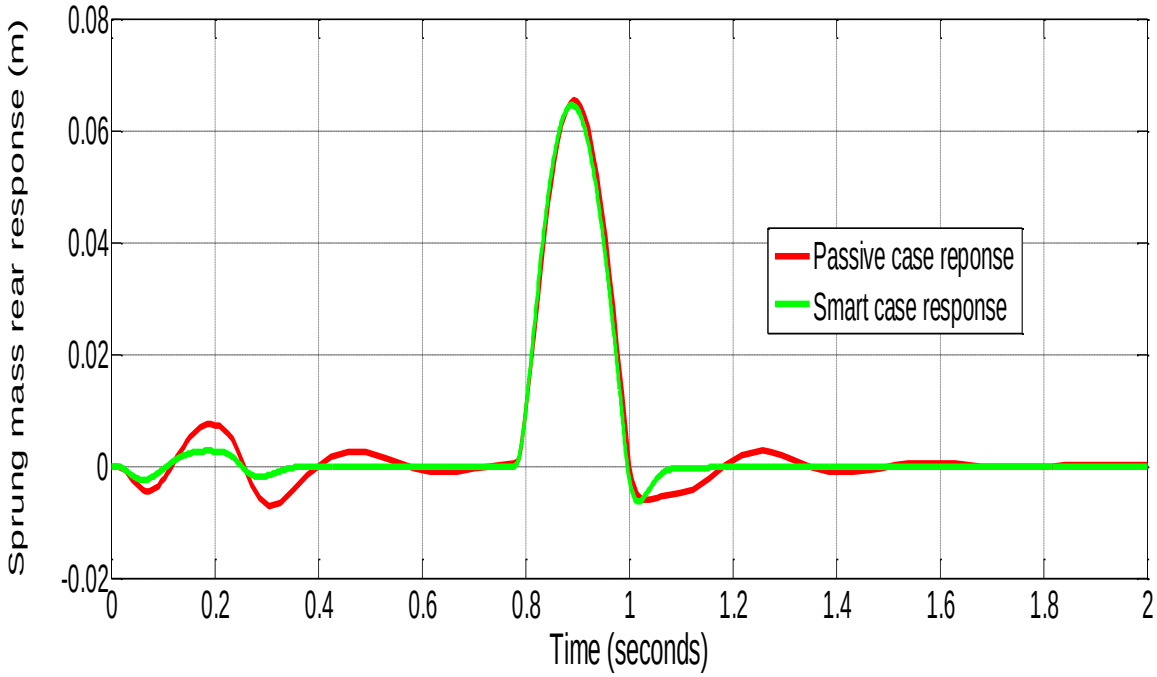

Figure (6-14):): Experimental response of sprung mass at rear side due to two impulse excitationsat front & rear tires respectively of 0.34 m in lenght and 0.06 m in amplitude at a speed of 1.6 m/s. The excitation takes 0.2125 s duration.

Figures (6-15) and (6-16) are plotted to investigate the difference between the theoretical and experimental response of the half-automobile model at the sprung mass center for passive and smart dampers. The results are due to sine excitation applied at the front tire of 0.34 m in length and 0.06 m in amplitude at a speed of 1.6 m/s, the excitation takes a 0.2125 s duration. For the passive damper, the percentage error for the settling time is 37%, and for the smart damper is 33%. These figures show that the settling time is reduced by 65% when using the proposed smart damper compared to that for the traditional passive one.

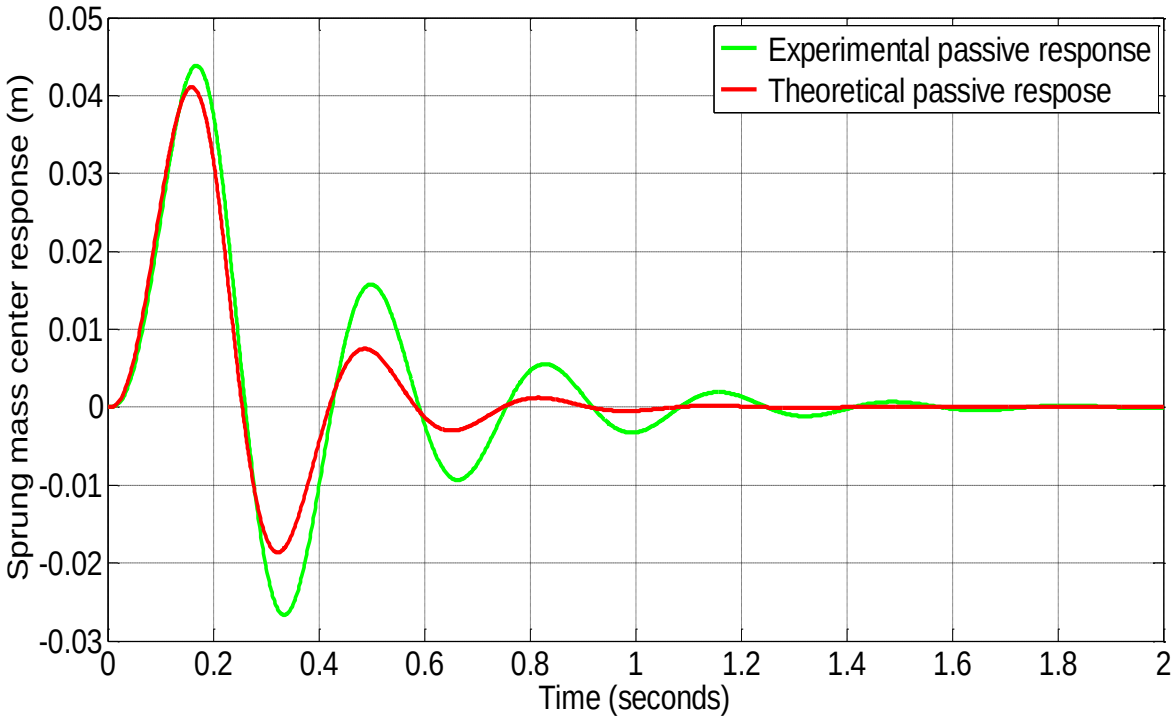

Figure (6-15): Experimental and theoretical comparision for sprung mass center passive response due to impulse excitation at front tire of 0.34 m in lenght and 0.06 m in amplitude at a speed of 1.6 m/s, the excitation takes 0.2125 s duration.

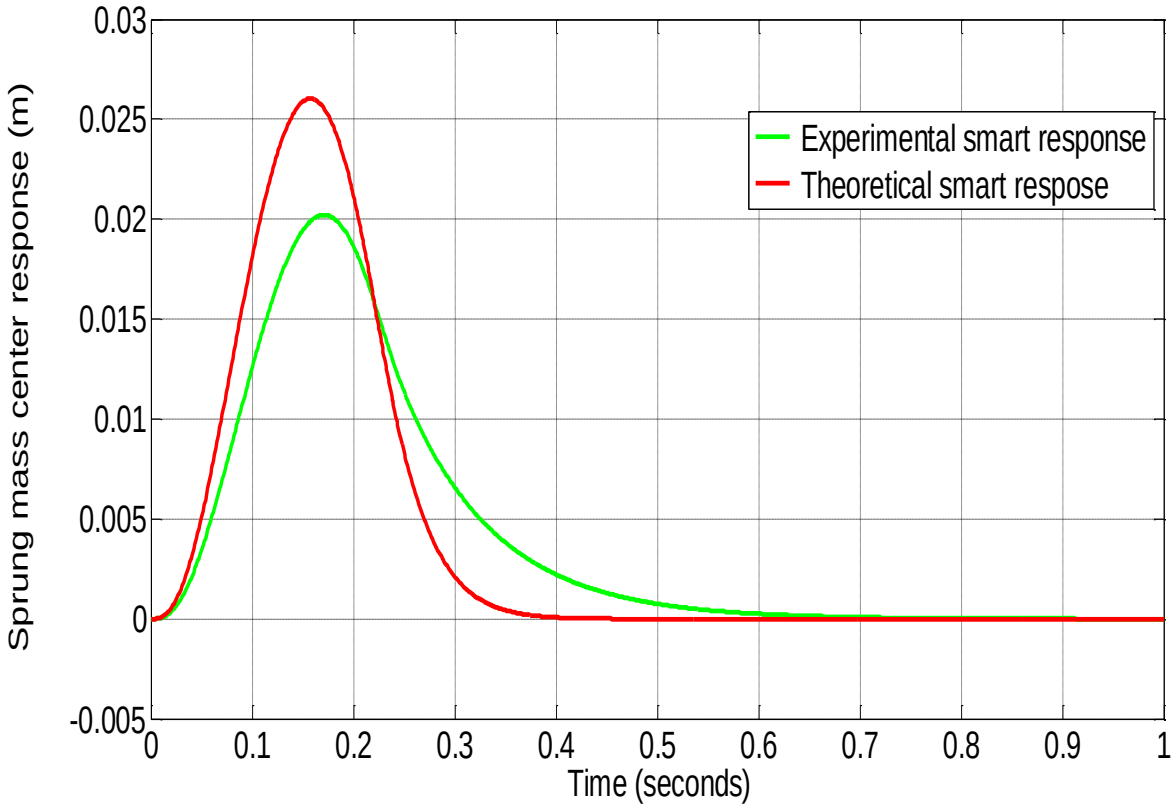

Figure (6-16): Experimental and theoretical comparision for sprung mass center response due to impulse excitation at front tire of 0.34 m in lenght and 0.06 m in amplitude at a speed of 1.6 m/s, the excitation takes0.2125 s duration.

6.2.4 Passive Response: Comparison with Previous Work

A prior work [43] illustrated the sprung mass center response for its parameter values listed in Table (6-3). The sprung mass center displacement provided by the prior work using its MATLAB Simulink software is depicted in Figure (6-17), and that using the MATLAB Simulink program is demonstrated in Figure (6-2) for the same prior work parameter values. The program may be relied upon because the variations between the two plots are so minor (maximum variation equals 0.106 %).

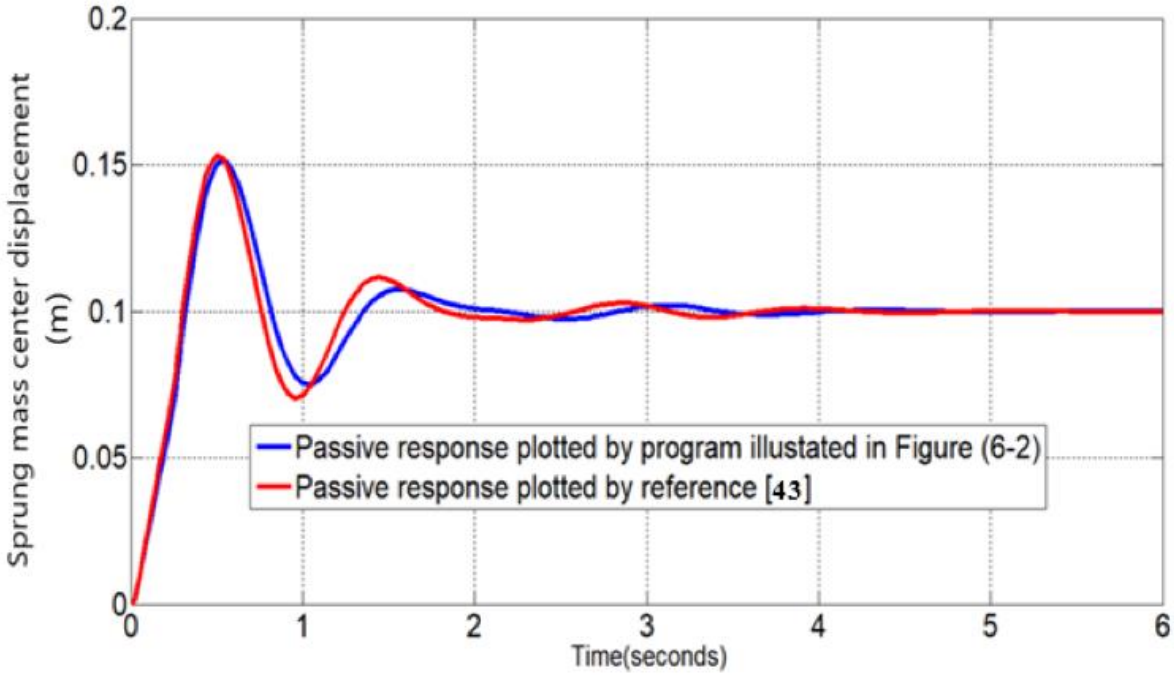

Figure (6-17): Sprung mass center passive response compared to previous work by reference [43]

Table (6-3): Half-car model parameter values [43].

Parameter	Value	Unit
L_2	1.011	m
L_1	1.803	m
b_3	0	$N.s/m$
b_4	0	$N.s/m$
b_1	1290	$N.s/m$
b_2	1620	$N.s/m$
H	0.225	s
J_c	2460	$kg.m^2$
k_1	19960	N/m

Parameter	Value	Unit
k_2	17500	N/m
k_3	175500	N/m
k_4	175500	N/m
m_s	730	Kg
m_{u1}	40	Kg
m_{u2}	35.5	Kg
v	12.5	m/s

6.3 Sprung Mass Angle of Rotation (θ)

In chapter three, it was assumed that the Sprung mass angle of rotation is very small to derive equations of motion. Experimental test rig results for passive and smart dampers show that this angle equals 0.037 radians (peak value), as illustrated in Figures (6-18, 6-19, and 6-20) for front, front and rear, and rear test rig tire excitations, respectively. This angle is the lowest in value for the smart case than the passive case due to the control valves of the smart dampers that provide the lowest sprung mass overshoot, affecting the rotational angle as a result.

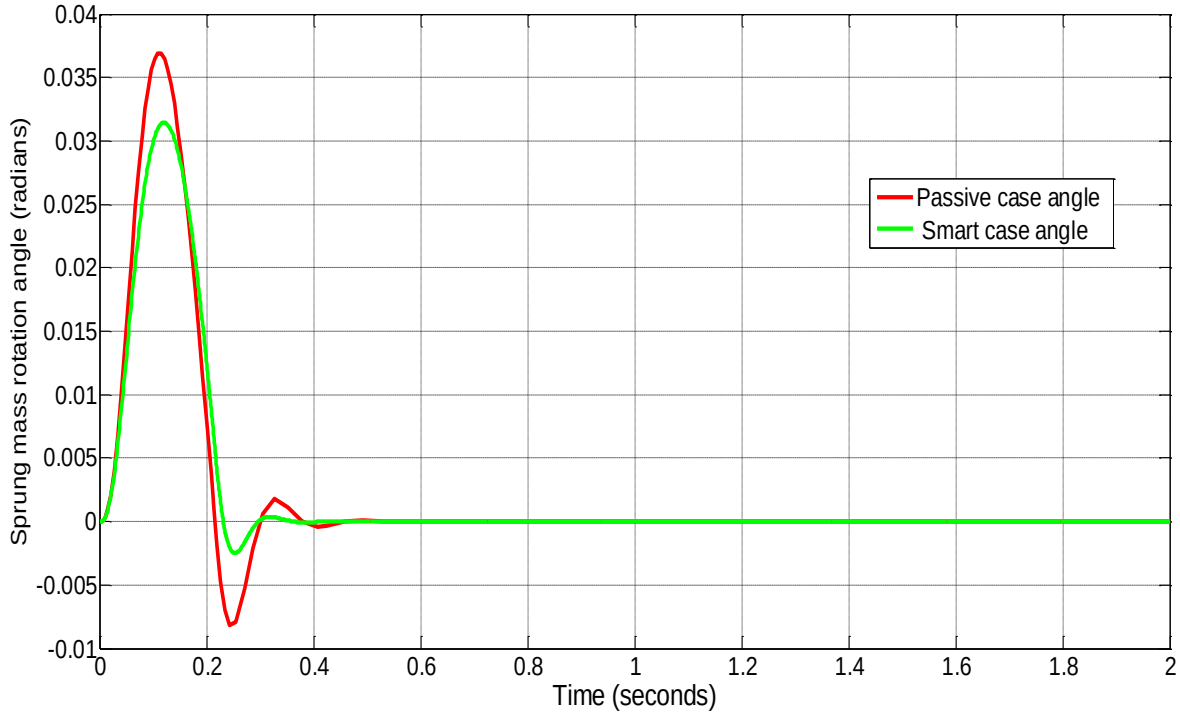

Figure (6-18): sprung mass rotation angle due to impulse excitation at front tire of 0.34 m in lenght and 0.06 m in amplitude at a speed of 1.6 m/s, the excitation takes0.2125 s duration.

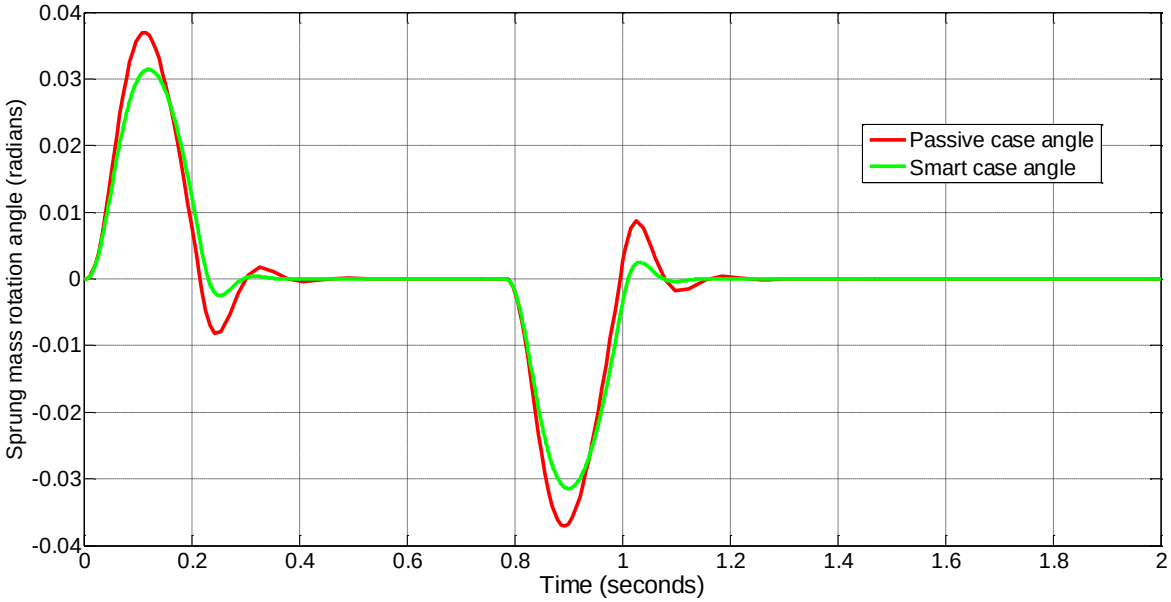

Figure (6-19): sprung mass rotation angle due to two impulse excitations at front & rear tires respectively of 0.34 m in lenght and 0.06 m in amplitude at a speed of 1.6 m/s. The excitation takes 0.2125 s duration.

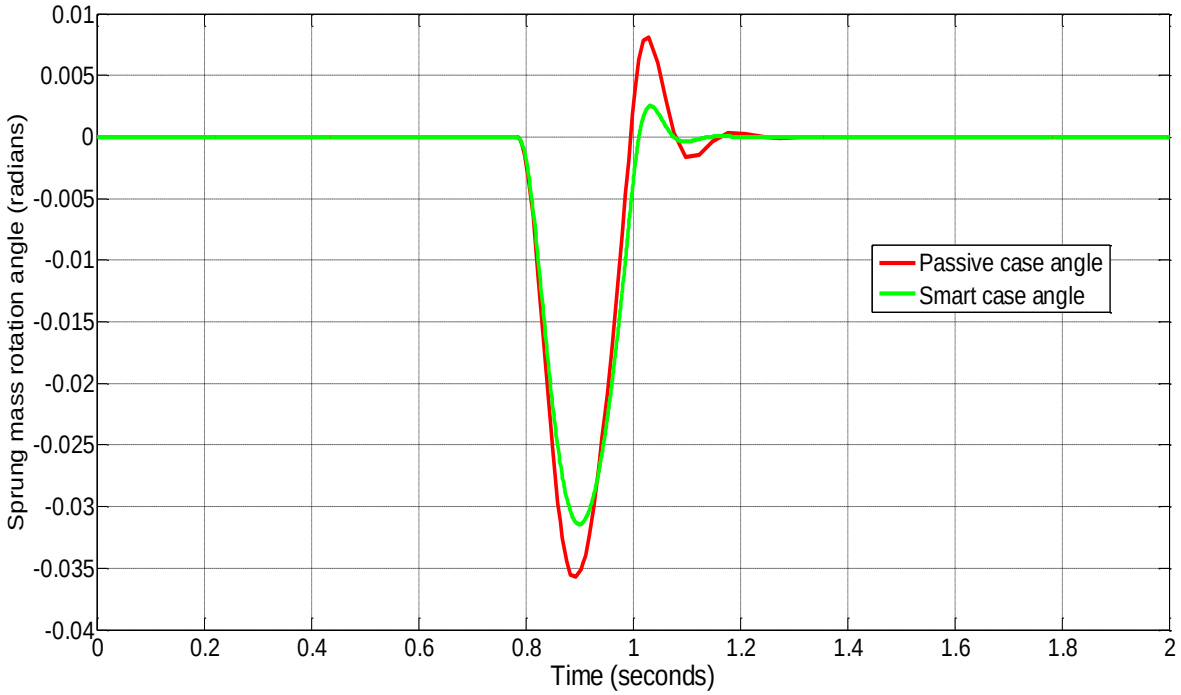

Figure (6-20): sprung mass rotation angle due to impulse excitation at rear tire of 0.34 m in lenght and 0.06 m in amplitude at a speed of 1.6 m/s, the excitation takes0.2125 s duration.

6.4 Damper Hydraulic Flow Rate

During the damper compression stroke, the damper hydraulic fluid flows from the bottom to the top of the damper through the check valve, while at the rebound stroke, the fluid flows inversely from the top to the bottom of the damper through the control valve. Figures (6-21) and (6-22) illustrate the smart and passive damper hydraulic flow rate against the compression and rebound stroke time, respectively. The front damper hydraulic flow rate is greater than the rear one because the front damper's relative velocity is greater than the rear damper's relative velocity, and hence, a lower flow rate; the flow rate is proportional directly to the relative velocity.

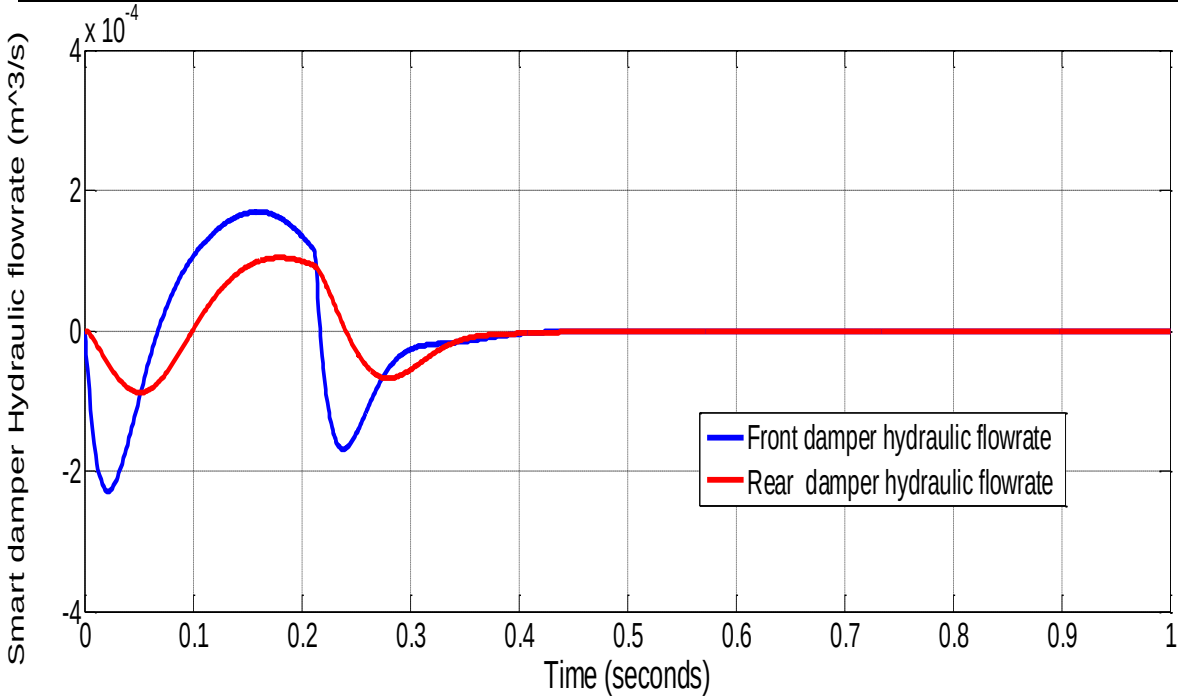

Figure (6-21): Smart damper hydraulic flow rate during the compression and rebound strokes due to impulse excitation at front tire of 0.34 m in length and 0.06 m in amplitude at a speed of 1.6 m/s, the excitation takes 0.2125 s duration.

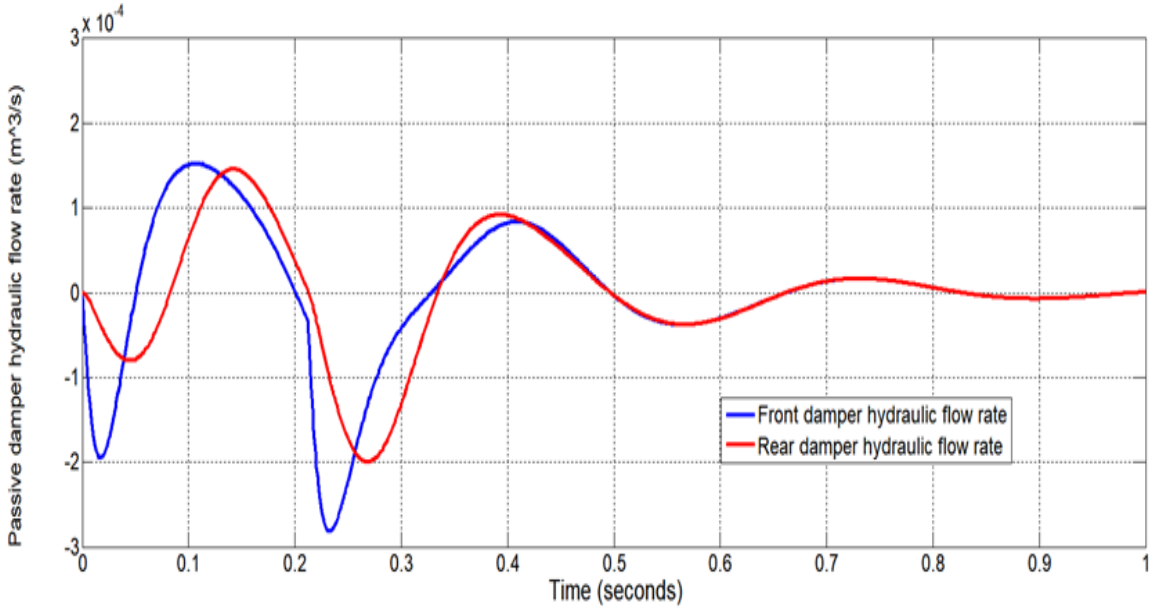

Figure (6-22): Passive damper hydraulic flow rate during the compression and rebound strokes due to impulse excitation at the front tire of 0.34 m in length and 0.06 m in amplitude at a speed of 1.6 m/s, the excitation takes 0.2125 s duration.

Chapter Seven

Conclusions and Future Work

Chapter Seven: Conclusions and Future Work

7.1 Introduction

The seventh chapter consists of the main conclusions observed from the work presented in the previous chapters, as well as the suggested future works that deserve to be points of investigation. The main aim of this study is to use a simple mechanical smart active to damp the vibration of automobiles when moving on irregular roads. This work is focused on using a hydraulic control valve to make the damping of the suspension system proportional to the hardness of the road's irregularity.

7.2 Conclusions

From the current work, the following findings are drawn:

1- The use of the half-car model is suitable for simulating automobile dynamics.

2- The optimization technique is suitable for finding the parameter values used in the smart damper. The Simulink program is suitable for this purpose.

3-The smart damper is effective in attenuating the vibration of the automobile where it resulting in a reduction of the overshoot of the sprung mass by about 65% and the settling time by about 55%..

4- The above result is very important in rising the riding comfort and increasing road handling with good automobile stability.

5- The constructed rig is suitable to verify theoretical work having the same parameters used in the rig.

7.3 Suggestions for Further Research

The following ideas are proposed for further research in light of the work that has been presented:

1- Using an entire automobile model with a smart damper.

2- Examining the system control's experimental performance and reaction when the system is activated by random excitation.

3- Analyzing the suspension system's response with a fuzzy controller and smart damper.

4- Measuring road handling and energy dissipation.

[1] Long, M.T., 2016. On the statistical correlation between the heave, pitch and roll motion of road transport vehicles (Doctoral dissertation, Victoria University).

[2] Ahmed, M.R., Yusoff, A.R. and Romlay, F.R.M., 2019. Adjustable valve semi-active suspension system for passenger car. *International Journal of Automotive and Mechanical Engineering*, *16*(2), pp.6470-6481.

[3] Kamelreiter, M., Kemmetmüller, W. and Kugi, A., 2012. Digitally controlled electrorheological valves and their application in vehicle dampers. *Mechatronics*, *22*(5), pp.629-638.

[4] Hassan, A.A.A.A.A., Vibration Control of Automobile Suspension System using Smart Damper.

[5] "Damper and Awe: 6 Types of Automotive Dampers Explained." Accessed: Dec. 17, 2024. [Online]. Available: https://www.caranddriver.com/features/a15094969/automotive-dampers-explained-how-6-common-types-work-feature.

[6] Dacova, D., 2021. Ride comfort in road vehicles: a literature review. *Trans Motauto World*, *6*(2), pp.65-69.

[7] S. Research, M. Eng, and A. Abdullah Hassan Al-Rajihy Assit Abdulkareem Abdulrazzaq Alhumdany, "REPUBLIC OF IRAQ MINISTRY OF HIGHER EDUCATION Vibration Control of Automobile Suspension System Using a Smart Damper ALI TEBA'AN HASSAN AL-GHIZ'ZY".

[8] C. V. Brandenburg, Dale C; Binder, "Handbook of Human," p. 1005, 1999, Accessed: Jan. 06, 2025. [Online]. Available: https://books.google.com/books/about/Handbook_of_Human_Vibration.html?id=-_JV63L6RMcC.

[9] P. S. Els, N. J. Theron, P. E. Uys, and M. J. Thoresson, "The ride comfort vs. handling compromise for off-road vehicles," *J. Terramechanics*, vol. 44, no. 4, pp. 303–317, Oct. 2007, doi: 10.1016/J.JTERRA.2007.05.001.

[10] V. Goga and M. Kl'Účik, "Optimization of Vehicle Suspension Parameters with use of Evolutionary Computation," *Procedia Eng.*, vol. 48, pp. 174–179, Jan. 2012, doi: 10.1016/J.PROENG.2012.09.502.

[11] P. Sharma, P., Saluja, N., Saini, D., & Saini, "Analysis of automotive passive suspension system with Matlab program generation.," *Int. J. Adv. Technol.*, vol. 4, no. 2, pp. 115-119., 2013.

[12] S. A., Rahman, K. A., & Tanvir, "Simulation and analysis of half-car passive suspension system," *Mech. Eng. Res. J.*, vol. 10, pp. 66–70, 2016.

[13] "MODELLING AND CONTROL OF MAGNETORHEOLOGICAL DAMPERS FOR VEHICLE SUSPENSION SYSTEMS HASSAN AHMED METERED SCHOOL OF MECHANICAL, AEROSPACE AND CIVIL ENGINEERING".

[14] P. Krauze and J. Kasprzyk, "Mixed Skyhook and FxLMS Control of a Half-Car Model with Magnetorheological Dampers," *Adv. Acoust. Vib.*, vol. 2016, no. 1, p. 7428616, Jan. 2016, doi: 10.1155/2016/7428616

[15] K. Hemanth, H. Kumar, and K. V Gangadharan, "Dynamic Analysis of Half Car Model with MR Damper as Semi-Active Suspension Element", doi: 10.20855/ijav.2018.23.21131.

[16] M. A. Ansari, P. K. Meher, A. Bisoi, and A. Biswas, "Augmentation of damping force by modifying the geometrical shape of the MR

damper," *J. Brazilian Soc. Mech. Sci. Eng.*, vol. 45, no. 6, pp. 1–13, Jun. 2023, doi: 10.1007/S40430-023-04243-5/METRICS.

[17] A. Yaghoubi, S., & Ghanbarzadeh, "Modeling and optimization of car suspension system in the presence of magnetorheological damper using Simulink-PSO hybrid technique," *Commun. Nonlinear Sci. Numer. Simul.*, vol. 125, p. 107378, 2023, doi: 10.1016/J.CNSNS.2023.107378.

[18] S. Tyagi and C. Sandu, "Development of a Semi Active Suspension System for Lightweight Automobiles." Aug. 09, 2016. Accessed: Jan. 01, 2025. [Online]. Available: http://hdl.handle.net/10919/72131

[19] O. Mokhiamar, M. Ghoniem, and T. Awad, "Implementation of fuzzy logic control on a new low cost semi-active vehicle shock absorber," *J. Mech. Eng. Sci.*, vol. 16, no. 2, pp. 8965–8975, Jun. 2022, doi: 10.15282/JMES.16.2.2022.13.0709.

[20] A. R. Rajasekharan Unnithan and S. Subramaniam, "Enhancing Ride Comfort and Stability of a Large Van Using an Improved Semi-active Stability Augmentation System," *SAE Int. J. Veh. Dyn. Stability, NVH*, vol. 6, no. 4, pp. 385–403, 2022, doi: 10.4271/10-06-04-0026.

[21] B. Zhang, H. Zhao, and X. Zhang, "Adaptive variable domain fuzzy PID control strategy based on road excitation for semi-active suspension using CDC shock absorber," *https://doi.org/10.1177/10775463231152287*, vol. 30, no. 3–4, pp. 860–875, Feb. 2023, doi: 10.1177/10775463231152287.

[22] M. H. Mohamad Haniff Bin Zamahsari, "Studies And Simulations Of Semi-Active Vehicle Suspension System," 2010.

[23] B. Ebrahimi, "Development of Hybrid Electromagnetic Dampers for Vehicle Suspension Systems." University of Waterloo, 2009.

Accessed: Dec. 23, 2024. [Online]. Available: http://hdl.handle.net/10012/4375

[24] Y. Mustafa, G. I., Wang, H., & Tian, "Model-free adaptive fuzzy logic control for a half-car active suspension system," *Stud. Informatics Control*, vol. 28(1), pp. 13–24, 2019.

[25] N. Hamza, A., & ben Yahia, "Heavy trucks with intelligent control of active suspension based on artificial neural networks.," *https://doi.org/10.1177/0959651820958516*, vol. 235, no. 6, pp. 952–969, 2020, doi: https://doi.org/10.1177/0959651820958516.

[26] D. ; Rodriguez-Guevara *et al.*, "An MPC-LQR-LPV Controller with Quadratic Stability Conditions for a Nonlinear Half-Car Active Suspension System with Electro-Hydraulic Actuators," *Mach. 2022, Vol. 10, Page 137*, vol. 10, no. 2, p. 137, Feb. 2022, doi: 10.3390/MACHINES10020137.

[27] D. N. Nguyen and T. A. Nguyen, "The Dynamic Model and Control Algorithm for the Active Suspension System," *Math. Probl. Eng.*, vol. 2023, no. 1, p. 2889435, Jan. 2023, doi: 10.1155/2023/2889435.

[28] M. Montazeri-Gh and O. Kavianipour, "Investigation of the passive electromagnetic damper," *Acta Mech.*, vol. 223, no. 12, pp. 2633–2646, Dec. 2012, doi: 10.1007/S00707-012-0735-8/METRICS.

[29] Y. Liao, P. Liu, J. Zhao, P. Kin Wong, D. Ning, and H. Du, "A novel closed-loop current control unit for decoupling vibration control of semi-active electrically interconnected suspension," *Mech. Syst. Signal Process.*, vol. 212, p. 111308, Apr. 2024, doi: 10.1016/J.YMSSP.2024.111308.

[30] A. M. A. Soliman, M. A. H. Galal, and N. A. Mansour, "Evaluation of Ride Performance through a Comparative Study of Switchable

Damper and Active Suspension by Using Fuzzy and Linear Quadratic Regulator Controller's Strategies," *SAE Int. J. Veh. Dyn. Stability, NVH*, vol. 5, no. 1, pp. 15–30, 2021, doi: 10.4271/10-05-01-0002.

[31] Makowski, M., Knap, L. and Grzesikiewicz, W., 2011. Vibration investigation of vehicle equiped with controlled piezoelectric dampers. *Journal of KONES*, *18*(4), pp.251-257.

[32] A. A. A.-R. A. M. A. Khafaji, "vibration vontrol of automobiles by smart damper based on half-car model," Kerbala, Iraq, 2024.

[33] A. A. A.-R. A. M. A. Khafaji, "Reducing the Vibration of Automobiles using Smart Damper (Experimental Approach)," Baghdad, Iraq, 2025.

[34] Rao, C.L., Lakshinarashiman, J., Sethuraman, R. and Sivakumar, S.M., 2003. Engineering Mechanics: Statics and Dynamics; PHI Learning Pvt. *Ltd.: Delhi, India*.

[35] Krauze, P. and Kasprzyk, J., 2016. Mixed Skyhook and FxLMS Control of a Half-Car Model with Magnetorheological Dampers. *Advances in Acoustics and Vibration*, *2016*(1), p.7428616.

[36] Cengel, Y. and Cimbala, J., 2013. *Ebook: Fluid mechanics fundamentals and applications (si units)*. McGraw Hill.

[37] Luo, Y., 2006. *System modeling and control design of a two-stage metering poppet-valve system* (Doctoral dissertation, University of Missouri--Columbia).

[38] Barbara Zardin, Massimo Borghi, Giovanni Cillo, Carlo Alberto Rinaldini, and Enrico Mattarelli, "Design of Two-Stage On/Off Cartridge Valves for Mobile Applications," Energy Procedia, vol. 126, pp. 1123–1130, 2017.

[39] G. A. Hassaan, "Car dynamics using quarter model and passive

suspension, part I: effect of suspension damping and car speed.," *Int. J.Comput. Tech.*, vol. 1, no. 2, pp. 1–9, 2014.

[40] "Moment-of-Inertia-1.png (2000×1200)." Accessed: Apr. 23, 2025. [Online]. Available: https://st.adda247.com/https://s3-ap-south-1.amazonaws.com/adda247jobs-wp-assets-adda247/jobs/wp-content/uploads/sites/2/2022/04/26094458/Moment-of-Inertia-1.png

[41] "(1620) Oğuzhan Ahan - YouTube." Accessed: Apr. 17, 2024. [Online]. Available: https://www.youtube.com/@oguzhanahan

[42] C. W. (1973). Bert, "Material damping: An introductory review of mathematic measures and experimental technique," *J. Sound Vib.*, vol. 29, no. 2, pp. 129-153., doi: https://doi.org/10.1016/S0022-460X(73)80131-2.

[43] Matrood, M. M., & Nassar, A. A. (2023). Improving the Dynamic Response of Half-Car Model using Modified PID Controller. *Iraqi Journal for Electrical and Electronic Engineering, 19,* 52-58.

الخلاصة

تتعرض السيارات للاهتزاز بسبب عدم انتظام الطرق، مما يؤثر على السلامة وأداء القيادة وراحة الركاب. تهدف هذه الدراسة إلى معالجة هذه المشكلة من خلال اعتماد نموذج "نصف سياره" الذي يتضمن أربعة درجات من الحرية. تم افتراض وجود حركات عمودية في الجانبين الأمامي والخلفي وحركه دورانية في المسافة بينهما، وتم اختبار النموذج في حالتين, الحاله الاولى باستخدام مخمدات تقليديه والثانيه باستخدام مخمدات ذكيه تم صناعتها بواسطه تعديل المخمدات التقليديه المستخدمه في الحاله الاولى باضافه صمامات تحكم هيدروليكية خارجية و تركيب صمامات ذات اتجاه جرياني واحد للمخمدات الأمامية والخلفية، مما حولها إلى ممتصات ذكية. تم تحليل استجابة النموذج عند تعرضه لمدخل طريقي مفاجئ، مع تعديل المعلمات مثل الكتلة ومعامل التخميد وصلابة النوابض للصمامات الهيدروليكيه المضافه لتحقيق استجابة سريعة تتماشى مع معايير الأداء المثلى (مثل زمن الاستقرار ونسبة الزيادة في الذروة والاستجابة في الحالة المستقرة) باستخدام تقنية تحسين تقليدية تُعرف باسم "طريقة البحث الخطي". ولتقليل الوقت والتكاليف استخدمت الدراسه برنامج الماتلاب- سميولنك وأظهرت النتائج أن هذا النهج يحسن من استجابة النظام الديناميكي مقارنة بالممتصات التقليدية. تم العثور على القيم المثلى لمعايير صمام التحكم الأمامي (الكتلة 2 غم، معامل التخميد 7 نيوتن.ثانية/متر و جساءة النابض 9000 نيوتن/متر)، بينما بالنسبة للصمام الخلفي، فهي (الكتلة 2غم، معامل التخميد 8 نيوتن.ثانية/متر و جساءة النابض 13000 نيوتن/متر). تُظهر النتائج أن هذه الطريقة تعزز استجابة النظام الديناميكي بالكامل مقارنة بالمخمد التقليدي الأول؛ حيث تم تقليل زمن استقرار الكتلة المعلقة في حالة المخمد الذكي بنسبة 65% وذروه التجاوزالقصوى بنسبة 55% مقارنة بالمخمد التقليدي، مما يوفر راحة أكبر في الركوب واستقرارًا أفضل للمركبة.

جمهورية العراق

وزارة التعليم العالي و البحث العلمي

جامعة كربلاء

كلية الهندسة

قسم الهندسة الميكانيكيه

التحكم في اهتزازات نموذج نصف سيارة بواسطة مخمد ذكي

رسالة مقدمة الى مجلس كلية الهندسة / جامعة كربلاء وهي جزء من متطلبات نيل درجة الماجستير في علوم الهندسة الميكانيكيه

المؤلف:

أحمد محمد علي حسن الخفاجي

باشراف :

البروفيسور الدكتور أحمد عبد الله حسن الراجحي

ذو القعده - 1446 ايار - 2025